## REPORT DOCUMENTATION PAGE

READ INSTRUCTIONS BEFORE COMPLETING FORM

1. REPORT NUMBER

2. GOVT ACCESSION NO.

3. RECIPIENT'S CATALOG NUMBER

4. TITLE (and Subtitle)
Prediction and Control of Residual Stresses and Distortion in HY-130 Thick Pipe Weldments

5. TYPE OF REPORT & PERIOD COVERED
THESIS

6. PERFORMING ORG. REPORT NUMBER

7. AUTHOR(s)
Mabry, John P.

8. CONTRACT OR GRANT NUMBER(s)

9. PERFORMING ORGANIZATION NAME AND ADDRESS
Massachusetts Institute of Technology
Cambridge, MA

10. PROGRAM ELEMENT, PROJECT, TASK AREA & WORK UNIT NUMBERS

11. CONTROLLING OFFICE NAME AND ADDRESS
CODE 031
NAVAL POSTGRADUATE SCHOOL
MONTEREY, CALIFORNIA 93940

12. REPORT DATE
May 1979

13. NUMBER OF PAGES
127

14. MONITORING AGENCY NAME & ADDRESS(if different from Controlling Office)

15. SECURITY CLASS. (of this report)
UNCLASS

15a. DECLASSIFICATION/DOWNGRADING SCHEDULE

16. DISTRIBUTION STATEMENT (of this Report)

APPROVED FOR PUBLIC RELEASE; DISTRIBUTION UNLIMITED

17. DISTRIBUTION STATEMENT (of the abstract entered in Block 20, if different from Report)

18. SUPPLEMENTARY NOTES

19. KEY WORDS (Continue on reverse side if necessary and identify by block number)
Naval Engineering
Welding
Thermal Stress
HY-130 Steel

20. ABSTRACT (Continue on reverse side if necessary and identify by block number)

SEE REVERSE

## ABSTRACT

In order to validate existing techniques for computer simulation of the weldin process, an experiment is designed and carried out in which seam and girth wel are produced on a high strength steel cylinder. Fabrication of the HY-130 cylinder, selection of welding parameters for the seam and girth welds, and the selection and arrangement of instrumentation are described. The theoretical background of finite element computer simulation of heat flow in weldments as well as techniques for axisymmetric finite element analysis of thermal stress and metal movement during welding are discussed. Finite element representatio of weldment geometry for heat flow and stress analysis is presented. Metallur cal properties of the HY-130 cylinder seam weld are presented in the form of photo-micrographs and electron scan micrographs.

Temperature, strain, and radial distortion are measured at various locations o the HY-130 cylinder and the measured values are compared in tabular and graphi form with those values predicted by use of the heat flow and stress analysis programs. Excellent agreement is achieved between measured and analytically predicted temperature distributions, but only qualitative agreement is shown f strains and radial distortion.

1

# PREDICTION AND CONTROL OF RESIDUAL STRESSES AND DISTORTION IN HY-130 THICK PIPE WELDMENTS

by

LIEUTENANT JOHN PAUL MABRY, U.S. NAVY

B.E., Vanderbilt University

1973

SUBMITTED IN PARTIAL FULFILLMENT

OF THE REQUIREMENTS FOR THE

DEGREES OF

OCEAN ENGINEER

and

MASTER OF SCIENCE

IN NAVAL ARCHITECTURE AND MARINE ENGINEERING

at the

MASSACHUSETTS INSTITUTE OF TECHNOLOGY

May, 1979

# PREDICTION AND CONTROL OF RESIDUAL STRESSES AND DISTORTION IN HY-130 THICK PIPE WELDMENTS

by

LIEUTENANT JOHN PAUL MABRY, U.S. NAVY

Submitted to the Department of Ocean Engineering
on 11 May 1979 in partial fulfillment of the requirements
for the Degrees of Ocean Engineer and
Master of Science in
Naval Architecture and Marine Engineering

## ABSTRACT

In order to validate existing techniques for computer simulation of the welding process, an experiment is designed and carried out in which seam and girth welds are produced on a high strength steel cylinder. Fabrication of the HY-130 cylinder, selection of welding parameters for the seam and girth welds, and the selection and arrangement of instrumentation are described. The theoretical background of finite element computer simulation of heat flow in weldments as well as techniques for axisymmetric finite element analysis of thermal stress and metal movement during welding are discussed. Finite element representation of weldment geometry for heat flow and stress analysis is presented. Metallurgical properties of the HY-130 cylinder seam weld are presented in the form of photo-micrographs and electron scan micrographs.

Temperature, strain, and radial distortion are measured at various locations on the HY-130 cylinder and the measured values are compared in tabular and graphical form with those values predicted by use of the heat flow and stress analysis programs. Excellent agreement is achieved between measured and analytically predicted temperature distributions, but only qualitative agreement is shown for strains and radial distortion.

Thesis Supervisor: Dr. Koichi Masubuchi

Title: Professor of Ocean Engineering and Materials Science

ACKNOWLEDGEMENTS

Professor Koichi Masubuchi has guided and supported my research effort and it is with gratitude and admiration that this report is submitted to him for certification.

I will be forever indebted to the U.S. Navy for providing an opportunity for me to study and grow at the Massachusetts Institute of Technology.

Many organizations and individuals have contributed to the success of this study. Their interest, advice, assistance, and support are greatly appreciated. Those persons whose efforts were particularly noteworthy include:

Dr. Chon-Liang Tsai, Vassilios Papazoglou, and Jim Averback of the MIT Ocean Engineering Department.

Professor Tom Eagar, Tony Zona, and Bruce Russell of MIT's Materials Joining Laboratory.

Fred Merlis of MIT's Aerolastics Laboratory.

Abraham Pollack of the Naval Ship Research and Development Center at Annapolis, Maryland.

Russ Van Billiard, Richard Wormwood, and Mitch Avery of the Portsmouth Naval Shipyard in Portsmouth, New Hampshire.

Paul Ryder, Roger M. Lamothe, and Theodore LaFrance of the Army Materials and Mechanics Research Center at Watertown, Massachusetts.

Bob Bennett of Bethlehem Steel Corporation Shipyard in East Boston, Massachusetts.

Art Greagor and Len Sudenfield of the MIT Materials Department.

This list is far from complete. The patience and understanding of my lovely wife, Barbara, also contributed.

# TABLE OF CONTENTS

TITLE 1

ABSTRACT 2

ACKNOWLEDGEMENTS 3

TABLE OF CONTENTS 5

LIST OF TABLES 7

LIST OF FIGURES 9

TABLE OF SYMBOLS 12

CHAPTER I: 13

A. INTRODUCTION

B. BACKGROUND

C. SCOPE OF RESEARCH

CHAPTER II: MATERIAL CONSIDERATIONS 20

A. GENERAL

B. COMPOSITION

C. TEMPERATURE DEPENDENCE OF MATERIAL PROPERTIES

CHAPTER III: DESCRIPTION OF EXPERIMENTAL PROCEDURE 35

A. FABRICATION OF THE WELD SPECIMEN

B. SELECTION OF WELDING CONSUMABLES

C. SELECTION OF WELDING PARAMETERS

1. GEOMETRY OF JOINT

2. HEAT INPUT

3. WIRE FEED RATE

D. ARRANGEMENT OF APPARATUS

E. TESTING OF WELDING EQUIPMENT

F. SELECTION AND ARRANGEMENT OF INSTRUMENTATION TO MEASURE TEMPERATURE, STRAIN, AND DISTORTION DURING WELDING

G. PRODUCTION OF THE INSTRUMENTED SEAM AND GIRTH WELDS

CHAPTER IV: METALLURGICAL CONSIDERATIONS 65

CHAPTER V: DESCRIPTION OF ANALYTICAL TOOLS AND PROCEDURES 73

A. INTRODUCTION

B. DESCRIPTION OF HEAT FLOW PROGRAM

1. THEORETICAL BACKGROUND

2. GEOMETRY OF WELD SPECIMEN AND DESCRIPTION OF FINITE ELEMENT REPRESENTATION OF TEMPERATURE DISTRIBUTION DURING GIRTH WELD

C. DESCRIPTION OF COMPUTER PROGRAM TO CALCULATE STRAIN, STRESS, AND DISTORTION

1. THEORETICAL BACKGROUND

2. GEOMETRY OF WELD SPECIMEN AND FINITE ELEMENT REPRESENTATION OF WELDMENT

CHAPTER VI: COMPARISON OF STRESS MEASURED DURING WELDING WITH VALUES PREDICTED BY ANALYTICAL METHODS 101

CHAPTER VII: CONCLUSIONS 123

CHAPTER VIII: RECOMMENDATIONS 124

# LIST OF TABLES


| | | |
|---|---|---|
| I-A | PAST EXPERIMENTAL STUDIES OF THERMAL STRESSES AND METAL MOVEMENT DURING WELDING | 18 |
| II-A | COMPOSITIONAL RANGES OF HY-130 STEEL | 21 |
| II-B | SUMMARY OF MECHANICAL PROPERTIES OF HY-130 STEEL | 33 |
| II-C | SUMMARY OF PHYSICAL PROPERTIES OF HY-130 STEEL | 34 |
| III-A | HY-130 CYLINDER WELDING PARAMETERS | 42 |
| III-B | TEMPERATURE PENETRATION DISTANCES DETERMINED BY TEMPILAQ | 46 |
| III-C | STRAIN GAGE CHARACTERISTICS | 48 |
| III-D | CHARACTERISTICS OF LINEAR MOTION POTENTIOMETERS | 57 |
| III-E | SEAM AND GIRTH WELD PASSES | 64 |
| V-A | NODAL COORDINATES FOR HEAT FLOW ANALYSIS | 77 |
| V-B | NODAL COORDINATES USED BY THE MURAKI PROGRAM | 97 |
| V-C | FINITE ELEMENT CONNECTIVITY USED BY THE MURAKI PROGRAM | 99 |
| VI-A | EXPERIMENTALLY DETERMINED TEMPERATURE DISTRIBUTION | 102 |
| VI-B | EXPERIMENTAL AND ANALYTICAL STRAIN 1.0 IN FROM WELD CENTERLINE | 107 |
| VI-C | EXPERIMENTAL AND ANALYTICAL STRAIN 1.5 IN FROM WELD CENTERLINE | 108 |
| VI-D | EXPERIMENTAL AND ANALYTICAL STRAIN 2.0 IN FROM WELD CENTERLINE | 109 |
| VI-E | EXPERIMENTAL AND ANALYTICAL STRAIN 2.5 IN FROM WELD CENTERLINE | 110 |
| VI-F | PREDICTED X AND Z DIRECTION STRESSES 1.0 IN FROM WELD CENTERLINE | 111 |

LIST OF TABLES (Cont'd)


| | | |
|---|---|---|
| VI-G | PREDICTED X AND Z DIRECTION STRESSES 1.5 IN FROM WELD CENTERLINE | 112 |
| VI-H | PREDICTED X AND Z DIRECTION STRESSES 2.0 IN FROM WELD CENTERLINE | 113 |
| VI-I | PREDICTED X AND Z DIRECTION STRESSES 2.5 IN FROM WELD CENTERLINE | 114 |
| VI-J | EXPERIMENTAL AND ANALYTICAL DISTORTION 0.5 IN AND 1.0 IN FROM WELD CENTERLINE | 115 |

# LIST OF FIGURES


| | | |
|---|---|---|
| II-1 | TYPICAL STRESS-STRAIN DIAGRAM FOR HY-130 AT ROOM TEMPERATURE | 23 |
| II-2 | ESTIMATED EFFECT OF TEMPERATURE ON 0.2% OFFSET YIELD STRESS FOR HY-130 | 24 |
| II-3 | ESTIMATED EFFECT OF TEMPERATURE ON YOUNG'S MODULUS FOR HY-130 | 25 |
| II-4 | TANGENT MODULUS CURVES FOR HY-130 | 26 |
| II-5 | ESTIMATED EFFECT OF TEMPERATURE ON TANGENT MODULUS FOR HY-130 | 27 |
| II-6 | ESTIMATED EFFECT OF TEMPERATURE ON POISSON'S RATIO FOR HY-130 | 28 |
| II-7 | ESTIMATED COEFFICIENT OF THERMAL EXPANSION FOR HY-130 | 29 |
| II-8 | EFFECT OF TEMPERATURE ON DENSITY OF HY-130 | 30 |
| II-9 | ESTIMATED EFFECT OF TEMPERATURE ON THERMAL CONDUCTIVITY OF HY-130 | 31 |
| II-10 | ESTIMATED EFFECT OF TEMPERATURE ON SPECIFIC HEAT OF HY-130 | 32 |
| III-1 | STAGES 1 AND 2 OF CYLINDER FABRICATION | 37 |
| III-2 | STAGES 3, 4, AND 5 OF CYLINDER FABRICATION | 38 |
| III-3 | WELD JOINT GEOMETRY FOR HY-130 CYLINDER SEAM WELDS | 40 |
| III-4 | POSITION OF CYLINDER AND WELDING TORCH FOR PRODUCTION OF SEAM WELD | 43 |
| III-5 | ARRANGEMENT OF STRAIN GAGES AND THERMOCOUPLES | 50 |
| III-6 | CYLINDER SECTIONS | 53 |
| III-7 | GIRTH WELD GEOMETRY | 54 |
| III-8 | PHOTOGRAPH OF CYLINDER SUPPORT STRUCTURE | 55 |

LIST OF FIGURES (Cont'd)


| | | |
|---|---|---|
| III-9 | PHOTOGRAPH OF GIRTH WELD PRODUCTION | 56 |
| III-10 | DISPLACEMENT TRANSDUCER CIRCUITRY | 59 |
| III-11 | ARRANGEMENT OF LINEAR MOTION POTENTIOMETERS | 59 |
| III-12 | DISPLACEMENT TRANSDUCER CALIBRATION RESULTS | 60 |
| III-13 | ARRANGEMENT AND OPERATION OF INSTRUMENTATION | 61 |
| III-14 | SEAM WELD PASSES | 62 |
| III-15 | GIRTH WELD PASSES | 63 |
| IV-1 | LOCATION OF PHOTO-MICROGRAPHS AND ELECTRON SCAN MICROGRAPHS | 66 |
| IV-2 | 500X PHOTO-MICROGRAPH OF HY-130 WELD METAL | 67 |
| IV-3 | 500X PHOTO-MICROGRAPH OF HY-130 FUSION ZONE | 67 |
| IV-4 | 500X PHOTO-MICROGRAPH OF HY-130 HAZ | 68 |
| IV-5 | 500X PHOTO-MICROGRAPH OF HY-130 PARENT METAL | 68 |
| IV-6 | 1200X ELECTRON SCAN MICROGRAPH OF HY-130 WELD METAL | 69 |
| IV-7 | 6000X ELECTRON SCAN MICROGRAPH OF HY-130 WELD METAL | 69 |
| IV-8 | 1200X ELECTRON SCAN MICROGRAPH OF HY-130 FUSION ZONE | 70 |
| IV-9 | 6000X ELECTRON SCAN MICROGRAPH OF HY-130 FUSION ZONE | 70 |
| IV-10 | 1200X ELECTRON SCAN MICROGRAPH OF HY-130 HAZ | 71 |
| IV-11 | 6000X ELECTRON SCAN MICROGRAPH OF HY-130 HAZ | 71 |
| IV-12 | 1200X ELECTRON SCAN MICROGRAPH OF HY-130 PARENT METAL | 72 |

LIST OF FIGURES (Cont'd)


| | | |
|---|---|---|
| IV-13 | 6000X ELECTRON SCAN MICROGRAPH OF HY-130 PARENT METAL | 72 |
| V-1 | FINITE ELEMENT REPRESENTATION OF WELDMENT GEOMETRY FOR HEAT FLOW ANALYSIS | 76 |
| V-2 | FINITE ELEMENT REPRESENTATION OF WELDMENT GEOMETRY FOR STRAIN, STRESS, AND DISTORTION ANALYSIS | 96 |
| VI-1 | PLOT OF EXPERIMENTAL TEMPERATURE DISTRIBUTION DURING GIRTH WELD | 103 |
| VI-2 | PLOT OF ANALYTICAL TEMPERATURE DISTRIBUTION DURING GIRTH WELD | 104 |
| VI-3 | COMPARATIVE PLOT OF EXPERIMENTAL AND ANALYTICAL STRAIN 1.0 IN FROM WELD CENTERLINE | 116 |
| VI-4 | COMPARATIVE PLOT OF EXPERIMENTAL AND ANALYTICAL STRAIN 1.5 IN FROM WELD CENTERLINE | 117 |
| VI-5 | COMPARATIVE PLOT OF EXPERIMENTAL AND ANALYTICAL STRAIN 2.0 IN FROM WELD CENTERLINE | 118 |
| VI-6 | COMPARATIVE PLOT OF EXPERIMENTAL AND ANALYTICAL STRAIN 2.5 IN FROM WELD CENTERLINE | 119 |
| VI-7 | PREDICTED X AND Z DIRECTION STRESSES 1.0 IN AND 1.5 IN FROM WELD CENTERLINE | 120 |
| VI-8 | PREDICTED X AND Z DIRECTION STRESSES 2.0 IN AND 2.5 IN FROM WELD CENTERLINE | 121 |
| VI-9 | COMPARATIVE PLOT OF EXPERIMENTAL AND ANALYTICAL RADIAL DISTORTION 0.5 IN AND 1.0 IN FROM WELD CENTERLINE | 122 |

# TABLE OF SYMBOLS

| | | |
|---|---|---|
| $\sigma$ | Stress | (ksi) |
| E | Elastic Modulus | (ksi x $10^{-3}$) |
| H | Tangent Modulus | (ksi x $10^{-3}$) |
| $\nu$ | Poisson's Ratio | |
| I | Welding Current | (Amperes) |
| V | Arc Voltage | (Volts) |
| v | Welding Arc Travel Speed | (inches/second) |
| Q | Heat Input | (Joules/inch) |
| $\rho$ | Density | ($lbm/_{in^3}$) |
| $\alpha_T$ | Coefficient of Thermal Expansion | (microstrain/$^{o}_{F}$) |
| C | Thermal Conductivity | (BTU/$_{hr\ ft\ ^{o}F}$) |
| $\kappa$ | Specific Heat | (BTU/$_{lbm\ ^{o}F}$) |
| q | Heat Intensity | (Joules/$_{sec\ inch}$) |
| K | Thermal Diffusivity | ($in^2$/sec) |
| $\eta_{arc}$ | Welding Arc Efficiency | |
| h | Plate Thickness | (inches) |
| T | Temperature | ($^{o}$F) |
| t | Time | (seconds) |

# CHAPTER I

## I.A INTRODUCTION:

Welding has been used as the primary means of fabricating ocean structures for the past forty years. Design tools for the fabrication of welded structures have evolved primarily as the result of experimentation. These tools are usually expressed as empirical relationships among welding parameters, some of which include structure and weld joint geometry, physical properties of the structural materials and welding consummables, as well as methods and rates of energy transfer during the joining process. In most cases the use of these empirical relationships has been adequate to ensure the achievement of good quality weld joints in a production environment.

As design tools become more sophisticated, and the interrelationships among physical properties of welding and structural materials are better understood, design practices relating to allowable stresses in welded structures converge toward material limits. Development and refinement of techniques for detecting and classifying flaws in weldments is another design consideration which tends to increase confidence in welded structures subjected to more demanding requirements, allowing design engineers to increase allowable stresses or to reduce factors of safety or uncertainty.

An area of welding technology which requires further definition and refinement is the occurrence of residual stresses and structural distortion during and as the result of the welding process. Extreme non-uniform thermal cycles of weld metal and of structural metal in areas near the weldment produce unevenly distributed thermal stresses which cause localized plastic deformations, with resultant residual stresses and structural distortion. These residual stresses can significantly contribute to structural failure, particularly when the failure mechanism is dependent upon low applied stress, such as brittle fracture or failure resulting from stress corrosion cracking. Distortions caused by welding can also cause structural failure by reducing a structure's ability to withstand buckling loads.

The ability to accurately predict the magnitude and type of residual stresses and distortion resulting from the welding of ocean structures would greatly enhance a design engineer's ability to estimate total stresses which materials must withstand during loading. More accurate estimation of total stresses would allow for more effective use of materials and the increased predictability of structural failure would ultimately result in the production of more reliable ocean structures.

I.B BACKGROUND:

Attempts to analytically predict or to simulate thermal stresses and metal movement which occur during the welding process have been the subject of considerable research effort during the past ten years. The complexity of the interrelationships among welding parameters which contribute to the formation of residual stresses in weldments does not allow the development of empirical relationships which are useful for more than one type of material, joint geometry, or welding process. Welding variables were too numerous and their interrelationships too complex for the development of a general technique for the analysis of transient thermal stresses, residual stresses, and distortion in weldments. Design engineers usually relied upon trial and error, or the use of design lanes derived from similar applications of proposed welding processes.

Computer simulation of the welding process has offered reasonable opportunities to develop techniques which apply to wide ranges of materials, weld geometries, and processes. A description of the chronological and systematic development of techniques used for analysis of thermal stresses and metal movement during the welding process is contained in a paper presented by Masubuchi[1] to an international conference on Residual Stresses in Welded Construction and their Effects. This conference was held in London 15-17 November 1977,

hosted by the Welding Institute, Abington Hall, Abington, Cambridge, England. Systematic development of computer techniques for welding simulation began with a one-dimensional analysis by Tall[2] in 1961. This research involved the simulation of thermal stresses occurring during the bead welding of a strip. Efforts at Massachusetts Institute of Technology by Masubuchi[3] in 1968 expanded Tall's analysis into a one-dimensional FORTRAN program. This research was expanded into the development of a two-dimensional FORTRAN program in 1970 by Iwaki[4]. Iwaki attempted to apply two-dimensional finite analysis to bead on plate welding. The most recent computer program to be used at MIT was developed by Muraki[5]. Muraki's program uses finite element analysis techniques to predict thermal stresses and metal movement based upon temperature distributions within the weldment which are calculated by heat flow programs also developed at MIT.

## I.C SCOPE AND OBJECTIVES OF THIS STUDY:

The purpose of this research is to design and carry out an experimental procedure to generate data which can be used to validate the existing heat flow program and the program which uses finite element analysis to predict the occurrence of thermal stresses and distortion during welding. The production of seam and girth welds in a high strength steel cylinder under very carefully controlled conditions

while measuring temperature, strain, and distortion as a function of time and location with respect to arc travel would serve as a valuable aid in evaluating the accuracy and potential usefulness of the heat flow program and of Muraki's axisymmetric finite element program for analysis of thermal stress and metal movement during welding. This research is part of a continuing effort at MIT to validate computer analysis of welding. A summary of past experimental studies of thermal stresses and metal movement during welding was presented by Masubuchi[1] and is reproduced and updated here as Table I-A.

PAST EXPERIMENTAL STUDIES OF THERMAL
STRESSES AND METAL MOVEMENT DURING WELDING

| NO. | PRINCIPAL PERSONNEL | SPONSOR | MATERIAL, JOINT TYPE, ETC. |
|---|---|---|---|
| 1. | Arita[6] | NASA | Bead-on-plate welding of 2219-o aluminum alloy plates (18 x 30 x ¼ in.) gas-metal-arc process |
| 2. | Klein[7,8] | U.S. Navy | Multi-pass welding of butt welds (up to 1 in. thick and twenty passes) in several types of steel (low carbon, HY-80, HY-130, and higher strength steels), GMA |
| 3. | Johnson[9] | USCG | Strain changes during flame heating along a straight line of several steel plates |
| 4. | Hirsch[10] | NASA | Bead-on-plate welding of niobium and tantalum sheets, 0.012 to 0.015 in. thick, gas-tungsten-arc process |
| 5. | Bryan[11,12] | NASA | Bead-on-plate and butt welds in 6061-T6 aluminum alloy plates ¼ in. thick, GMA |
| 6. | Yamamoto[13,14] | NSF,WRC, and a group of Japanese companies | Welding along the longitudinal edge of rectangular plates, ½ in. thick, GMA and GTA |
| 7. | Serotta[15] | NSF,WRC, and a group of Japanese companies | Longitudinal distortion during welding along the longitudinal edge of rectangular plates and welding T joints, steel and aluminum |

TABLE I-A

| | | | |
|---|---|---|---|
| 8. | Hwang[16] | A group of Japanese Companies | Welding along the longitudinal edge of rectangular plates in low carbon steel, quenched and tempered steels, stainless steel, and a titanium alloy |
| 9. | Nishida[17] | NSF,WRC, and a group of Japanese companies | Several methods for calculating thermal stresses and metal movement during welding were revised. Analytical results were compared with experimental data |
| 10. | Schrodt[18] | U.S. Navy | Strain response of high restraint slit-type welds during welding of HY-130 |
| 11. | Lipsey[19] | U.S. Navy | Thermal strains in high strength quenched and tempered steels. Multi-pass butt welds in 1 in. thick HY-130 |

TABLE I-A (Continued)

# CHAPTER II

## MATERIAL CONSIDERATIONS

### II.A GENERAL:

The Office of Naval Research is sponsoring an ongoing program to investigate thermal stresses and distortion in high strength steel (HY-130) structures. HY-130 steel is a high quality, low carbon, quenched and tempered steel with a yield strength of 130-150 ksi. This material was produced by the United States Steel Company, primarily for use by the U.S. Navy.

### II.B COMPOSITION:

Acceptable ranges of chemical composition for HY-130 steel are shown in Table II-A. These ranges, reported by Shackleton,[20] are compositional limits of HY-130 steel as received for production.

Mechanical properties of HY-130 steel in the "as received" quenched and tempered condition, as reported by Schrodt,[21] are:

| | |
|---|---|
| Yield Strength: | 130-145 ksi |
| Elongation in 2 inches: | 15% |
| Reduction of Area: | 50% minimum transverse<br>70% through thickness |
| Impact requirements: | 60 ft-lbf at $0^{\circ}$ F |

A Rockwell hardness test conducted on the material to be used in this experimental study yielded a Rockwell "C" Scale Hardness of 32.

COMPOSITIONAL RANGES OF HY-130 STEEL (%)[20]

| | |
|---|---|
| C | 0.08 - 0.12 |
| Mn | 0.60 - 0.90 |
| Si | 0.20 - 0.35 |
| Ni | 4.75 - 5.25 |
| Cr | 0.40 - 0.70 |
| Mo | 0.30 - 0.65 |
| V | 0.05 - 0.10 |
| S | 0.015 Max |
| P | 0.010 Max |
| Ti | 0.020 Max |
| Cu | 0.25 Max |

TABLE II-A

## II.C TEMPERATURE DEPENDENCE OF MATERIAL PROPERTIES:

Subroutines within the axisymmetric finite element program developed by Muraki for analysis of thermal stresses and metal movement during welding require that material properties be specified as a function of temperature. A search of the literature failed to produce detailed temperature relationships among the various material properties required by the Muraki program for HY-130 at elevated temperatures. Graphical presentation of these relationships reported by Schrodt[21] are reproduced in Figures II-1 through II-10. A tabular summary of this information is included as Tables II-B and II-C.

The Muraki program which is to be verified by experimental data assumes a linear relationship between various material properties and temperature. Assumed linear relationships which served as input data to the Muraki program are indicated by a dashed line on the appropriate figures.

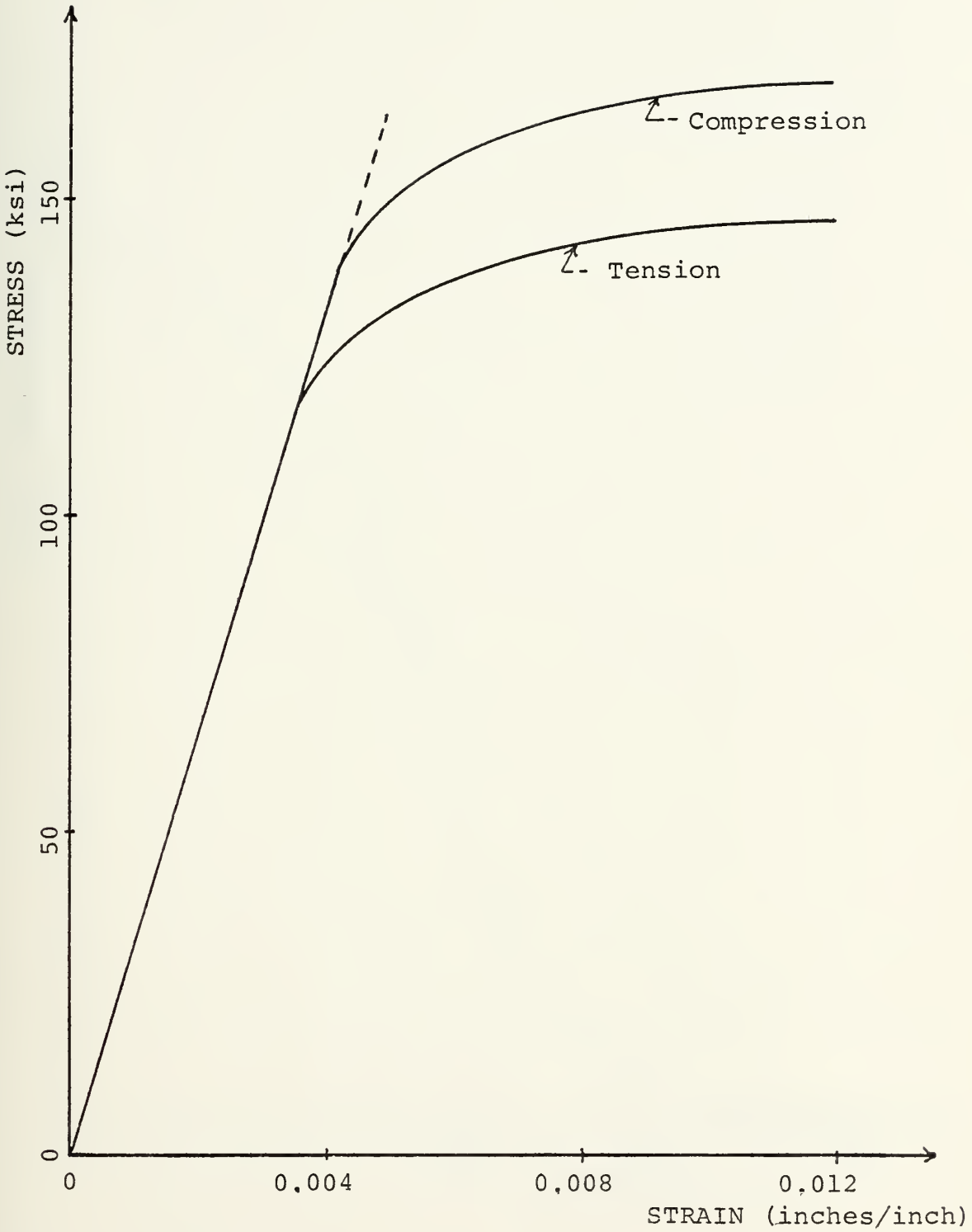


FIGURE II-1 TYPICAL STRESS-STRAIN DIAGRAM FOR HY-130 AT ROOM TEMPERATURE

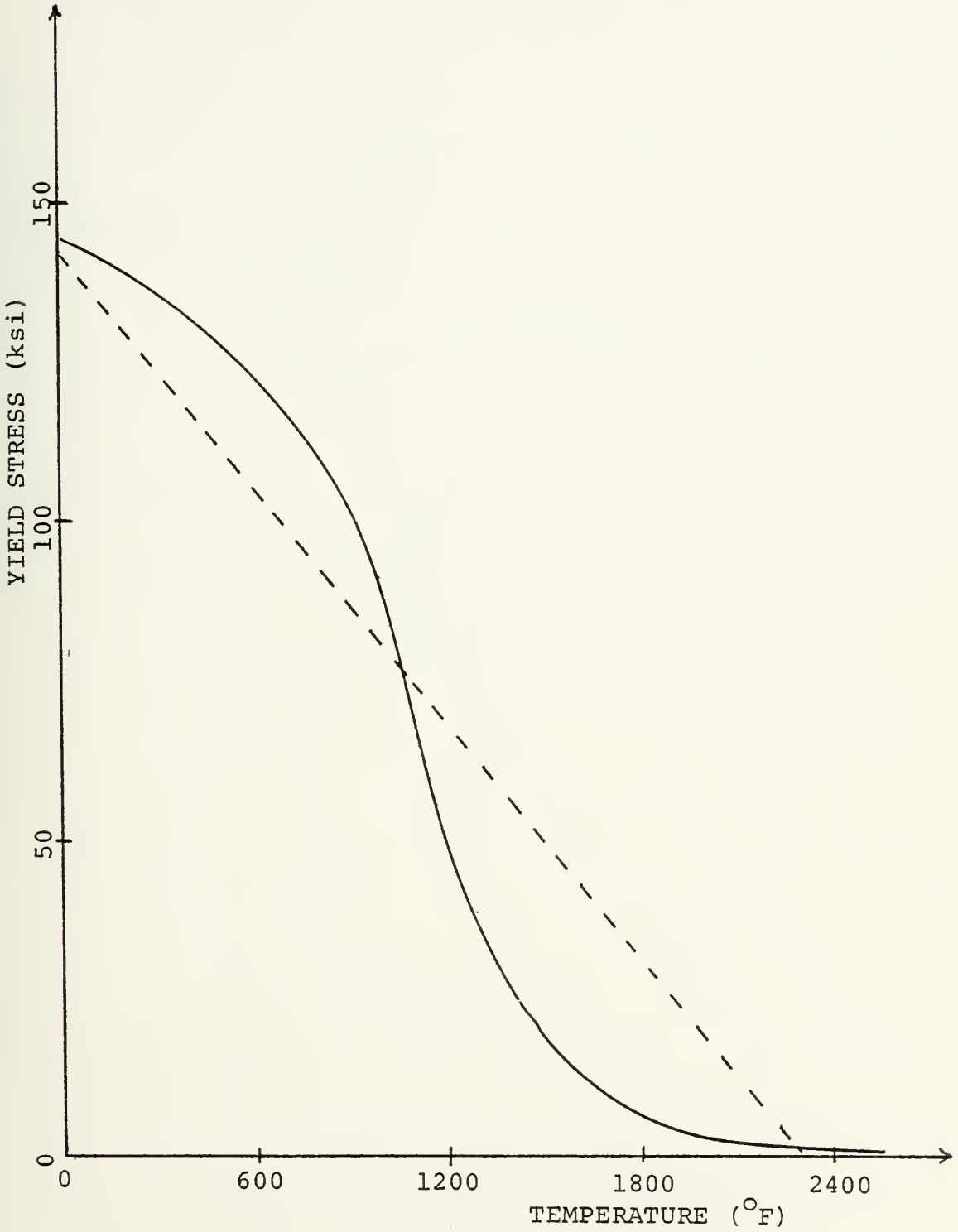


FIGURE II-2 ESTIMATED EFFECT OF TEMPERATURE ON 0.2% OFFSET YIELD STRESS FOR HY-130

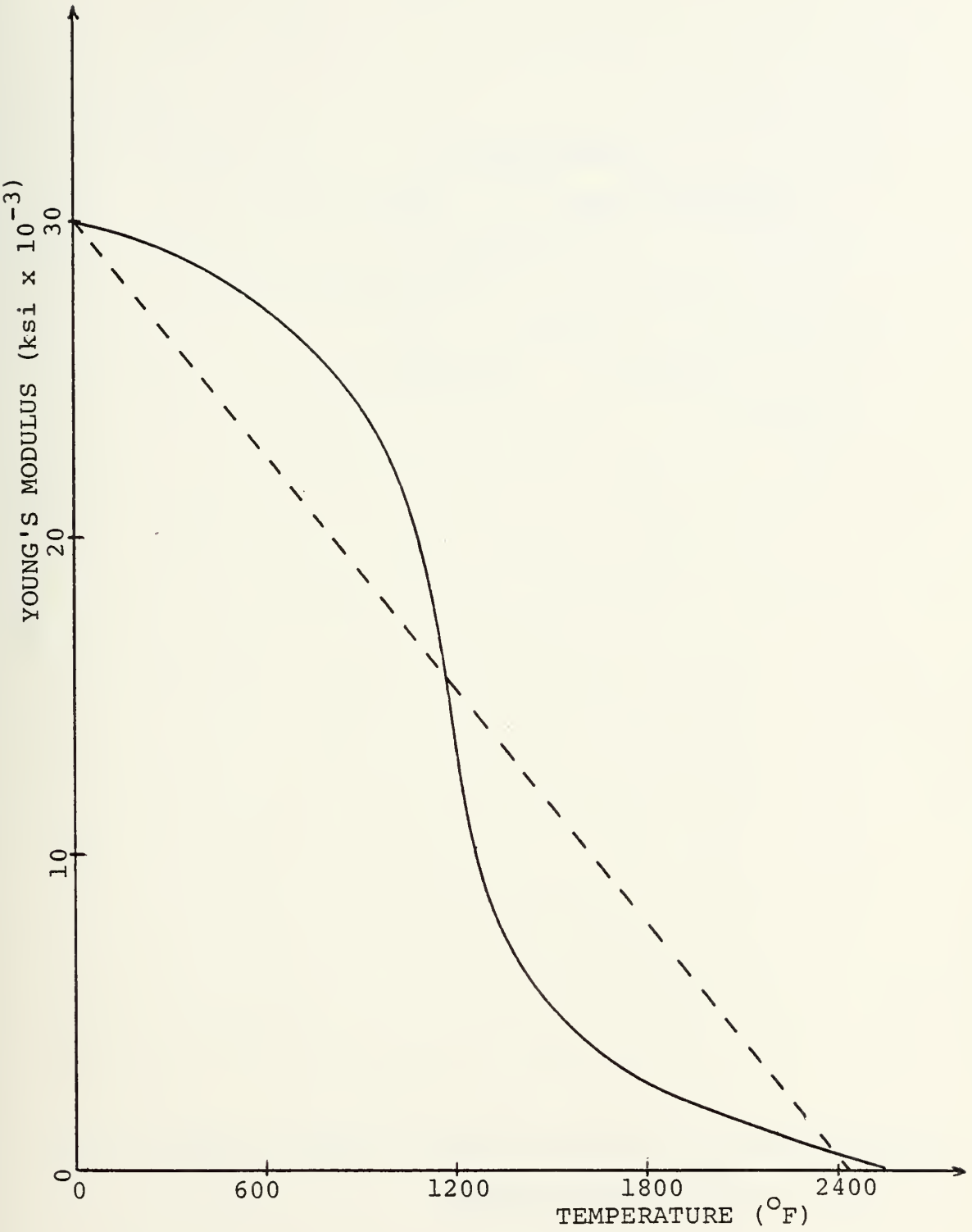


FIGURE II-3 ESTIMATED EFFECT OF TEMPERATURE ON YOUNG's MODULUS FOR HY-130

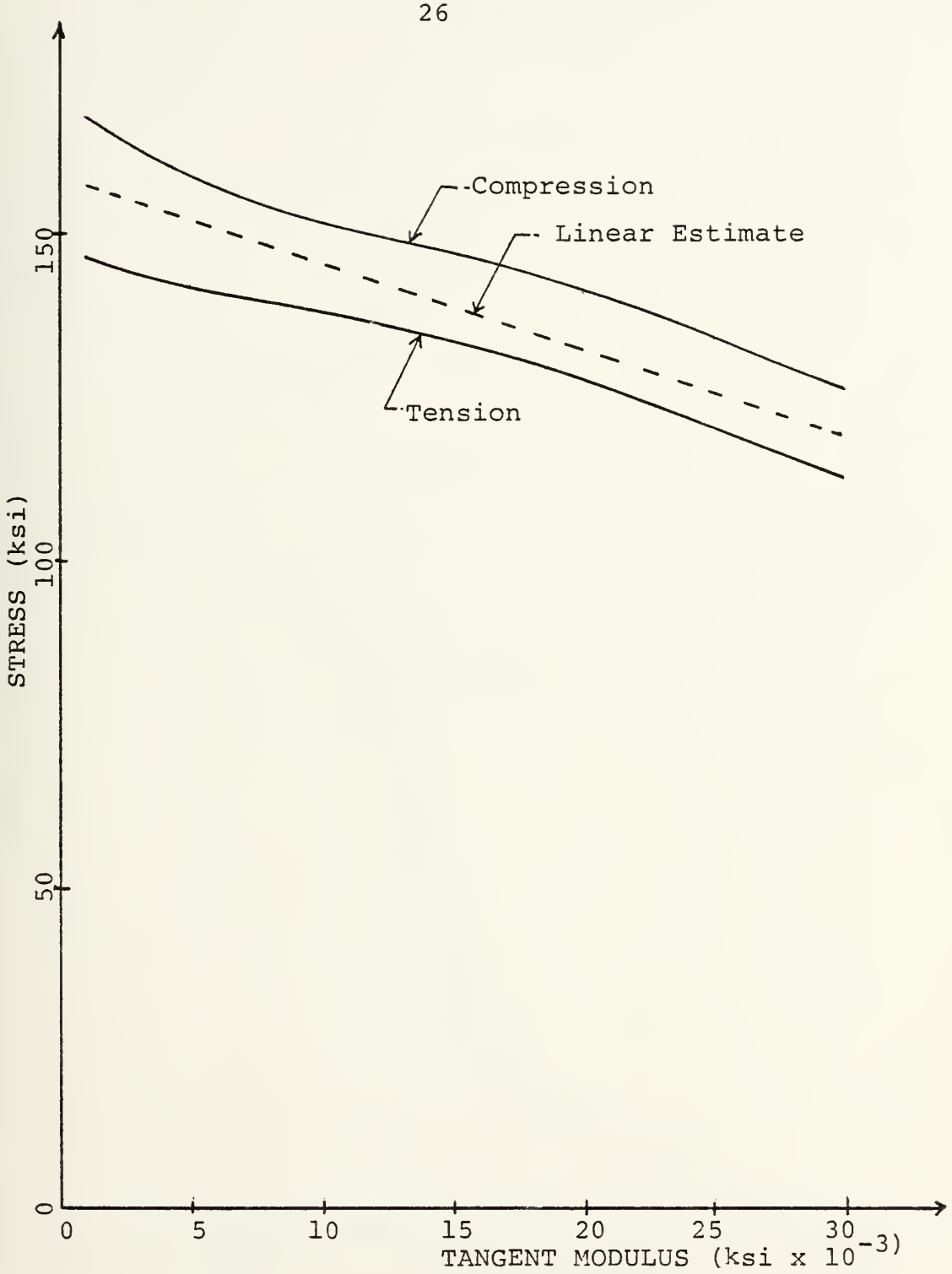


FIGURE II-4 TANGENT MODULUS CURVES FOR HY-130

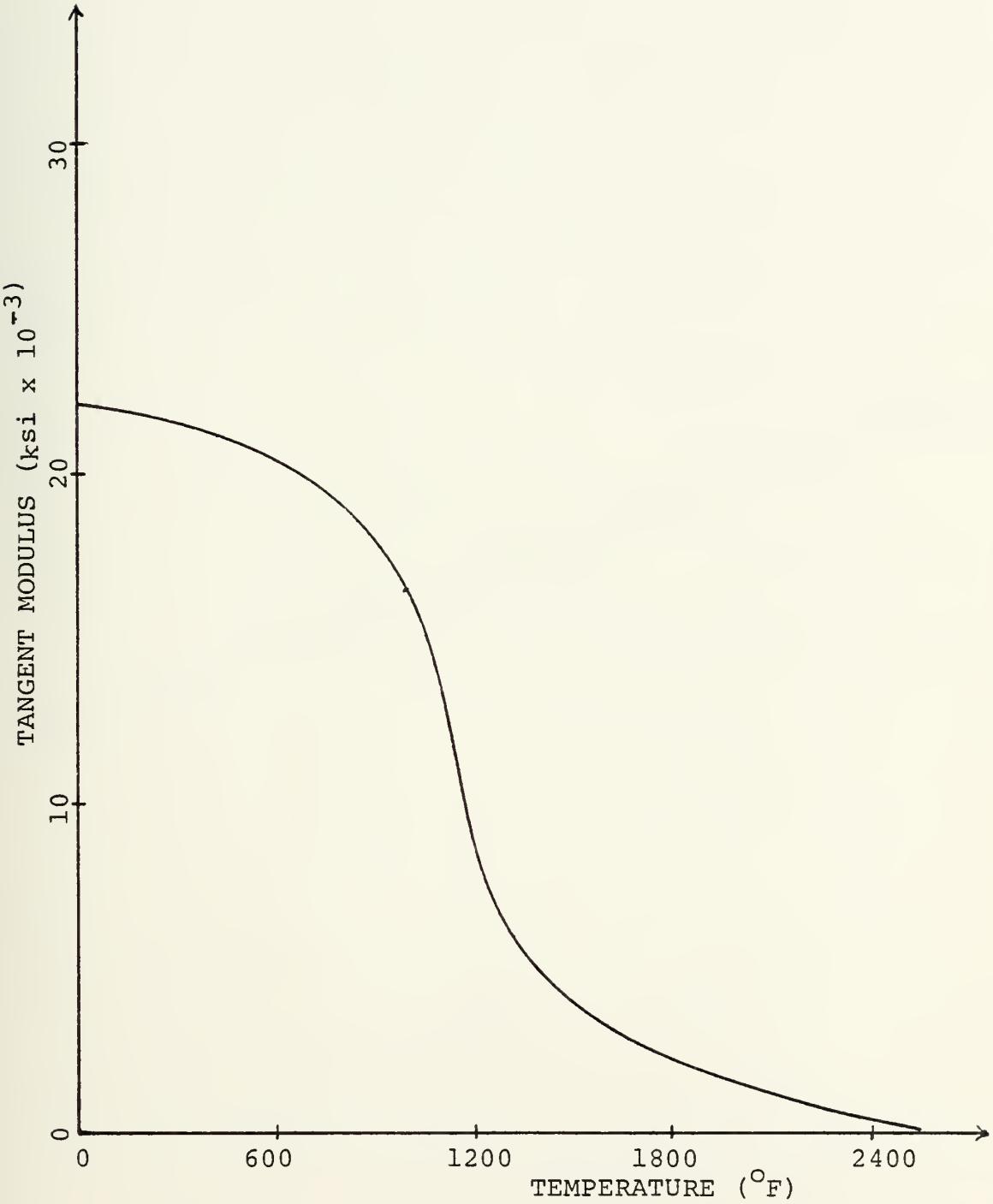


FIGURE II-5 ESTIMATED EFFECT OF TEMPERATURE ON TANGENT MODULUS FOR HY-130

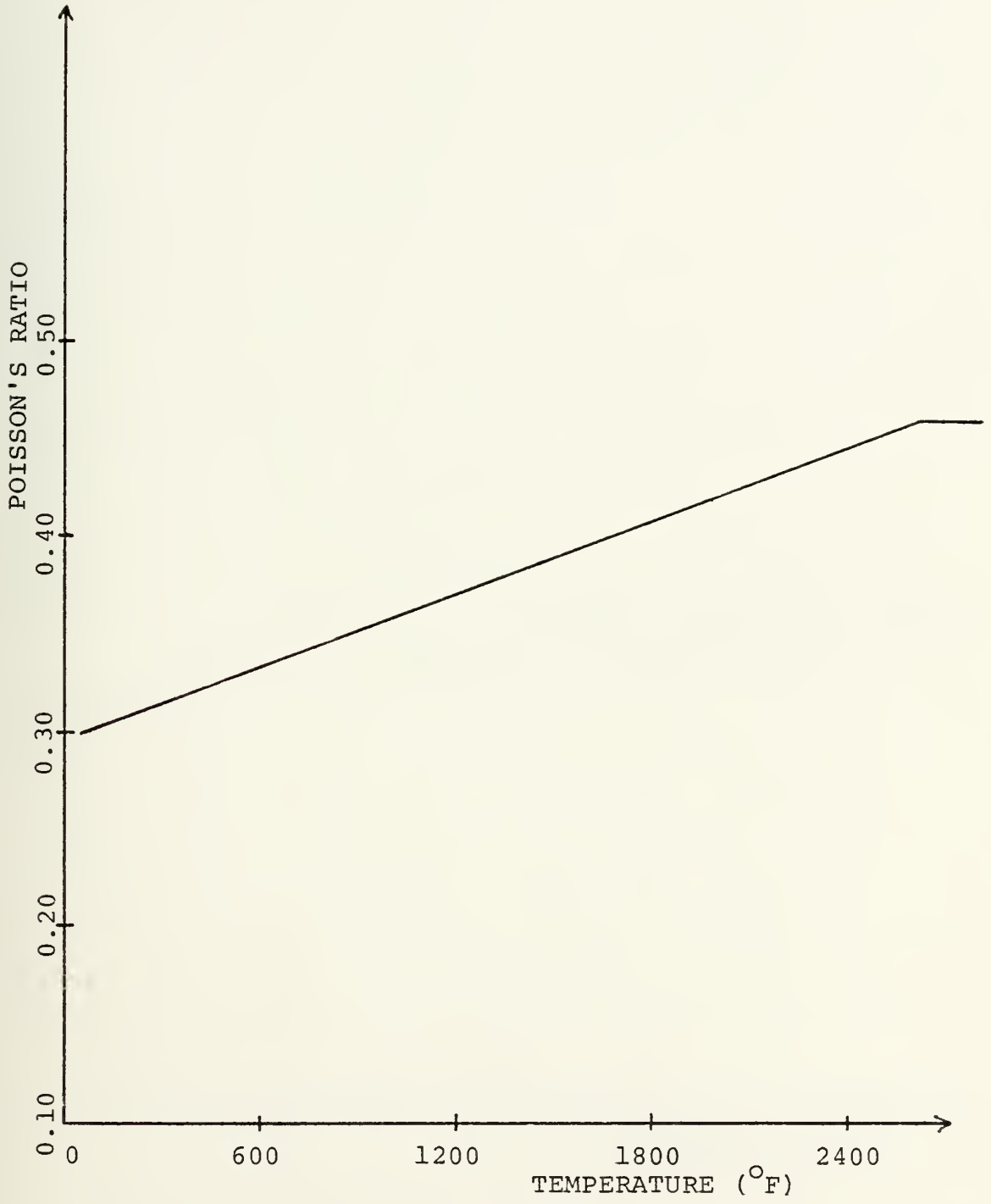


FIGURE II-6 ESTIMATED EFFECT OF TEMPERATURE ON POISSON'S RATIO FOR HY-130

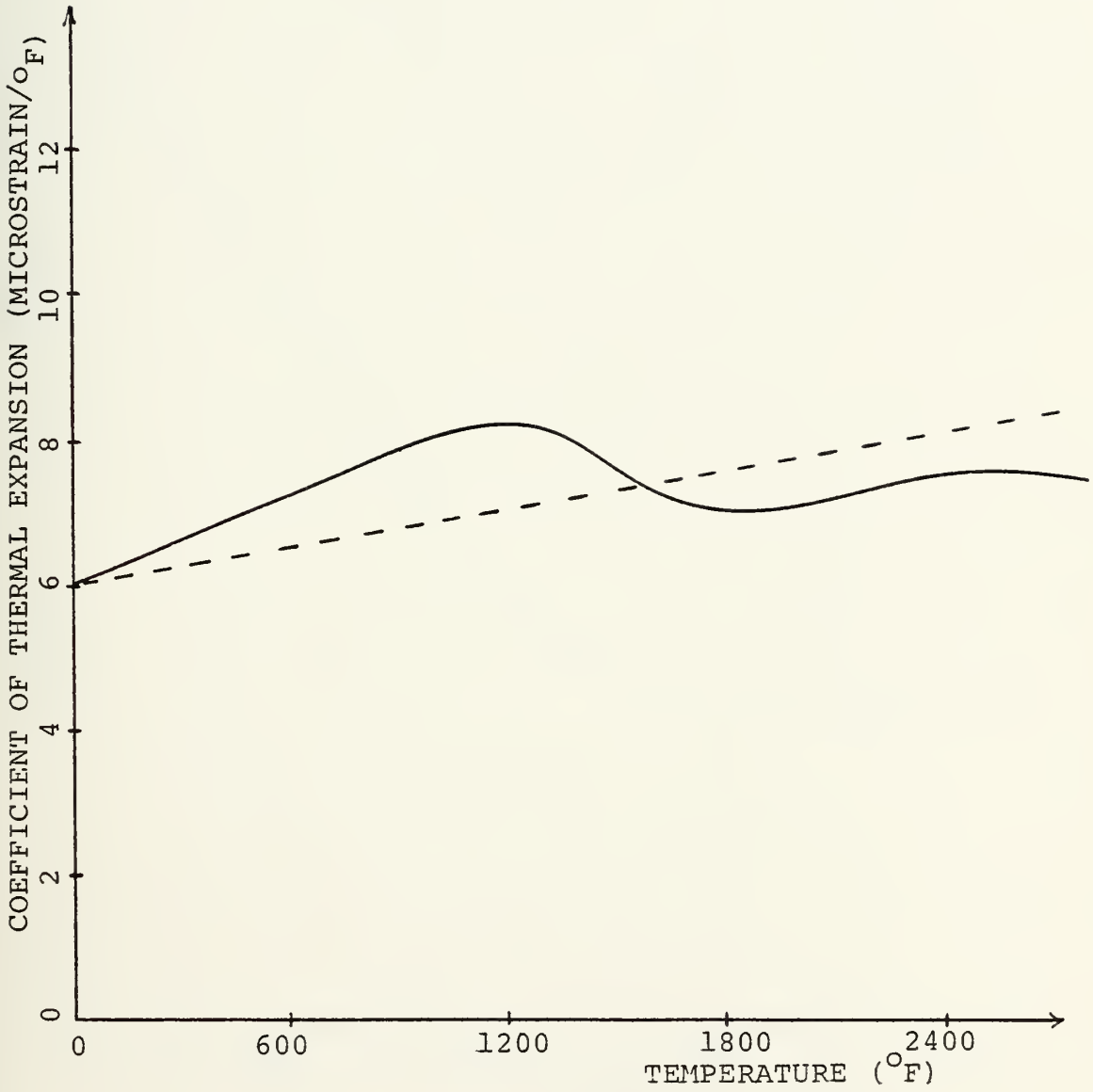


FIGURE II-7 ESTIMATED COEFFICIENT OF THERMAL EXPANSION FOR HY-130

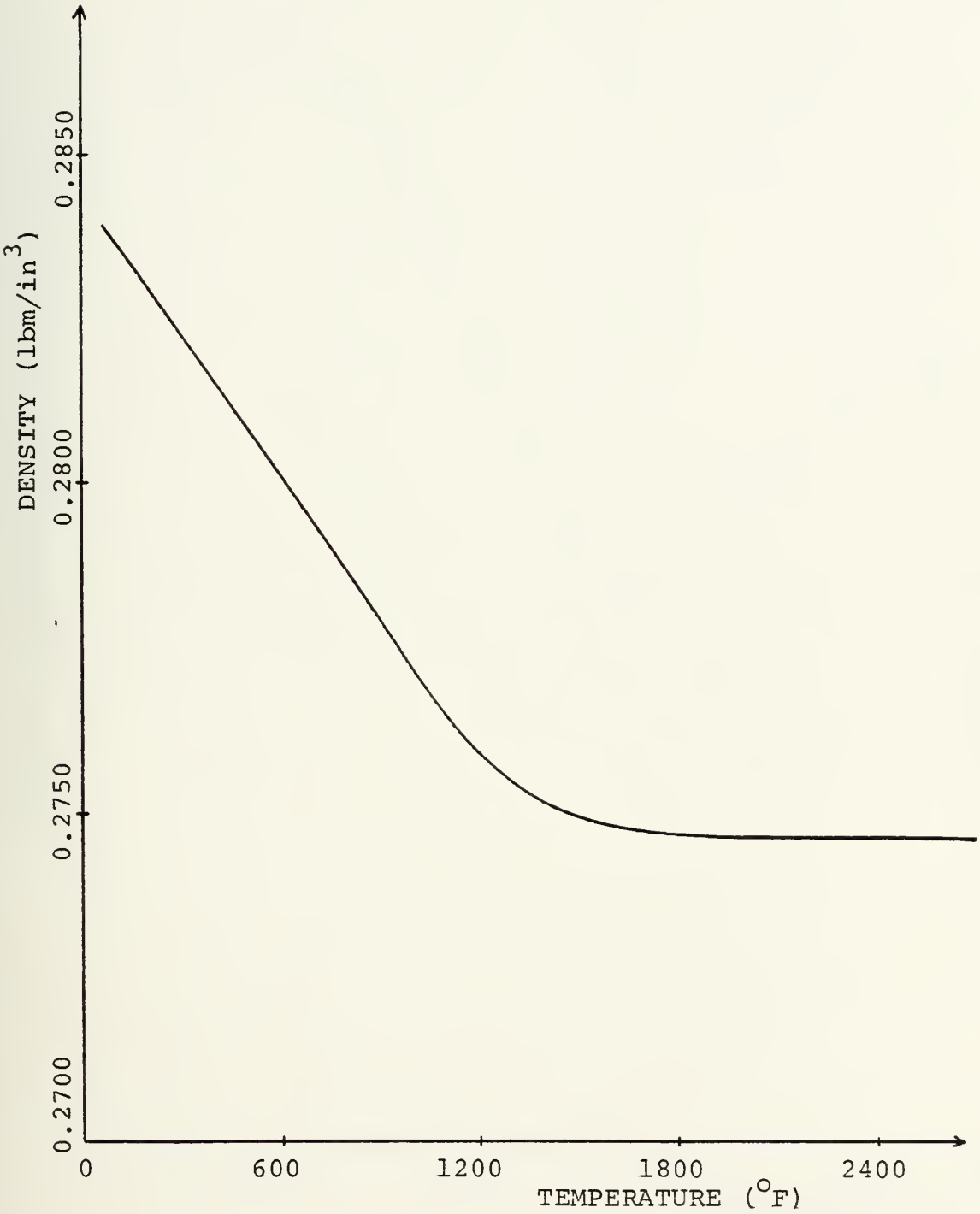


FIGURE II-8 EFFECT OF TEMPERATURE ON DENSITY OF HY-130


FIGURE II-9 ESTIMATED EFFECT OF TEMPERATURE ON THERMAL CONDUCTIVITY OF HY-130


FIGURE II-10 ESTIMATED EFFECT OF TEMPERATURE ON SPECIFIC HEAT OF HY-130

SUMMARY OF MECHANICAL PROPERTIES

FOR HY-130 STEEL

| TEMPERATURE ($^{o}$F) | $\sigma$ | E | H | $\nu$ |
|---|---|---|---|---|
| 68 | 143 | 30 | 22.2 | .30 |
| 200 | 138 | 29.6 | 21.8 | .308 |
| 400 | 131.5 | 28.8 | 21.2 | .321 |
| 600 | 122 | 27.7 | 20.5 | .334 |
| 800 | 110 | 26 | 19.2 | .346 |
| 1000 | 88 | 22.7 | 17.0 | .359 |
| 1200 | 50 | 14.0 | 9.2 | .372 |
| 1400 | 25,5 | 5.0 | 4.9 | .384 |
| 1600 | 11.2 | 4.0 | 3.1 | .397 |
| 1800 | 6.0 | 3.0 | 2.2 | .410 |
| 2000 | 4.0 | 2.0 | 1.5 | .422 |
| 2200 | 2.0 | 1.2 | .8 | .435 |
| 2400 | 1.0 | .4 | .4 | .447 |
| 2500 | 0 | 0 | 0 | .454 |

$\sigma$ = Yield Stress 2% Offset (ksi)

E = Elastic Modulus (ksi x $10^{-3}$)

H = Tangent Modulus (ksi x $10^{-3}$)

$\nu$ = Poisson's Ratio

TABLE II-B

## SUMMARY OF PHYSICAL PROPERTIES

## FOR HY-130 STEEL

| TEMPERATURE (°F) | $\rho$ | $\alpha_T$ | C | $\kappa$ |
|---|---|---|---|---|
| 68 | 0.284 | 6.1 | 19.4 | 0.107 |
| 200 | 0.283 | 6.5 | 20.4 | 0.11 |
| 400 | 0.282 | 6.95 | 21.5 | 0.118 |
| 600 | 0.280 | 7.3 | 21.8 | 0.126 |
| 800 | 0.279 | 7.7 | 21.2 | 0.136 |
| 1000 | 0.278 | 8.0 | 19.5 | 0.148 |
| 1200 | 0.276 | 8.3 | 17.1 | 0.168 |
| 1400 | 0.275 | 8.18 | 15.0 | 0.197 |
| 1600 | 0.275 | 7.05 | 13.4 | 0.255 |
| 1660 | 0.275 | 6.92 | 13.1 | 0.293 |
| 1800 | 0.275 | 7.0 | 14.0 | 0.18 |
| 2000 | 0.275 | 7.2 | 15.0 | 0.158 |
| 2200 | 0.275 | 7.3 | 16.0 | 0.158 |
| 2400 | 0.275 | 7.4 | 16.7 | 0.158 |
| 2600 | 0.275 | 7.5 | 17.0 | 0.158 |
| 2800 | 0.275 | 7.5 | 7.0 | 0.18 |

$\rho$ = Density (lbm/in$^3$)

$\alpha_T$ = Coefficient of Thermal Expansion (microstrain/$^oF$)

C = Thermal Conductivity (BTU/hr ft $^oF$)

$\kappa$ = Specific Heat (BTU/lbm $^oF$)

TABLE II-C

# CHAPTER III

## DESCRIPTION OF EXPERIMENTAL PROCEDURE

### III.A FABRICATION OF THE WELD SPECIMEN:

A circular cylinder of high strength steel was formed in order to test the MIT computer program for the analysis of heat flow in a weldment, with subsequent use of the temperature distributions from the heat flow program to validate the Muraki axisymmetric finite element program for analysis of thermal stress and metal movement during welding. The HY-130 circular cylinder was formed to dimensions suggested in the June 1977 proposal on Study of Residual Stresses and Distortion in Structural Weldments in High Strength Steels. This research proposal was made from Massachusetts Institute of Technology to the Office of Naval Research.

Material for forming the cylinder was obtained from the Naval Ship Research and Development Center, Annapolis Laboratory, Annapolis, Maryland. The material was received at Massachusetts Institute of Technology Welding Laboratory in the form of HY-130 plates 60" x 63" x 3/4". A request was made to Portsmouth Naval Shipyard in Portsmouth, New Hampshire, to roll the HY-130 plates into cylindrical shapes; Portsmouth Naval Shipyard being the only industrial activity in the vicinity of MIT with experience in forming HY-130. Detailed drawings and specific requirements were submitted to Portsmouth

Naval Shipyard and an agreement was reached for the shipyard to form the plates into cylinders. However, due to the thickness (3/4") of the plate to be formed to a small outside diameter (18"), Portsmouth Naval Shipyard engineers suggested that it would be necessary to form a cylinder by bending two plates to semi-circular cylindrical shapes and then welding the two halves together. In view of this requirement and in order to facilitate easier handling of the HY-130 plates, the two plates were flame cut to four plates 60" x 31½" x 3/4" at the MIT Welding Laboratory prior to transporting to Portsmouth, New Hampshire.

Stages of cylinder fabrication are depicted in Figures III-1 and III-2. In order to prevent heat resulting from the flame cutting operation from affecting thermal properties of the steel close to the proposed weld, Tsai[22] suggested that flats required for bending be removed by flame cutting no closer than ¼" to the proposed leading edges of the semi-circular cylindrical mating surfaces. The flats were removed in this manner and remaining material to be removed in order to form a $60^{\circ}$ Vee groove with 1/8" root, as illustrated in Figure III-2, was removed by mechanical grinding. The semi-circular cylinders were then transported back to the MIT Welding Laboratory for experimental welding.

STAGES OF CYLINDER FABRICATION

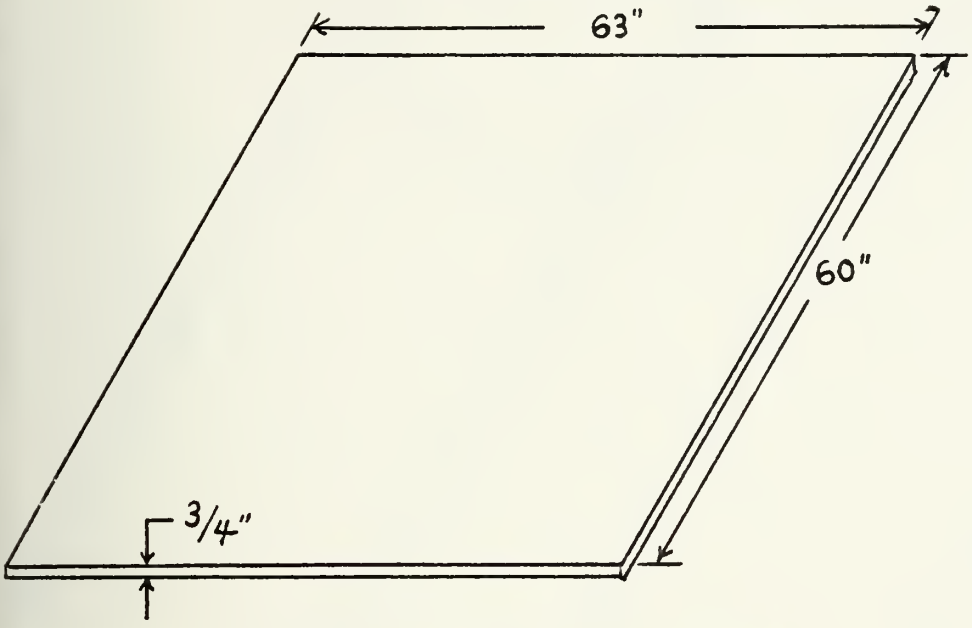


Stage 1 - HY-130 plate with dimensions shown.

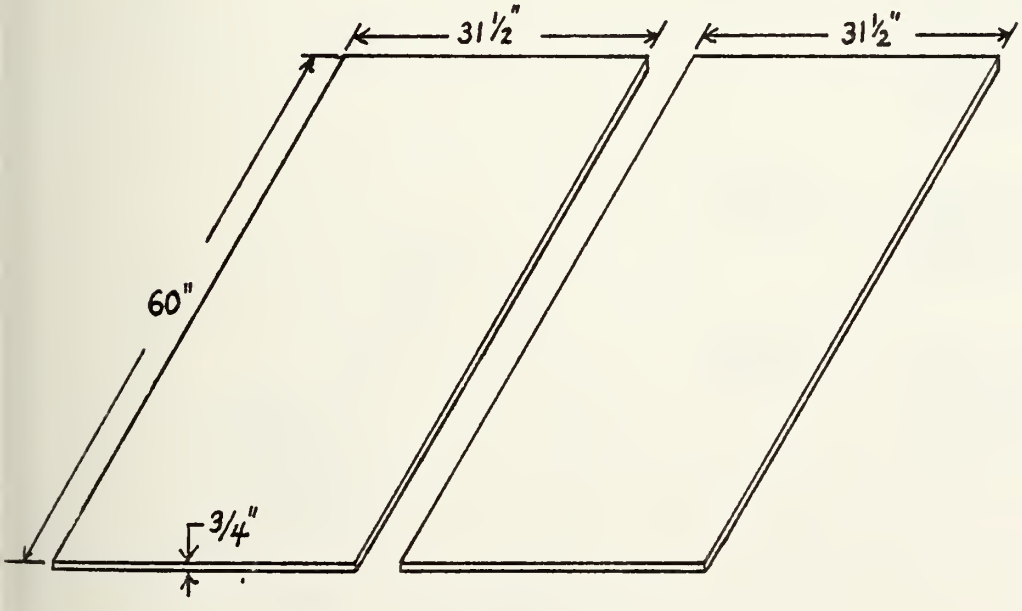


Stage 2 - Plate flame cut to dimensions shown

FIGURE III-1

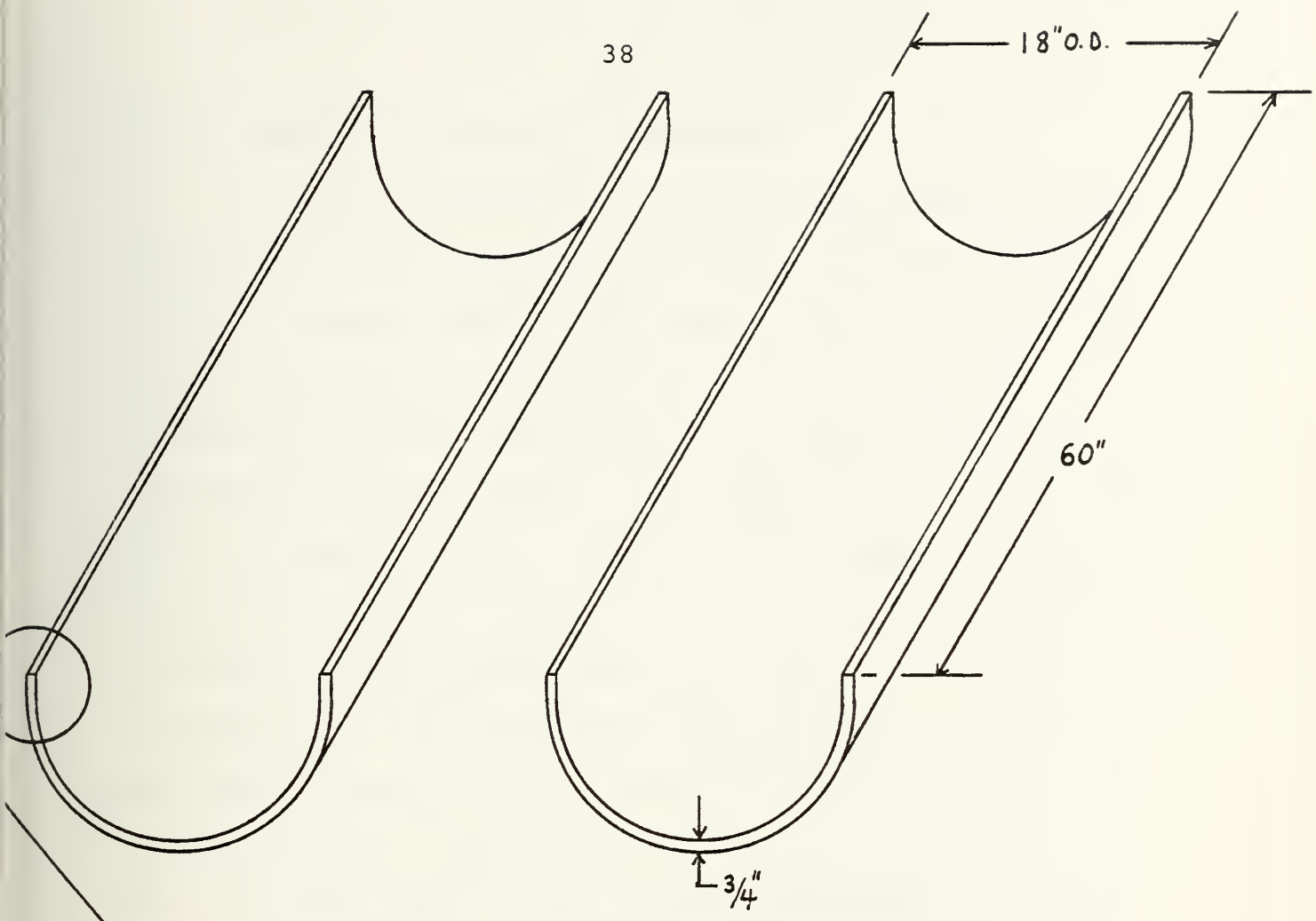


Stage 3 - Plate halves rolled to semi-circular cylindrical shapes with flats approximately 1 3/4" remaining on leading edges.

Stage 4 - Flats removed by flame cutting no closer than 1/4" to mating edges of semi-cylinders.

Stage 5 - 1/4" excess material removed from mating edges of semi-cylinders and 30° angle produced by mechanical grinding.

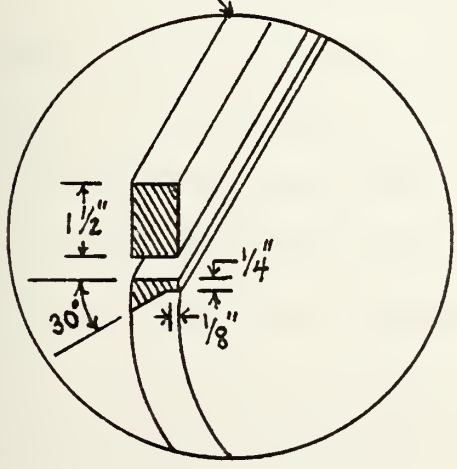


FIGURE III-2

## III.B SELECTION OF WELDING CONSUMABLES:

The type of welding suggested in the research proposal for girth welding of cylindrical shells was multi-pass gas metal arc welding (GMAW). This type of welding requires the use of shielding gas and filler wire, both of which can significantly affect weld quality. The most common type of shielding gas used in GMAW of low carbon steel is Argon with 25% $CO_2$. However, in the case of HY-130, experience has shown that the use of Argon with 25% $CO_2$ leads to inadequate fracture toughness properties in the weld deposit. Shackleton[20] recommends rich Argon with less than 5% Oxygen or 10% $CO_2$ to avoid deterioration in the fracture toughness properties of the weld deposit caused by Oxygen pickup from the shielding gas. Shielding gas selected and purchased for this experiment was Argon with 1% $O_2$. This gas was reported by Radziminski[23] as the gas most effective in shielding HY-130 welds.

Filler wire selected for the HY-130 cylindrical seam and girth welds was 1/16" diameter Linde 140S wire. This wire was developed by Union Carbide specifically for HY-130 weldments and was unanimously endorsed in the literature. During periods when the filler wire was not in use, it was stored in a drying oven containing desiccative material. This step was viewed as necessary in order to prevent moisture or other impurities, or oxides, from collecting on the wire surface.

III.C SELECTION OF WELDING PARAMETERS:

1. The variations in weldment geometry which could be considered for this experiment were somewhat restricted by the fact that cylinder size required that the weld be made only from the outside. Based upon several previous welding experiments reported by Doty[24] and the above mentioned restriction, a single 60° Vee groove was selected as near optimum for producing the seam and girth welds of the cylinder. Weld joint geometry for this experiment is depicted below in Figure III-3.

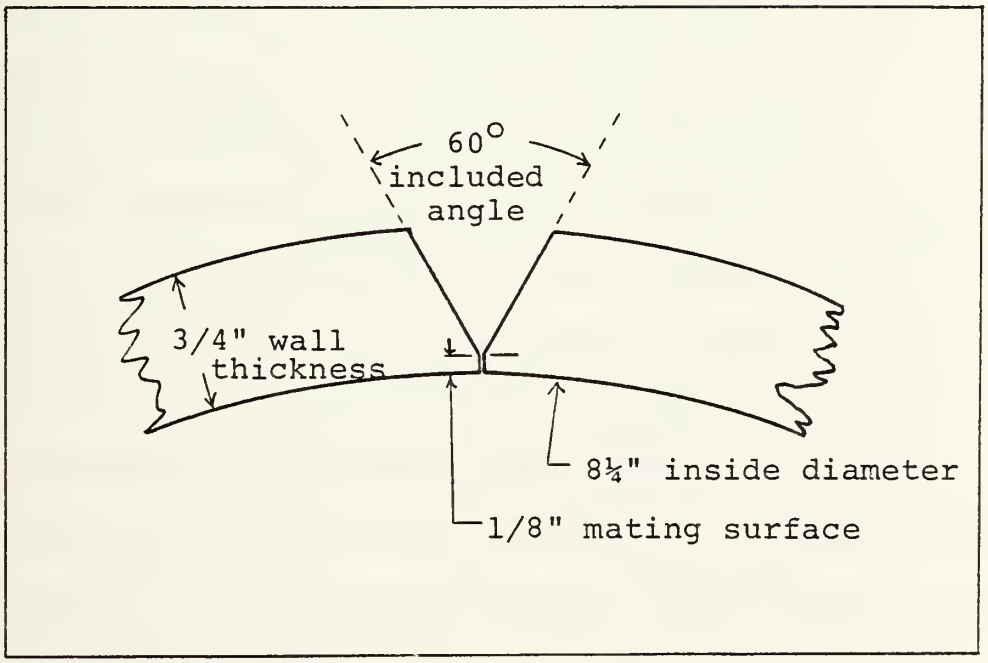


FIGURE III-3 WELD JOINT GEOMETRY FOR PRODUCING SEAM WELDS ON HY-130 CYLINDER

2. For the purposes of this study, heat input (Q) is defined in the conventional way as the product of arc voltage and welding current divided by arc travel speed, as expressed below in Equation 3-1:

$$\text{HEAT INPUT} = Q = \frac{V \times I}{v} \qquad \text{(Equation 3-1)}$$

There were some variations in welding literature regarding the upper level of heat input which would produce a good quality weld in 3/4" HY-130 steel. Shackleton[20] recommended a maximum heat input of 40,000 Joules/inch. This upper limit was also recommended by Nunez[25] and Conner.[26] Radziminski[23] recommended a maximum of 45,000 Joules/inch. Although there was some variation in the suggested upper limits of heat input, there seemed to be general agreement that 40,000 Joules/inch was a reasonable value for the production of good quality welds and this value was selected for production of the seam and girth welds on the HY-130 cylinder. Maximum and minimum allowable values of pre-heat and interpass temperature were also discussed in the above quoted references; general recommendations were more varied, but based on a rough average of recommended values, a common pre-heat and interpass temperature of 200 $^{o}$F was selected.

3. Filler wire feed rate is automatically controlled by the GMAW welding machine. A wire feed rate of approximately 87 inches/minute of the 1/16" Linde 140S filler wire

was measured during the production of a seam weld. The flow meter for the Argon/1% $O_2$ shielding gas was set at 40 $ft^3$/hr. A summary of welding parameters which remained unchanged during the course of this experiment is shown in Table III-A below. The only parameters which were varied between welding passes were the arc voltage, welding current, and in one instance the arc travel speed. Voltage, current, and arc travel speed were recorded for each pass and are included in the presentation of results.

| WELDING PARAMETERS | |
|---|---|
| JOINT GEOMETRY ..... | $60^{\circ}$ Single V Groove |
| MAXIMUM HEAT INPUT ..... | 40,000 Joules/in |
| FILLER WIRE ..... | 1/16" Diameter Linde 140S |
| feed rate - | 87 in/min |
| SHIELDING GAS ..... | Argon/1% $O_2$ |
| flow rate - | 40 $ft^3$/hr |

TABLE III-A

III.D ARRANGEMENT OF APPARATUS:

Welding equipment used for the entire experiment consisted of a Linde SVI-300 Power Supply with ST-2 Torch and associated arc travel and wire feed mechanisms. Seam welds were produced by placing the cylinder on an adjustable welding table and moving the welding torch along the groove of the seam weld. Prior to positioning the cylinder on the welding table, the two cylinder halves were tack welded at positions 6" from either end and at the center with 1" welds on the inside of each mating edge. Positions of the cylinder and welding torch for production of a seam weld are depicted in the photograph, Figure III-4, below.

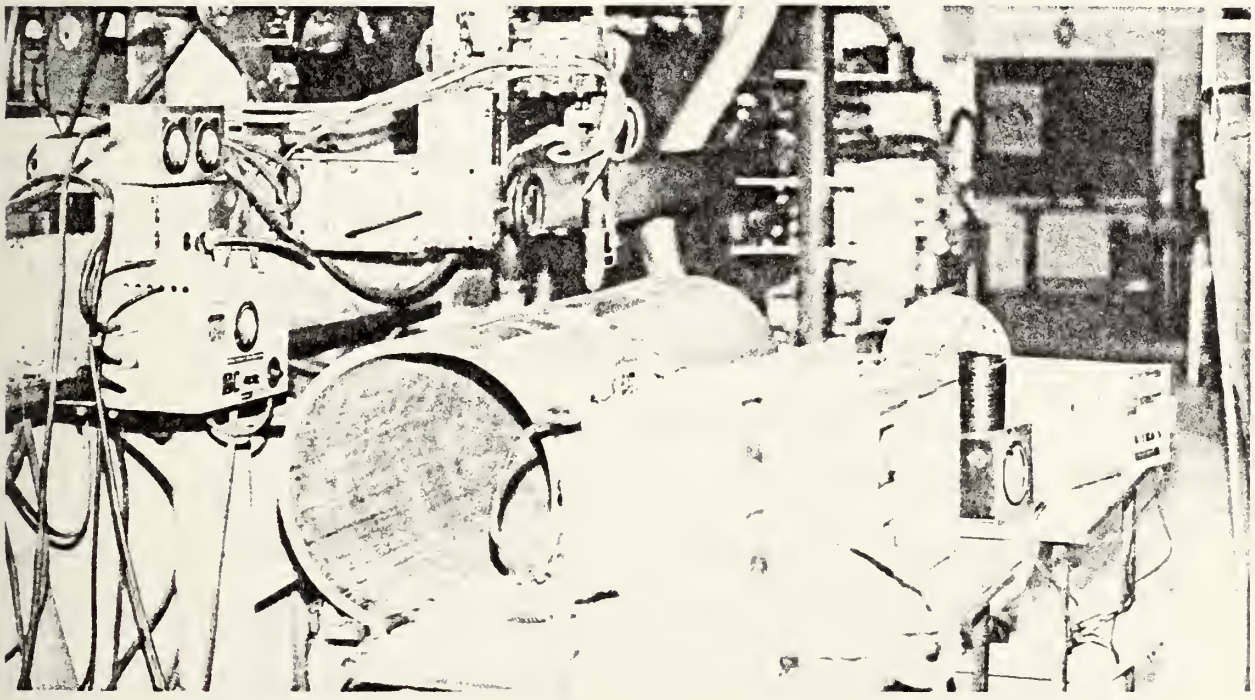

FIGURE III-4 POSITION OF CYLINDER AND WELDING TORCH FOR PRODUCTION OF SEAM WELD

III.E TESTING OF WELDING EQUIPMENT:

In order to determine approximate temperature distributions during actual welding and to facilitate a thorough checkout of welding equipment prior to welding passes for data gathering, it was deemed advantageous to produce a seam weld on one side of the cylinder without benefit of instrumentation to record temperature and strain. This allowed the wire feed mechanism, arc travel controls and indicators, gas flow regulators and meters, and the welding equipment electrical circuity and instrumentation to be tested and checked for accuracy under conditions expected during the actual test. This "test run" also provided an opportunity for operator training. A preliminary checkout of welding equipment had been conducted using "bead-on-plate" welds on scrap pieces of HY-130.

Approximate temperature distributions to be expected during the instrumented test were determined by the application of temperature indicating liquid (TEMPILAQ) in narrow bands transverse to the welding direction. TEMPILAQ liquids corresponding to temperature levels of 400 $^{o}$F, 600 $^{o}$F, 800 $^{o}$F, 1000 $^{o}$F, and 1100 $^{o}$F were applied to the chemically cleaned inner and outer surfaces of the cylinder. TEMPILAQ was reapplied between passes and distances of temperature penetration from the weld centerline on both the inside and outside

of the cylinder were recorded for each welding pass. Welding current, arc voltage, arc travel speed, and maximum distances from the weld centerline for the various TEMPILAQ levels were recorded for each welding pass and are shown in Table III-B. This tabulated data was used as a basis for determining strain gage and thermocouple locations for the instrumented seam and girth welds to be used in validating heat flow and thermal stress computer programs.

| WELDING PASS | | * TEMPERATURE PENETRATION DISTANCE | | | | |
|---|---|---|---|---|---|---|
| | | | OUTSIDE | | INSIDE | |
| | | | LEFT | RIGHT | LEFT | RIGHT |
| 1. I = 260A<br>V = 23V<br>v = 12 in/min | | 400F | .86 | - | .94 | .88 |
| | | 600F | - | - | .63 | .60 |
| | | 800F | - | - | .44 | .40 |
| | | 1000F | - | - | .38 | .35 |
| | | 1100F | - | - | .25 | .22 |
| 2. I = 260A<br>V = 23V<br>v = 12 in/min | | 400F | .61 | .38 | .69 | .75 |
| | | 600F | - | - | .38 | .56 |
| | | 800F | - | - | .22 | .38 |
| | | 1000F | - | - | .06 | .31 |
| | | 1100F | - | - | - | .19 |
| 3. I = 260A<br>V = 23V<br>v = 12 in/min | | 400F | .80 | - | .88 | .63 |
| | | 600F | - | - | .50 | .38 |
| | | 800F | - | - | .13 | - |
| | | 1000F | - | - | - | - |
| | | 1100F | - | - | - | - |
| 4. I = 260A<br>V = 23V<br>v = 12 in/min | | 400F | - | .92 | .50 | .88 |
| | | 600F | - | .49 | .19 | .50 |
| | | 800F | - | - | - | - |
| | | 1000F | - | - | - | - |
| | | 1100F | - | - | - | - |
| 5. I = 350A<br>V = 22V<br>v = 10 in/min | | 400F | .92 | 1.55 | 1.06 | 1.63 |
| | | 600F | - | .80 | .38 | .75 |
| | | 800F | - | .58 | - | .38 |
| | | 1000F | - | .09 | - | - |
| | | 1100F | - | .03 | - | - |
| 6. I = 330A<br>V = 21V<br>v = 10 in/ min | | 400F | 1.49 | 1.15 | 1.50 | .88 |
| | | 600F | .80 | .75 | .75 | - |
| | | 800F | .55 | - | .25 | - |
| | | 1000F | .49 | - | - | - |
| | | 1100F | .49 | - | - | - |
| 7. I = 350A<br>V = 22V<br>v = 20 in/min | | 400F | .46 | .78 | .38 | .75 |
| | | 600F | - | .40 | - | .13 |
| | | 800F | - | .25 | - | - |
| | | 1000F | - | .03 | - | - |
| | | 1100F | - | - | - | - |
| 8. I = 370A<br>V = 21V<br>v = 20 in/min | | TEMPERATURE PENETRATION DISTANCES NOT RECORDED | | | | |

* Temperature penetration distances are expressed in inches, measured in the direction indicated from the weld centerline.

TABLE III-B

## III.F SELECTION AND ARRANGEMENT OF INSTRUMENTATION TO MEASURE STRESS AND DISTORTION DURING WELDING:

Stresses occurring during the thermal cycles associated with seam and girth welding of the HY-130 cylinder were determined by measuring strains as a function of time (i.e. - location of the strain measurement with respect to the time history of welding arc location) and as a function of distance from the weld centerline. Strains were measured by placing electrical-resistance wire gages on the outside surface of the cylinder. Bi-axial strain gages were placed with one axis aligned with the cylinder axis and welding direction (herein called the longitudinal direction) and the other axis aligned in a direction normal to the welding direction (herein referred to as the transverse direction. Characteristics of the strain gages used for this experiment are shown in Table III-C.

In order to validate the MIT heat flow program, it was necessary to measure the heat distribution within the cylinder. Heat flow and temperature distribution within the HY-130 cylinder was viewed as critical to validation of the Muraki program, inasmuch as strain, stress, and distortion calculations are all based upon temperature distribution data which must be supplied as input to the program. Thermocouples used for measuring temperature distribution were Chromel/Alumel

| STRAIN GAGE CHARACTERISTICS | |
|---|---|
| Type Used: | FAET-12D-12S6(EL) |
| Manufacturer: | BLH Electronics, Inc.<br>Waltham, Massachusetts 02154 |
| Gage Factor: | 2.00 $\pm$ .1% |
| Resistance: | 120 $\pm$ .2 Ohms |
| Grid Length: | 0.125 inches |
| Cement Used: | BLH EPY-500 |

TABLE III-C

Strain indications were corrected for temperature by the following temperature error (apparent strain) equation:

$$EAP = -91.37 + 2.17T - 2.33 \times 10^{-2}T^2 + 5.31 \times 10^{-5}T^3 - 2.40 \times 10^{-8}T^4$$

wires which were peened into small (0.040") indentations drilled into the cylinder outer surface. Thermocouple circuit continuity was assured by the use of an inductive spot welder on the thermocouple connections. After circuit continuity was assured, the thermocouples were protected by the use of sealing cement.

Since longitudinal and transverse strains were to be measured with gages which required temperature correction, it was necessary to place thermocouples in positions which would give temperature-time histories consistent with strain gage locations. Arrangement of strain gages and thermocouples on the HY-130 cylinder outer surface is shown in Figure III-5. Arranging the strain gages and thermocouples in this manner allowed them to be used for measuring strain and temperature distributions during the production of the second seam weld (the first seam weld was made without instrumentation) and then to be used again after the cylinder had been cut into sections and mating edges prepared for a girth weld. Arranging the strain gages and thermocouples at a $45^{o}$ angle with respect to the seam weld and at equidistant locations with respect to each other allowed the strain gages and thermocouples to give strain-temperature distributions which could be adjusted in time so as to be coincident.

ARRANGEMENT OF STRAIN GAGES AND THERMOCOUPLES

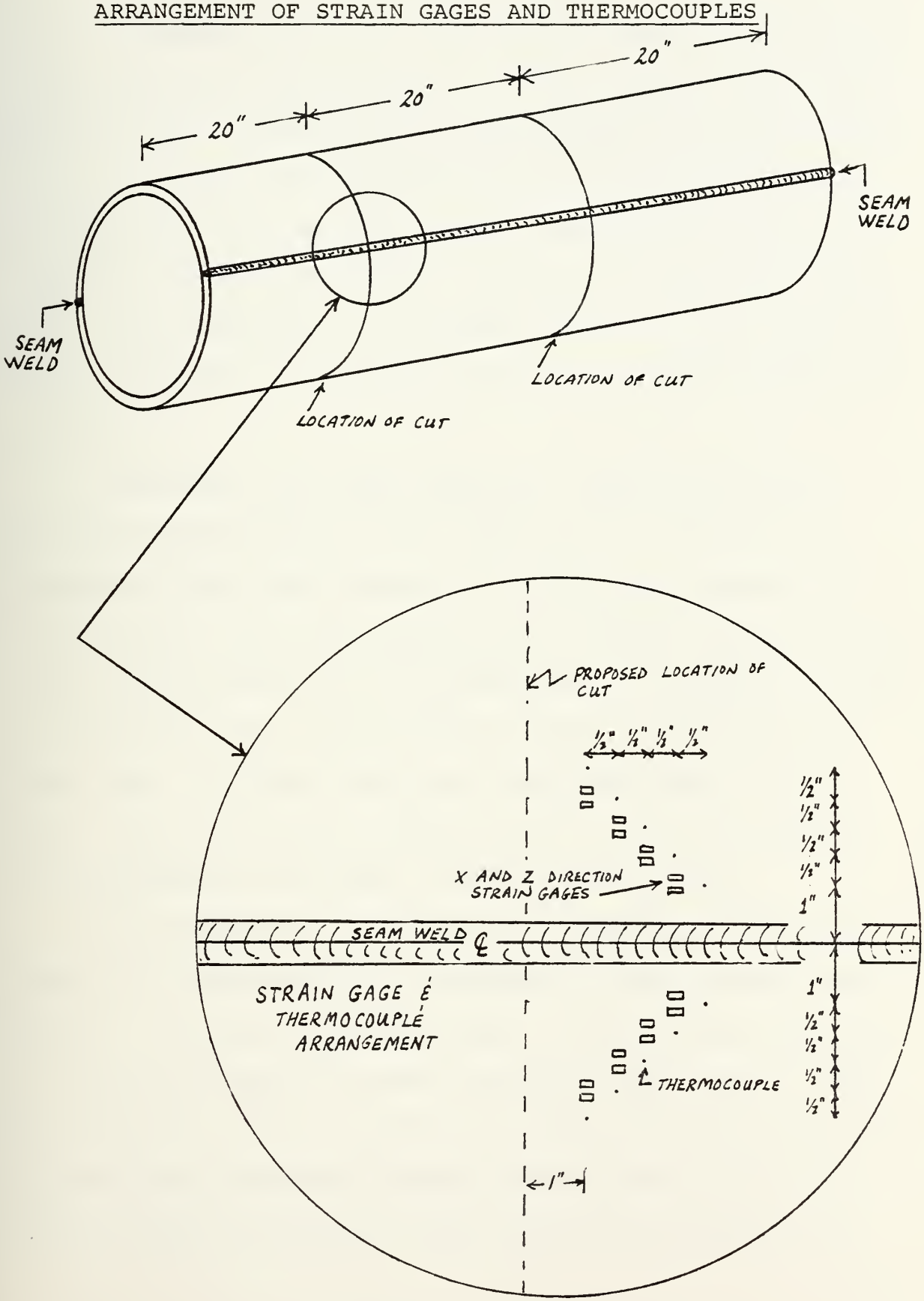


FIGURE III-5

It should be pointed out that the practice of locating strain gages and thermocouples so as to require time adjustment of their readings assumes quasi-steady-state heat flow (i.e. - the heat flow/temperature distribution with respect to the welding arc is the same at a position 40" along the length of the cylinder as at a position 41" along the cylinder). This assumption is necessary in view of the fact that strain gages and thermocouples cannot be located at the same position.

Arranging the strain gages and thermocouples at a $45^{\circ}$ angle with respect to the seam weld was viewed as advantageous since this scheme places the strain gages and thermocouples which were subjected to the most severe thermal cycle during production of the seam weld in a position which is subjected to the least severe thermal cycle during the girth weld. Failures occurring during the seam weld are most likely to occur at locations which are least critical to measurements to be taken during the girth weld.

After determining and marking the desired strain gage locations, strain gages were cemented to the cylinder outer surface. Physical size and weight of the cylinder prevented the usual technique of curing the strain gage bonding cement in laboratory ovens. In order to assure that the strain gage bonding would withstand expected temperatures, a 5 foot by 5 foot thermal insulating blanket (graciously manufactured

for this purpose by Bethlehem Steel Corporation Shipyard in Boston, Massachusetts) was placed around the cylinder and electrical heating elements placed inside. The temperature of the cylinder was slowly raised to 250 $^{o}$F and the strain gage bonding cement was cured at this temperature for a period of four hours, as directed by the strain gage manufacturer's instructions. The heating elements used for this purpose were later used to preheat the cylinder prior to welding.

For production of the girth weld, it was necessary to cut the HY-130 cylinder into sections. Original plans called for cutting the 60 inch cylinder into two 30 inch sections which would have mating edges prepared for a girth weld by machining a 60$^{o}$ single Vee groove. Due to physical limitations of laboratory facilities it was necessary to reduce the length of the two sections to be joined by a girth weld to 20 inches each. This required that the HY-130 cylinder be cut into three sections, each 20 inches in length. This decision was made prior to production of the instrumented seam weld, and the strain gages were placed so as to permit measurements during the seam weld as well as during production of the girth weld.

After completion of the seam weld, the 60 inch long HY-130 cylinder was transported to the Army Materials and Mechanics Research Center in Watertown, Massachusetts, where it was sawed into three sections, each 20 inches in length.

A large power hack saw was used to cut the cylinder into sections. The saw was used on slow speed and the blade and cylinder were continuously cooled by an oil and water cooling mixture during cutting. This procedure was viewed as necessary in order to prevent heat generated by the cutting action from affecting thermal properties of the mating edges to be joined by girth welding.

After the two saw cuts were made, producing the desired three 20 inch long cylindrical sections, a ½ inch thick ring was sawed from the section which would not be used in the girth weld; again paying particular attention to preventing heat buildup in the material being sawed. A diagram of the resulting sections appears below as Figure III-6.

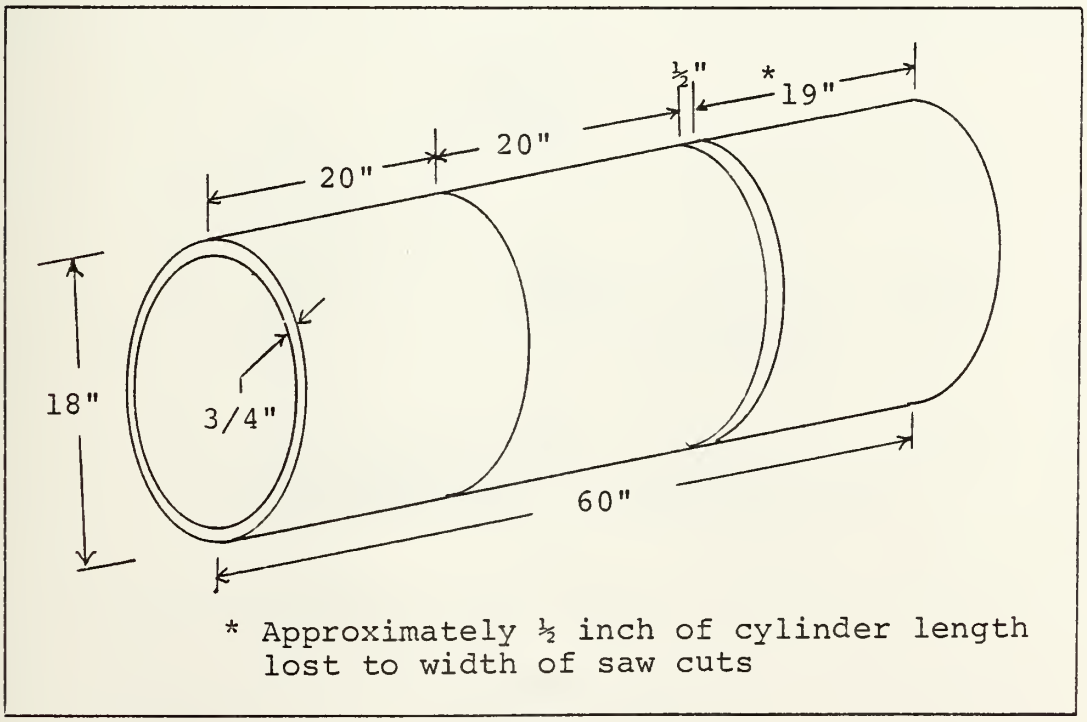


FIGURE III-6

A cross-section of the previously produced seam weld was removed from the ½ inch thick ring and later ground, polished, and etched for analysis of the metallurgical properties of the seam weld. Details of this procedure and a discussion of the results are contained in Chapter IV of this study.

Mating edges of the two sections to be joined by girth welding were then prepared for welding by machining a 60° single Vee groove as shown below in Figure III-7. Heat buildup during machining was prevented by the use of a continuously flowing oil and water cooling bath during machining.

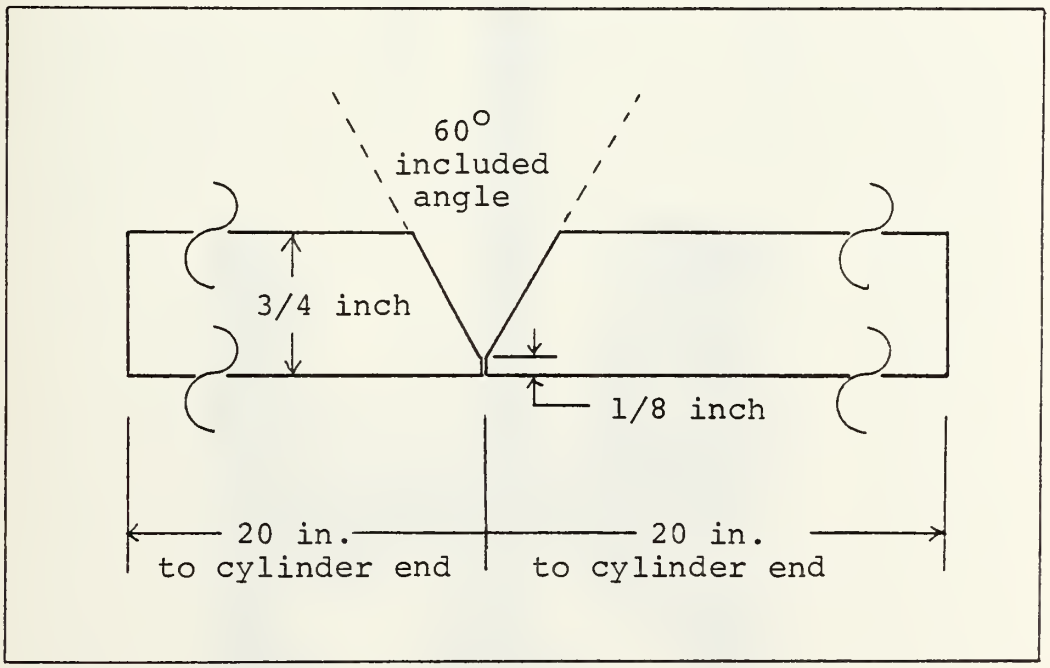


FIGURE III-7

The two 20 inch cylindrical sections were transported back to the MIT welding laboratory where apparatus required for production of the girth weld was assembled. In order to control arc travel speed during production of the girth weld, it was necessary to design and manufacture a supporting structure for the cylinder which would permit cylinder rotation at a controlled speed with respect to the fixed position of the GMAW torch. This was accomplished by producing a structure which was designed to support the two 20 inch cylinders from within. Details of this supporting structure are shown below in Figure III-8.

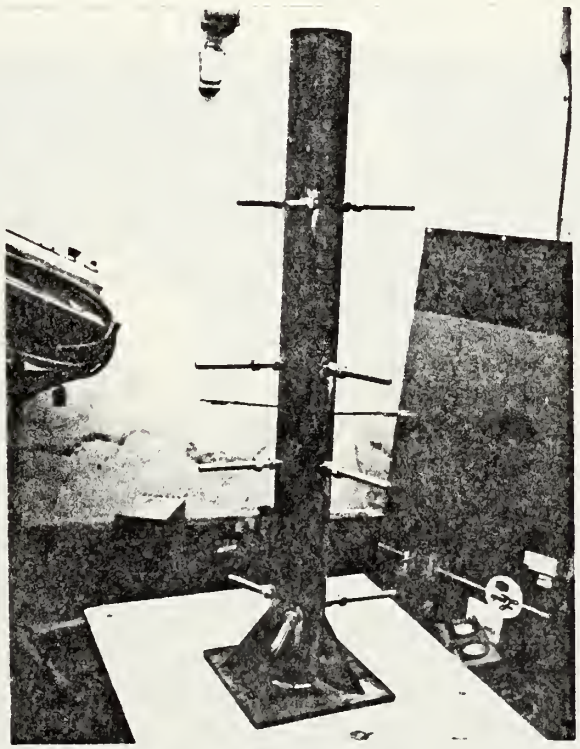

FIGURE III-8

The rectangular base of the supporting structure was bolted to the base of a tilting turntable and the 20 inch long cylinder halves were fixed to the support by force exerted on the interior walls of the cylinder by the threaded dowels. The turntable was then tilted so as to place the now 40 inch long cylinder (with $60^{\circ}$ Vee groove located in the center) in a horizontal position. The threaded dowels were adjusted in order to provide for constant clearance between the stationary GMAW torch and cylinder outer wall during cylinder rotation. Turntable controls were adjusted and calibrated in order to achieve desired arc travel speeds. A photograph of the apparatus in use during production of the girth weld appears below as Figure III-9.

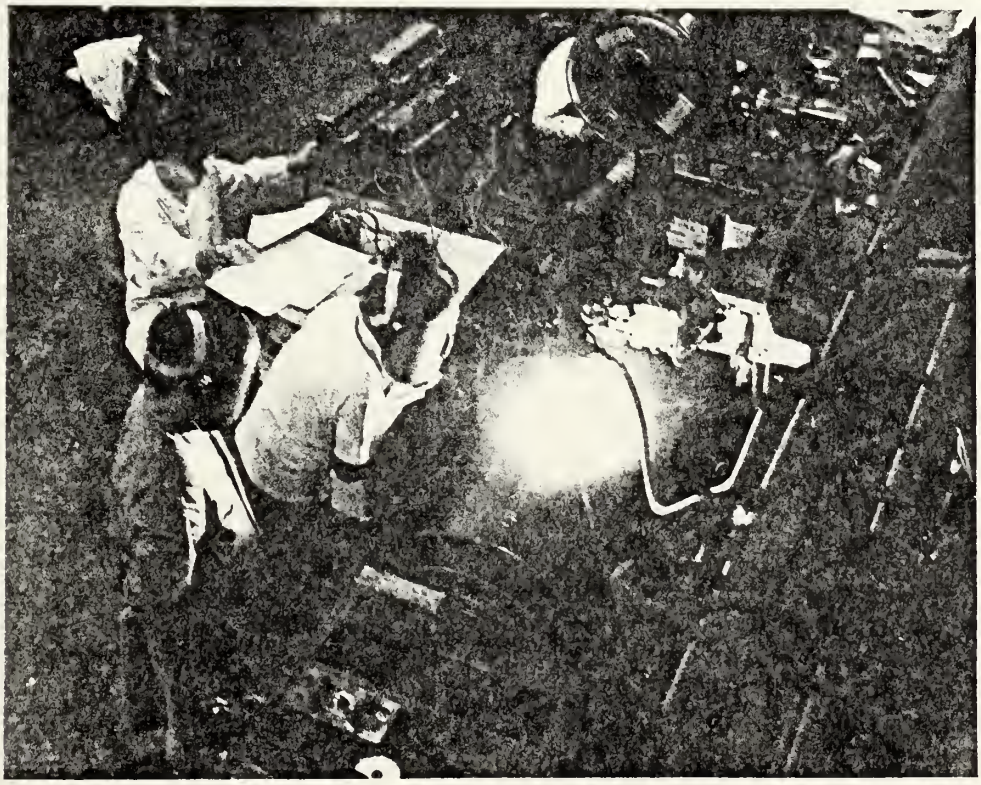

FIGURE III-9

In order to measure radial distortion during production of the girth weld, two Bourns Linear Motion Potentiometers were placed at the inner surface of the cylinder. Characteristics of the linear motion potentiometers are shown below in Table III-D.

ACCEPTANCE TEST RECORD

FOR LINEAR MOTION POTENTIOMETERS

| TESTS PERFORMED | SPEC LIMITS |
|---|---|
| MECHANICAL TRAVEL ..... | 0.44 in max |
| ACTUATION FORCE ..... | 4 oz min |
| TOTAL ELEMENT RESISTANCE ..... | 4750 to 5250 Ohms |
| INSULATION RESISTANCE ..... | 50 Megohms min at 500 V DC |
| NOISE OR CONTACT RESISTANCE VARIATION..... | 100 ohms max |
| END SETTINGS ..... | 0.1 to 5.0% each end |
| LINEARITY ..... | $\pm$ 1.0% VR max |

TABLE III-D

Displacement transducer circuitry and arrangement of linear motion potentiometers within the HY-130 cylinder are indicated in Figures III-10 and III-11 respectively. Prior to mounting the displacement transducers in position within the cylinder, a calibration test was conducted by deflecting the displacement transducers through measured distances and recording resultant voltages. A plot of this calibration test appears as Figure III-12. After completion of calibration tests, the linear motion potentiometers were installed within the cylinder as indicated in Figure III-11. Holes were drilled and threaded in the cylinder support mechanism and the linear motion potentiometer support rods were threaded and screwed into these holes at diametrically opposed locations within the cylinder. Potentiometers corresponding to Channels 1 and 2 of the recorder were located at positions 1/2 inch and 1 inch respectively in the cylinder axial direction from the weld centerline.

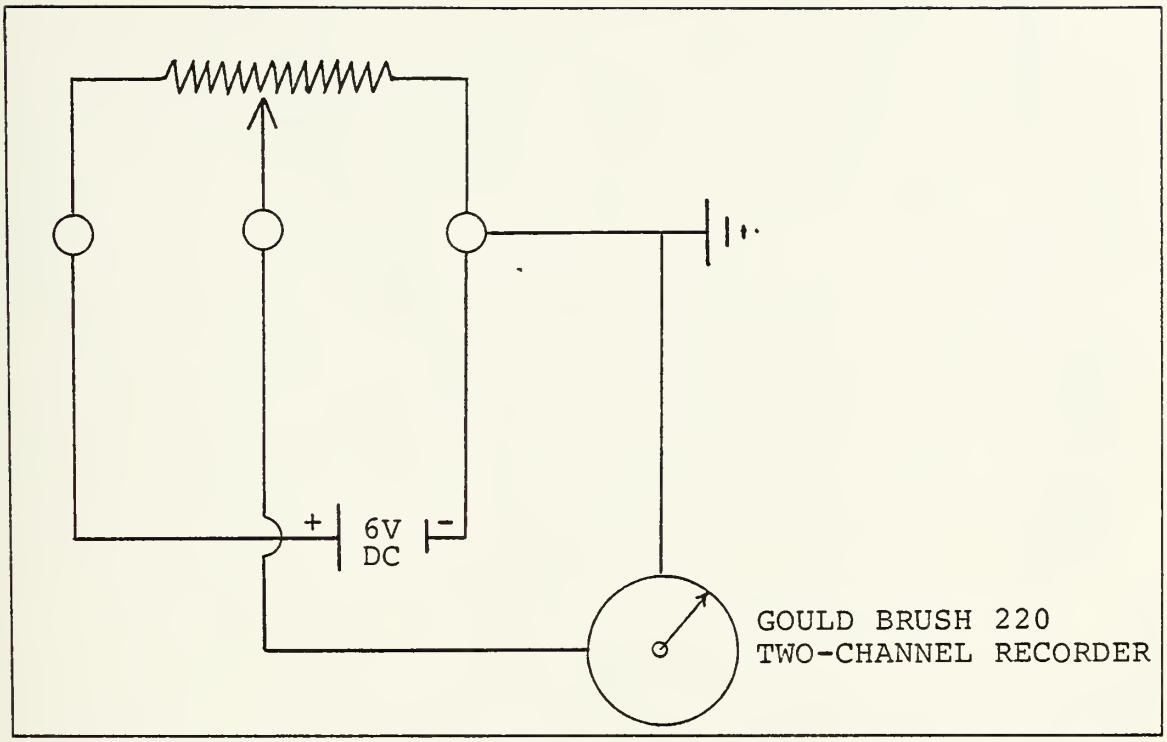


FIGURE III-10 DISPLACEMENT TRANSDUCER CIRCUITRY

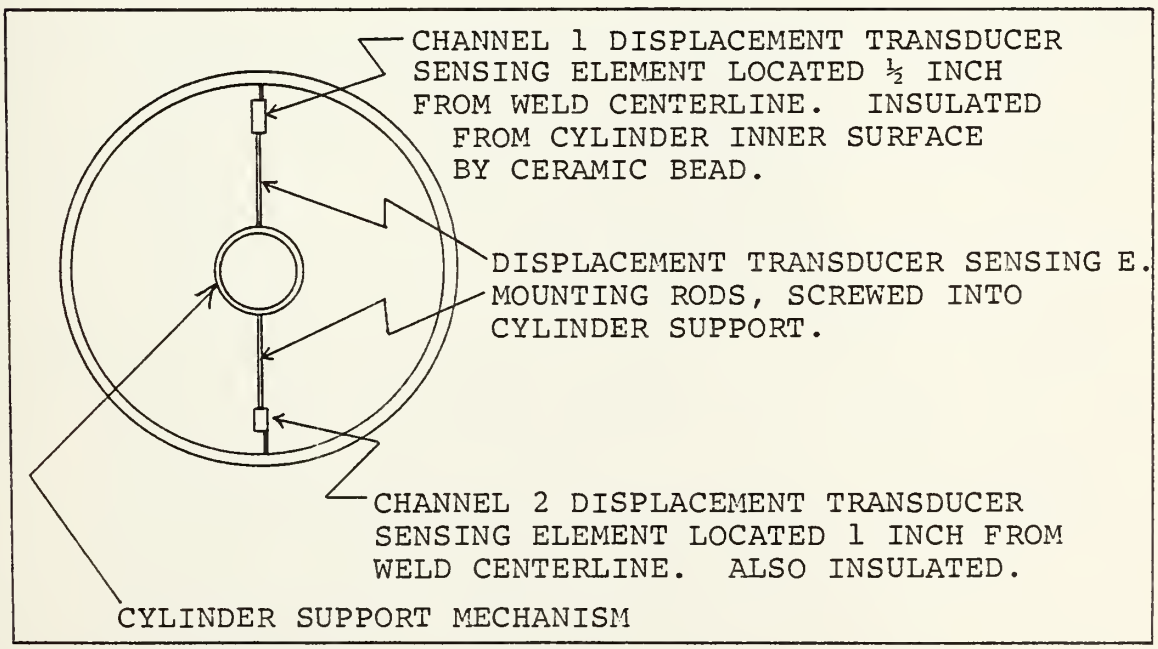


FIGURE III-11 DISPLACEMENT TRANSDUCER SENSING ELEMENT LOCATIONS

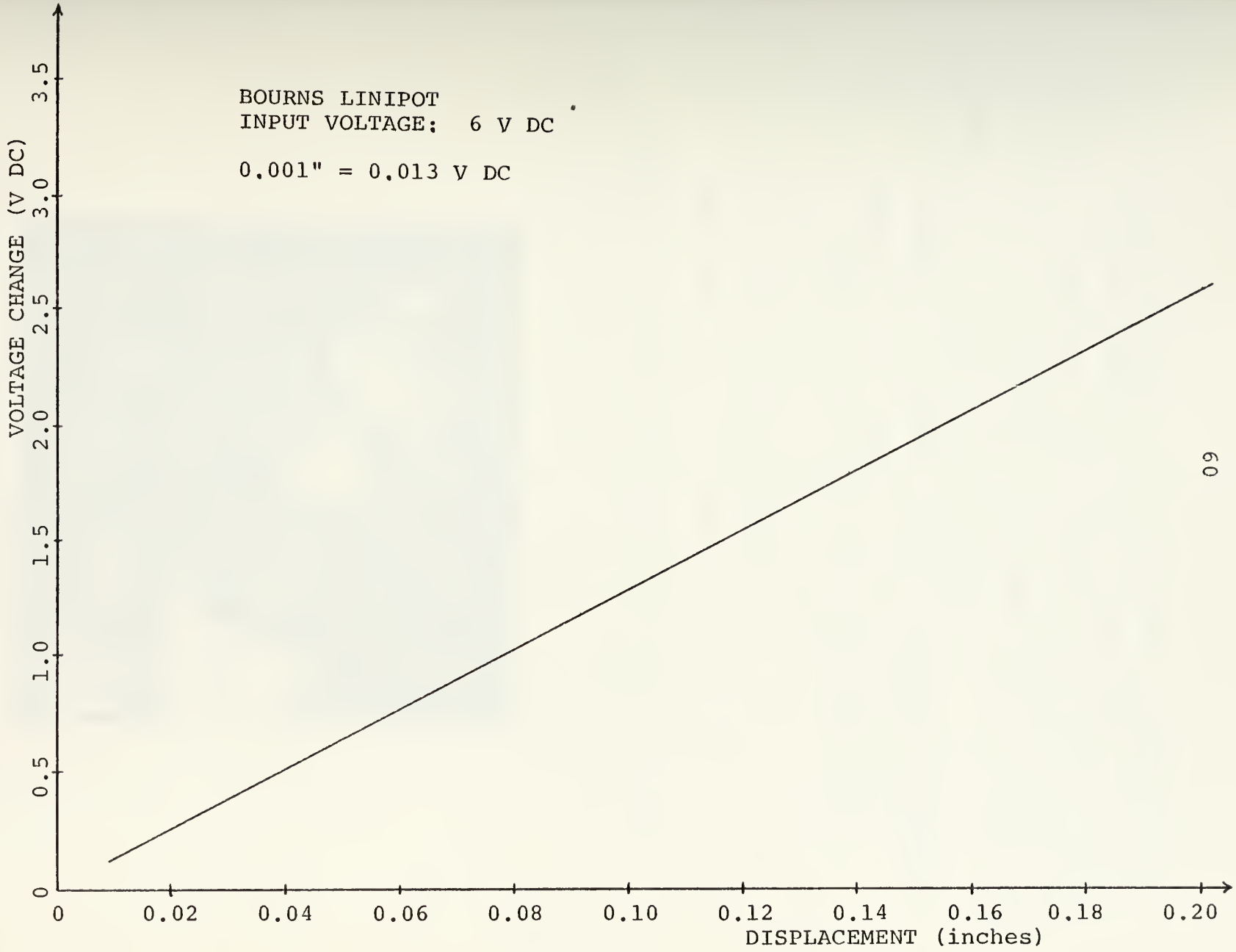


FIGURE III-12

Strain and temperature were measured at the indicated locations during production of the instrumented seam weld; and strain, temperature, and distortion were measured during production of the girth weld. Equipment used to record the measured values included the following:

Minneapolis-Honeywell H1508 24 Channel Visicorder

Three Helland Universal Bridge Balancer Units, Model no. 82-6 (ser no's 1332,1307,1312)

16 Channel Strain Gage Calibrator (one arm bridge adapter)

Gould Brush 220 Two-Channel Recorder (distortion)

General arrangement and operation of this equipment during production of the girth weld are indicated below in Figure III-13.

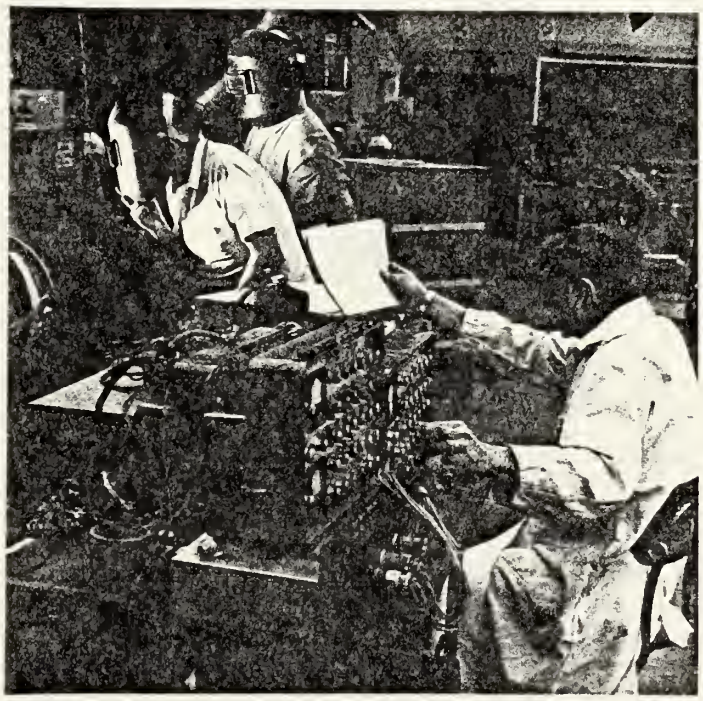

FIGURE III-13

III.G PRODUCTION OF THE INSTRUMENTED SEAM AND GIRTH WELDS:

1. The Seam Weld: After the HY-130 cylinder had been suitably supported and aligned; instrumentation and other apparatus arranged, checked and calibrated, the instrumented seam weld was produced by making seven passes. Figure III-14 below shows approximate dimensions and location of each pass. Values of weld parameters for each pass are tabulated in Table III-E.

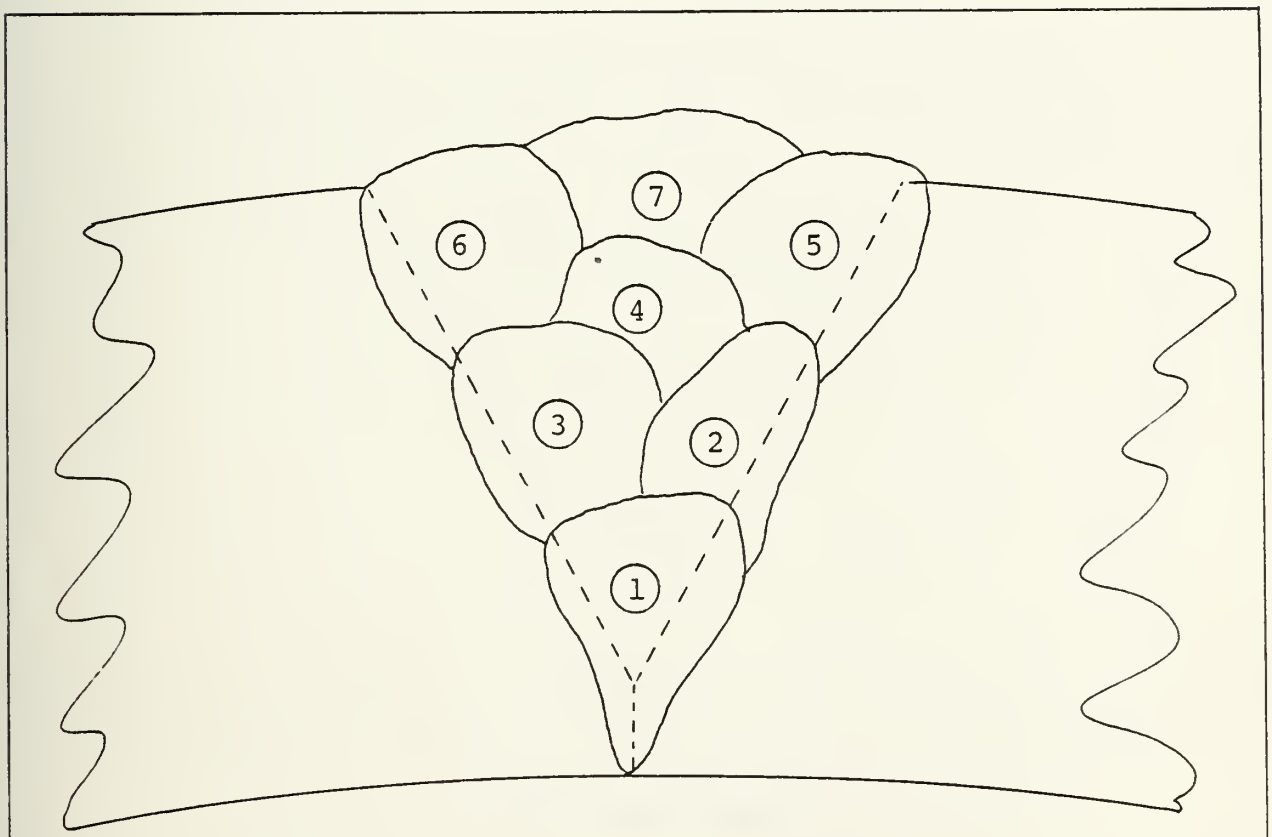


SEAM WELD PASSES

FIGURE III-14

2. The Girth Weld: Production of the girth weld required careful positioning of the rotating HY-130 cylinder with respect to the GMA welding torch. The girth weld required six passes with approximate dimensions shown below in Figure III-15. Girth weld parameters are also included in Table III-E.

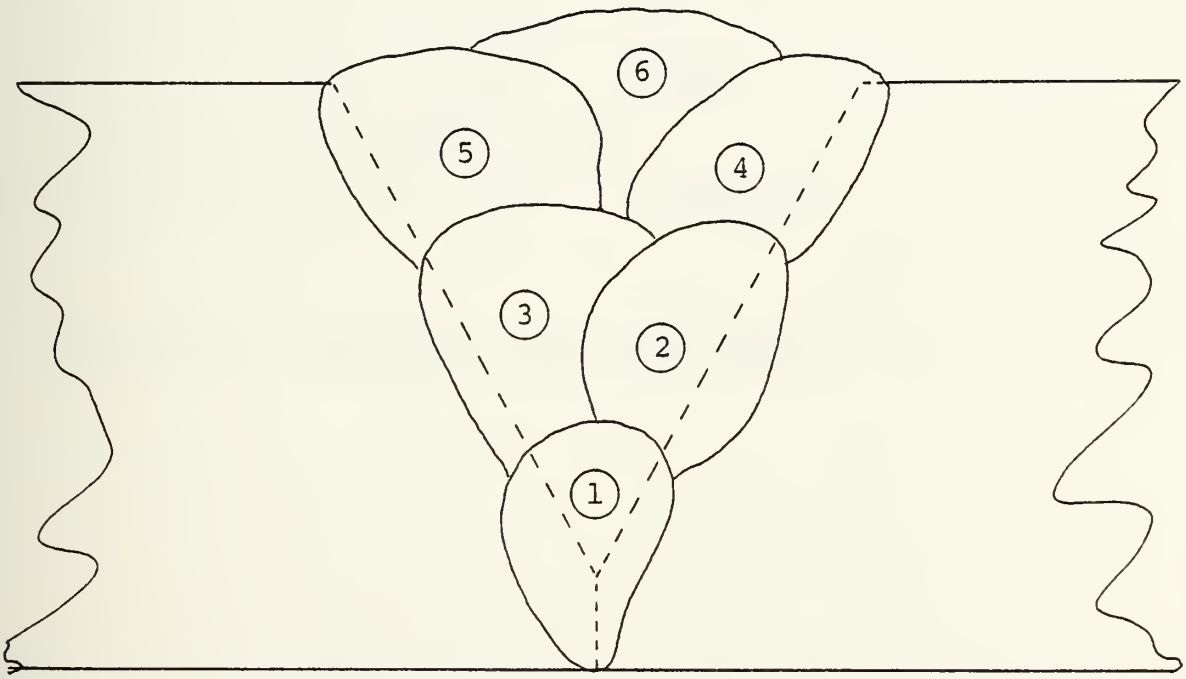


GIRTH WELD PASSES

FIGURE III-15

| | SEAM WELD PASSES | | | GIRTH WELD PASSES | | |
|---|---|---|---|---|---|---|
| WELD PASS NO. | I | V | v | I | V | v |
| 1. | 320 | 26 | 0.20 | 270 | 26 | 0.20 |
| 2. | 320 | 25 | 0.20 | 290 | 25.5 | 0.20 |
| 3. | 320 | 25 | 0.20 | 270 | 26 | 0.20 |
| 4. | 300 | 26 | 0.27 | 285 | 25.5 | 0.20 |
| 5. | 285 | 25 | 0.20 | 280 | 26 | 0.20 |
| 6. | 280 | 25 | 0.20 | 290 | 26 | 0.20 |
| 7. | 290 | 25 | 0.40 | - | - | - |

I = Welding Current in Amperes

V = arc voltage in Volts

v = arc travel speed in inches/sec

TABLE III-E SEAM AND GIRTH WELD PASSES

# CHAPTER IV

# METALLURGICAL CONSIDERATIONS

## IV.A PREPARATION OF SPECIMEN:

When the 60 inch cylinder was sawed into sections, as previously discussed in Chapter III, a cross-section of the instrumented weld was cut from the ½ inch ring. The weld specimen was cut to approximately 3/4 inch by 3/4 inch and marked for identification as shown in Figure IV-1. Mounting for polishing was in thermo-setting bakelite resin, pressed into a 1¼ inch diameter by 3/4 inch long cylindrical shape under hydraulic pressure of 4200 psi at 250 $^{o}$F for 2 minutes using a Buehler press.

The specimen was then rough polished by successive use of 60, 120, 180, 240, 320, and 400 grit 3M TRI-M-ITE Silicon Carbide paper. Fine polishing was accomplished by successive use of 1.0μ, 0.3μ, and 0.05μ alumina polishing powder. Etching for photo-micrographs required about 15 seconds with 5% NITAL. The 500X photo-micrographs, Figures IV-2 through IV-5, were produced by the use of a LEITZ WETZLAR microscope with NPL 50X/0.85 lens, using Polaroid type 52 POLAPAN film. Fine polishing was repeated and the specimen was etched using 1% NITAL prior to the production of 1200X and 6000X electron scan micrographs. These electron scan micrographs appear as Figures IV-6 through IV-13. Locations of the photomicrographs and the electron scan micrographs are indicated on Figure IV-1.

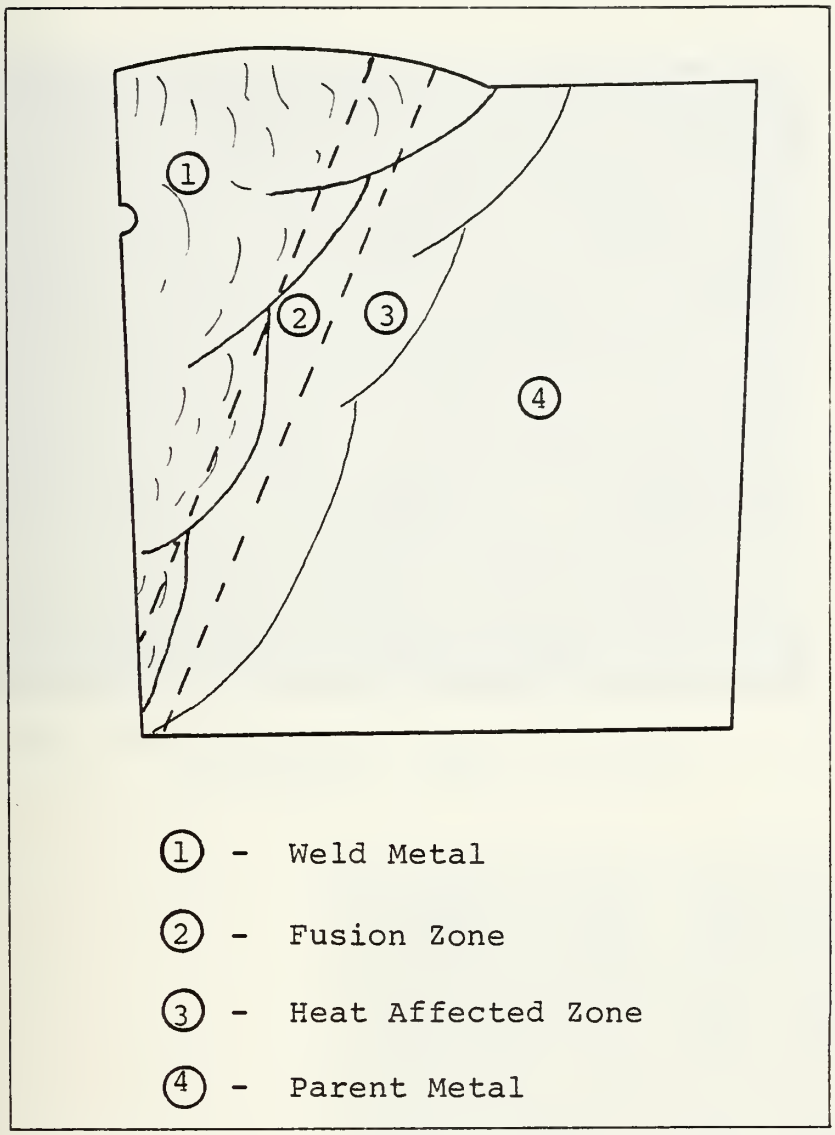


FIGURE IV-1 DIAGRAM SHOWING LOCATIONS OF PHOTO-MICROGRAPHS AND ELECTRON SCAN MICROGRAPHS. 3/4" SAMPLE WAS CUT FROM THE SEAM WELD (SHOWING CROSS SECTION OF WELD - WITH NOTCH IN UPPER LEFT CORRESPONDING TO WELD CENTERLINE). AFTER POLISHING AND ETCHING, 500X PHOTO-MICROGRAPHS AND 1200X/6000X ELECTRON SCAN MICROGRAPHS WERE PRODUCED AT THE LOCATIONS INDICATED.

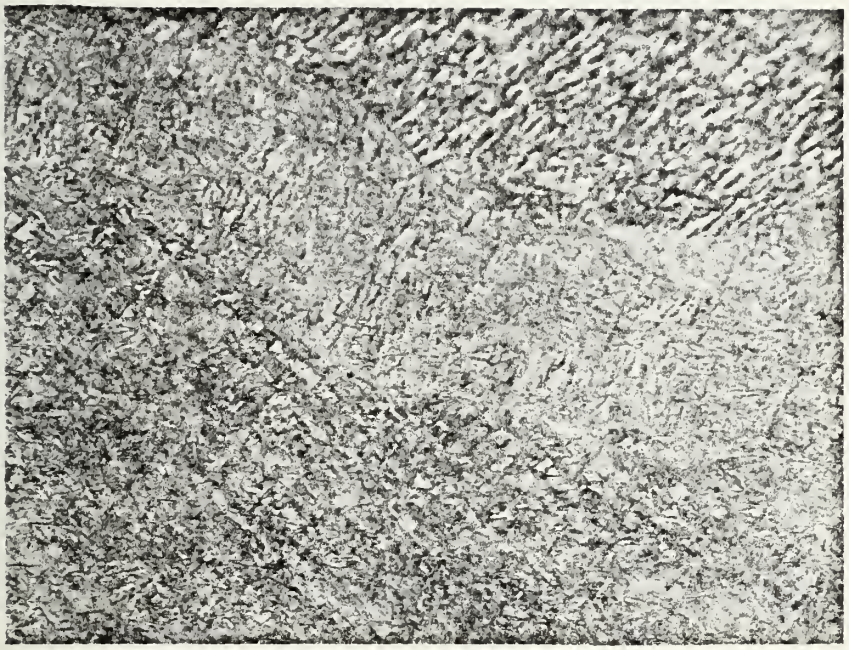

FIG IV-2 PHOTOMICROGRAPH OF HY-130
WELD METAL. 500X. 5% NITAL.

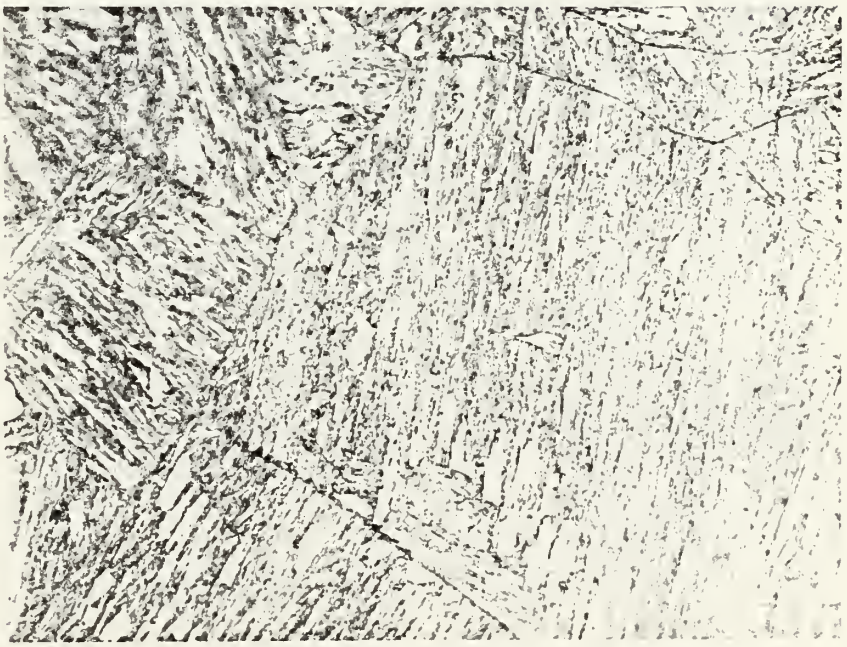

FIG IV-3 PHOTOMICROGRAPH OF HY-130
FUSION ZONE. 500X. 5% NITAL.

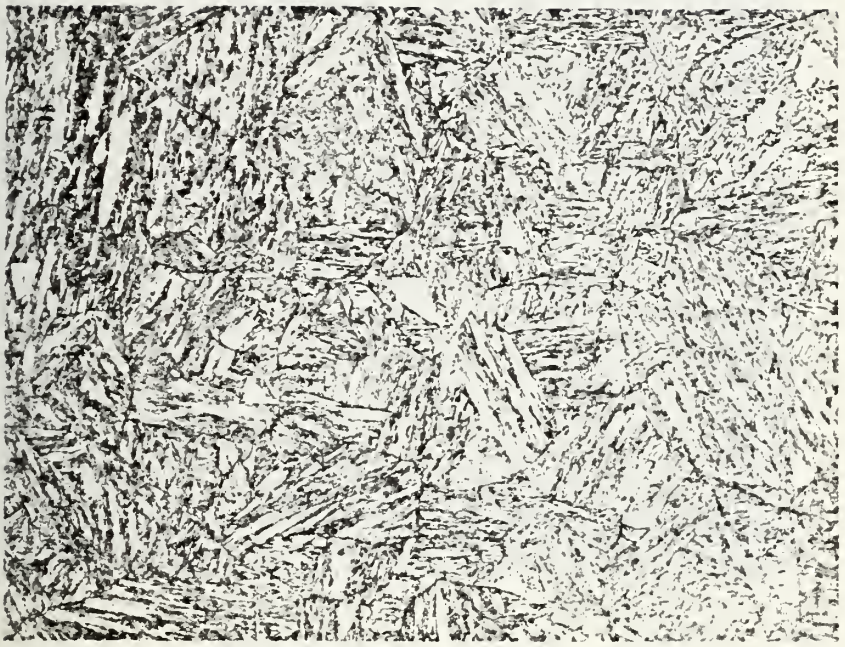

FIG IV-4 PHOTOMICROGRAPH OF HY-130
HAZ. 500X. 5% NITAL.

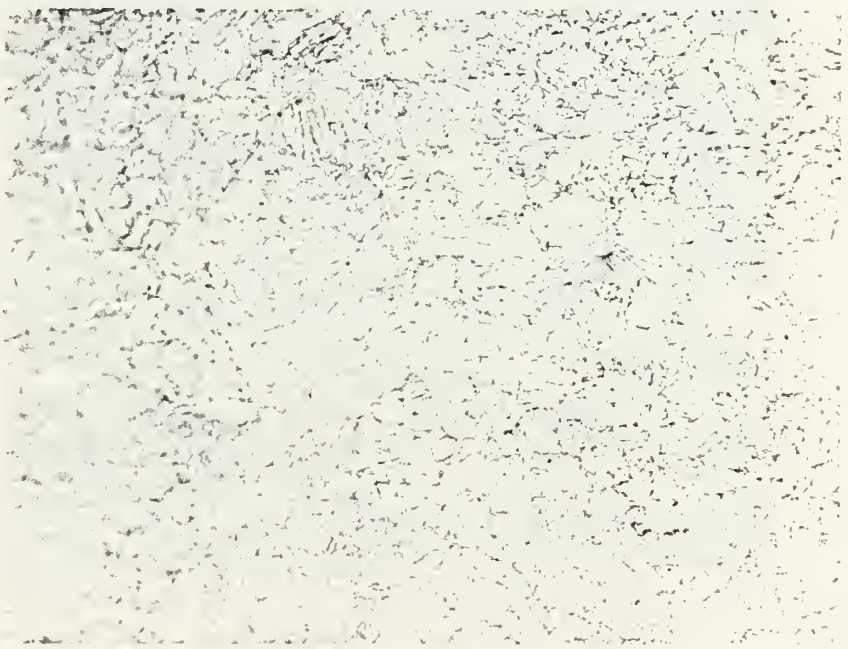

FIG IV-5 PHOTOMICROGRAPH OF HY-130
PARENT METAL. 500X. 5% NITAL.

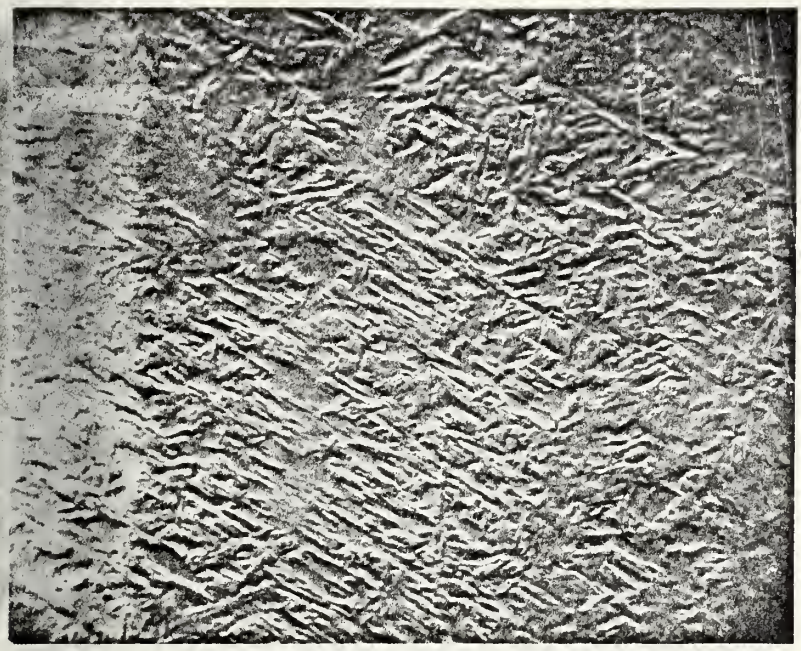

FIG IV-6 ELECTRON SCAN MICROGRAPH OF
HY-130 WELD METAL. 1200X.
1% NITAL.

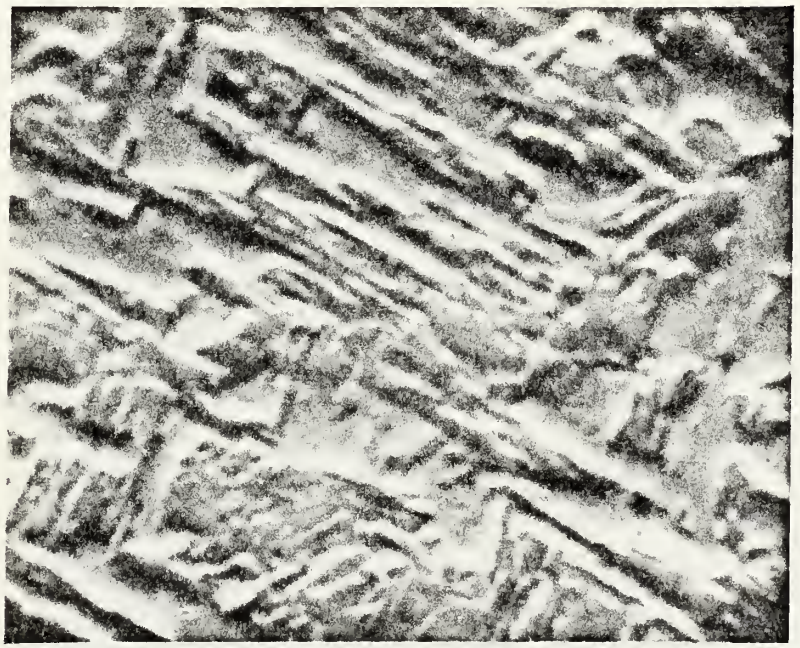

FIG IV-7 ELECTRON SCAN MICROGRAPH OF
HY-130 WELD METAL. 6000X.
1% NITAL.

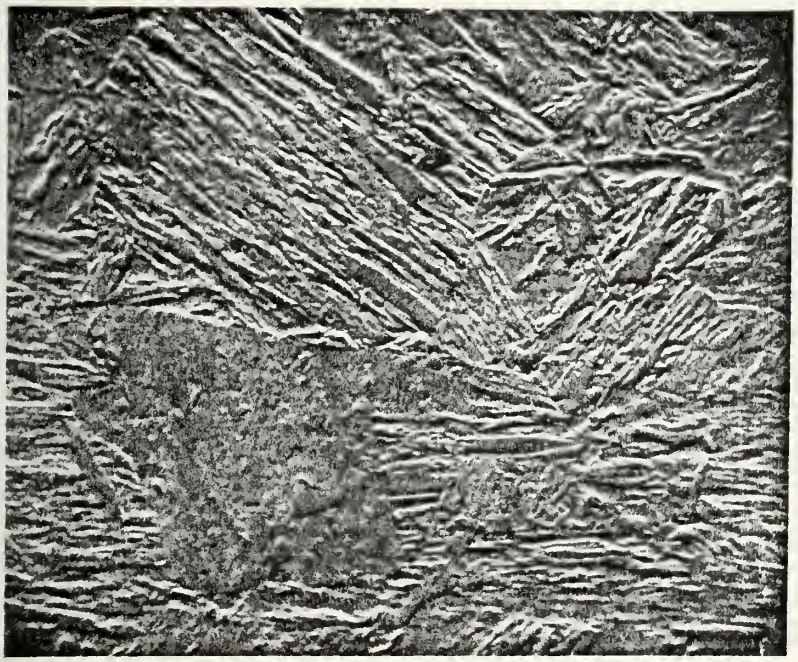

FIG IV-8 ELECTRON SCAN MICROGRAPH OF HY-130 FUSION ZONE. 1200X. 1% NITAL.

FIG IV-9 ELECTRON SCAN MICROGRAPH OF HY-130 FUSION ZONE. 6000X. 1% NITAL.

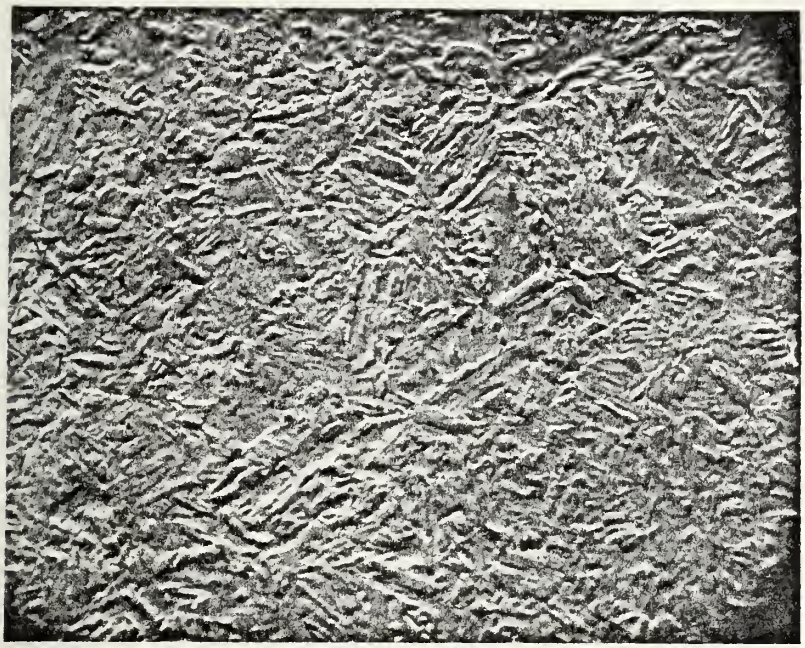

FIG IV-10 ELECTRON SCAN MICROGRAPH OF
HY-130 HAZ. 1200X. 1% NITAL.

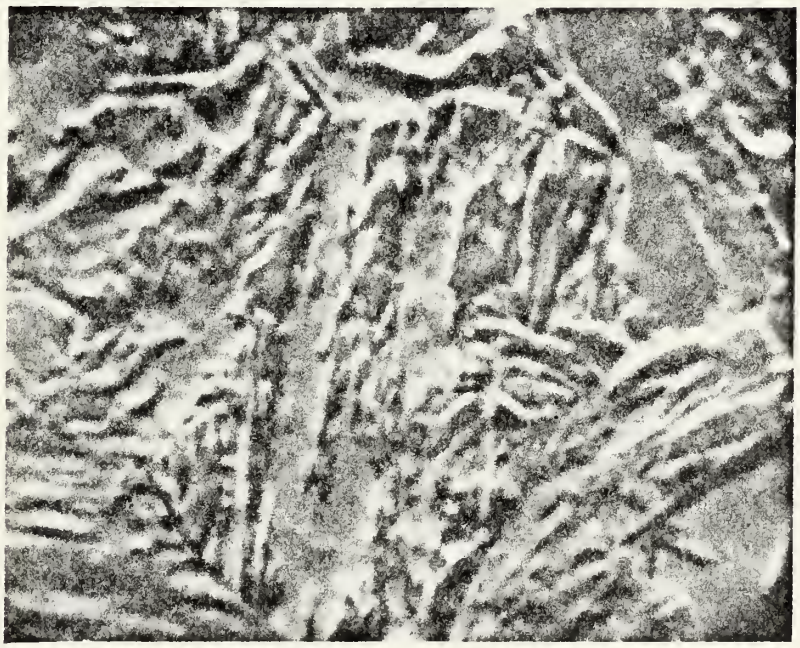

FIG IV-11 ELECTRON SCAN MICROGRAPH OF
HY-130 HAZ. 6000X. 1% NITAL.

FIG IV-12 ELECTRON SCAN MICROGRAPH OF HY-130 PARENT METAL. 1200X. 1% NITAL.

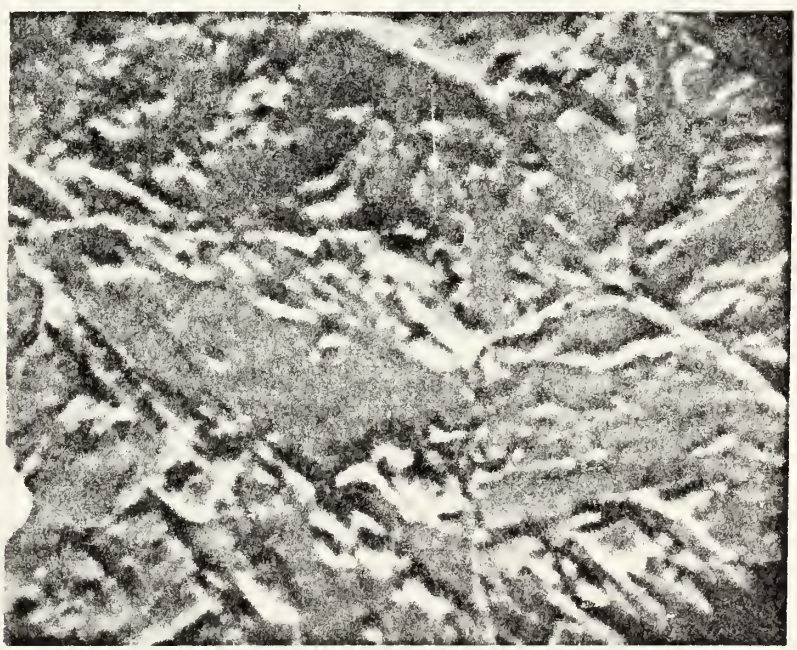

FIG IV-13 ELECTRON SCAN MICROGRAPH OF HY-130 PARENT METAL. 6000X. 1% NITAL.

# CHAPTER V

# DESCRIPTION OF ANALYTICAL TOOLS AND PROCEDURES

## V.A INTRODUCTION:

Analytical procedures used in this study to predict temperature distribution, strain, stress, and distortion occurring during production of a weldment were developed at Massachusetts Institute of Technology. Both the heat flow program and the program used to analyze thermal stress and metal movement use finite element techniques and are written in the FORTRAN-IV language.

Discussion of these programs within this study will be limited to a brief synopsis of their theoretical background, presentation of assumptions and applicable equations upon which they are based, and a summary of welding parameters pertinent to production of the HY-130 weldment which were used as input to the programs. Detailed discussion of these programs, lists, card decks, and manuals describing their use are located within the Department of Ocean Engineering at Massachusetts Institute of Technology.

## V.B DESCRIPTION OF THE HEAT FLOW PROGRAM:

1. Theoretical Background. The finite element computer program used in this study to generate temperature distribution in the HY-130 cylinder girth weld is Program B-4 in a report developed by Muraki[27] and Masubuchi entitled "Computer Programs

Useful for the Analysis of Heat Flow in Weldments" at MIT in 1974. This program develops temperature distribution based on heat conduction in quasi-stationary state from a moving point heat source in a plate of finite thickness. The solution assumes:

a. The size of the heat source is small compared to that of the body under consideration.

b. Heat is supplied instantaneously.

c. Thermophysical properties do not depend upon temperature.

d. Heat is transferred in conduction only (other modes such as radiation and convection are not considered).

e. The material of the body is uniform and isotropic in the thermophysical properties.

The solution is based upon the following equation which expresses the difference between the temperature at time t (in seconds after the arc is initiated) and the initial temperature:

$$T-T_o = \frac{q}{2\pi c} e^{\frac{-v\zeta}{2K}} \left[ \frac{e^{\frac{-vr}{2K}}}{r} + \sum_{n=1} \left( \frac{e^{\frac{-vr_n}{2K}}}{r_n} + \frac{e^{\frac{-vr'_n}{2K}}}{r'_n} \right) \right] \quad \text{(Eq. 5-1)}$$

Where: $\zeta = x - vt$

$r^2 = x^2 + y^2 + z^2$

$r_n = \zeta^2 + y^2 + (2nh - z)^2$

$r'_n = \zeta^2 + y^2 + (2nh + z)^2$

$q$ = heat intensity

2. Geometry of Weld Specimen and Description of Finite Element Representation of Temperature Distribution Program:

Division of the HY-130 cylinder girth weld into elements for use in the heat conduction program is illustrated in Figure V-1. Node coordinates (x, y, and z values) for each of the 114 nodes are listed in Table V-A. The weldment is represented by finite elements which are arranged so as to cause node locations for analytical determination of heat distribution to be coincident with locations of thermocouples which were actually placed on the cylinder outer surface in order to experimentally determine temperature distribution.

Node coordinates listed in Table V-A are based upon an origin (x=y=z=0) which is coincident with the starting point of the heat source (welding arc), with subsequent times of interest corresponding to location of the heat source (in nodal coordinates) at the referenced time. This analysis assumes that the heat source moves on the plane z=0 along the x-axis. The x direction (direction of welding arc travel) would appear on Figure V-1 as normal to the y-z plane, positive direction into the paper. In this figure the y-axis is along the cylinder length and the z-axis is in the radial direction.

# FINITE ELEMENT REPRESENTATION OF WELDMENT GEOMETRY FOR HEAT FLOW ANALYSIS

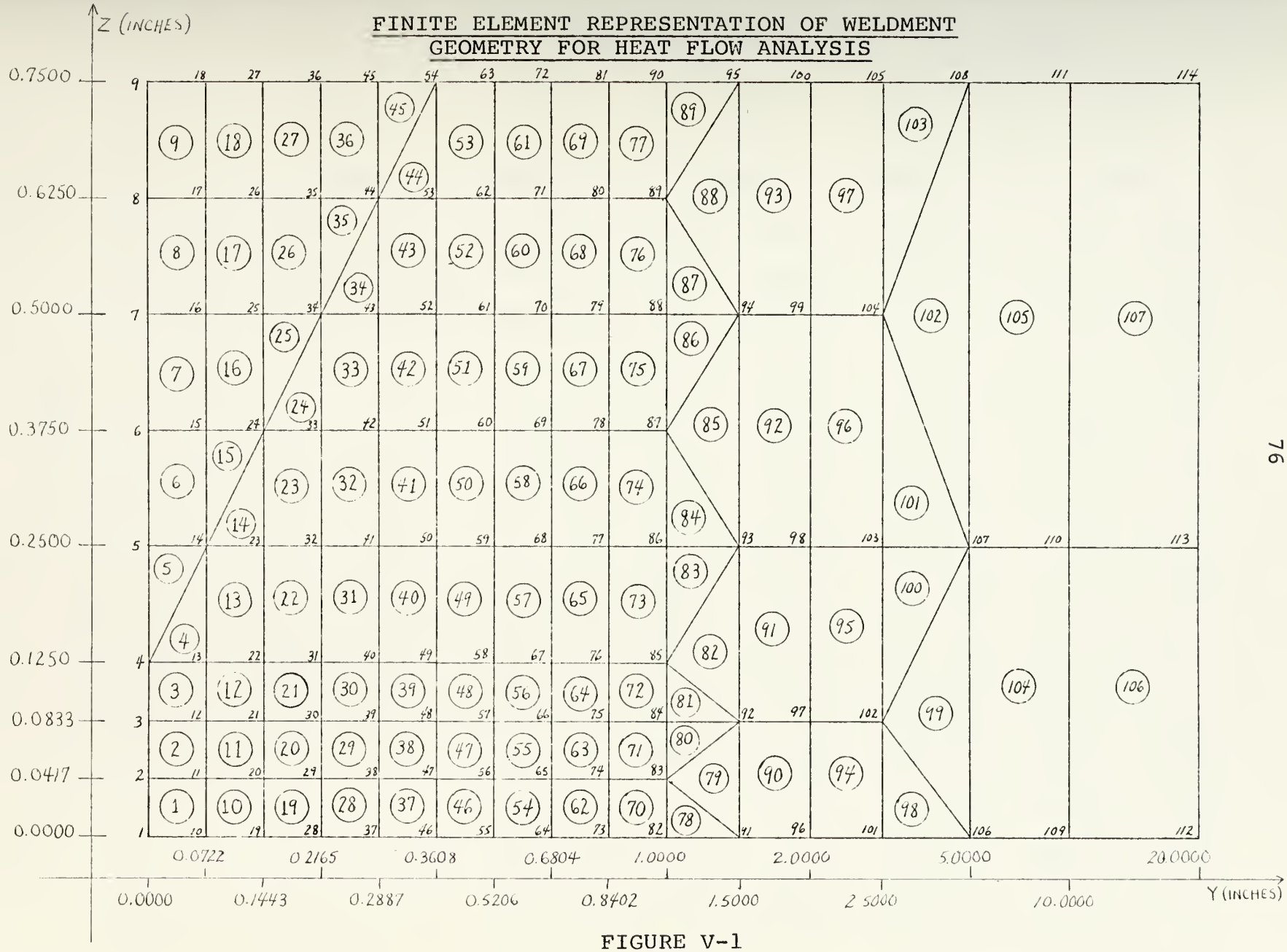


FIGURE V-1

NODE COORDINATES (HEAT FLOW PROGRAM)

| | | |
|---|---|---|
| 1(26.00, 0.0, 0.0) | 2(26.00, 0.0, 0.0417) | 3(26.00, 0.0, 0.0833) |
| 4(26.00, 0.0, 0.1250) | 5(26.00, 0.0, 0.2500) | 6(26.00, 0.0, 0.3750) |
| 7(26.00, 0.0, 0.5000) | 8(26.00, 0.0, 0.6250) | 9(26.00, 0.0, 0.7500) |
| 10(26.00, 0.0722, 0.0) | 11(26.00, 0.0722, 0.0417) | 12(26.00, 0.0722, 0.0833) |
| 13(26.00, 0.0722, 0.1250) | 14(26.00, 0.0722, 0.2500) | 15(26.00, 0.0722, 0.3750) |
| 16(26.00, 0.0722, 0.5000) | 17(26.00, 0.0722, 0.6250) | 18(26.00, 0.0722, 0.7500) |
| 19(26.00, 0.1443, 0.0) | 20(26.00, 0.1443, 0.0417) | 21(26.00, 0.1443, 0.0833) |
| 22(26.00, 0.1443, 0.1250) | 23(26.00, 0.1443, 0.2500) | 24(26.00, 0.1443, 0.3750) |
| 25(26.00, 0.1443, 0.5000) | 26(26.00, 0.1443, 0.6250) | 27(26.00, 0.1443, 0.7500) |
| 28(26.00, 0.2165, 0.0) | 29(26.00, 0.2165, 0.0417) | 30(26.00, 0.2165, 0.0833) |
| 31(26.00, 0.2165, 0.1250) | 32(26.00, 0.2165, 0.2500) | 33(26.00, 0.2165, 0.3750) |
| 34(26.00, 0.2165, 0.5000) | 35(26.00, 0.2165, 0.6250) | 36(26.00, 0.2165, 0.7500) |
| 37(26.00, 0.2887, 0.0) | 38(26.00, 0.2887, 0.0417) | 39(26.00, 0.2887, 0.0833) |
| 40(26.00, 0.2887, 0.1250) | 41(26.00, 0.2887, 0.2500) | 42(26.00, 0.2887, 0.3750) |
| 43(26.00, 0.2887, 0.5000) | 44(26.00, 0.2887, 0.6250) | 45(26.00, 0.2887, 0.7500) |
| 46(26.00, 0.3608, 0.0) | 47(26.00, 0.3608, 0.0417) | 48(26.00, 0.3608, 0.0833) |
| 49(26.00, 0.3608, 0.1250) | 50(26.00, 0.3608, 0.2500) | 51(26.00, 0.3608, 0.3750) |
| 52(26.00, 0.3608, 0.5000) | 53(26.00, 0.3608, 0.6250) | 54(26.00, 0.3608, 0.7500) |
| 55(26.00, 0.5206, 0.0) | 56(26.00, 0.5206, 0.0417) | 57(26.00, 0.5206, 0.0833) |

TABLE V-A

NODE COORDINATES (Cont'd) (HEAT FLOW PROGRAM)

| | | |
|---|---|---|
| 58(26.00, 0.5206, 0.1250) | 59(26.00, 0.5206, 0.2500) | 60(26.00, 0.5206, 0.3750) |
| 61(26.00, 0.5206, 0.5000) | 62(26.00, 0.5206, 0.6250) | 63(26.00, 0.5206, 0.7500) |
| 64(26.00, 0.6804, 0.0) | 65(26.00, 0.6804, 0.0417) | 66(26.00, 0.6804, 0.0833) |
| 67(26.00, 0.6804, 0.1250) | 68(26.00, 0.6804, 0.2500) | 69(26.00, 0.6804, 0.3750) |
| 70(26.00, 0.6804, 0.5000) | 71(26.00, 0.6804, 0.6250) | 72(26.00, 0.6804, 0.7500) |
| 73(26.00, 0.8402, 0.0) | 74(26.00, 0.8402, 0.0417) | 75(26.00, 0.8402, 0.0833) |
| 76(26.00, 0.8402, 0.1250) | 77(26.00, 0.8402, 0.2500) | 78(26.00, 0.8402, 0.3750) |
| 79(26.00, 0.8402, 0.5000) | 80(26.00, 0.8402, 0.6250) | 81(26.00, 0.8402, 0.7500) |
| 82(26.00, 1.0000, 0.0) | 83(26.00, 1.0000, 0.0417) | 84(26.00, 1.0000, 0.0833) |
| 85(26.00, 1.0000, 0.1250) | 86(26.00, 1.0000, 0.2500) | 87(26.00, 1.0000, 0.3750) |
| 88(26.00, 1.0000, 0.5000) | 89(26.00, 1.0000, 0.6250) | 90(26.00, 1.0000, 0.7500) |
| 91(26.00, 1.5000, 0.0) | 92(26.00, 1.5000, 0.0833) | 93(26.00, 1.5000, 0.2500) |
| 94(26.00, 1.5000, 0.5000) | 95(26.00, 1.5000, 0.7500) | 96(26.00, 2.0000, 0.0) |
| 97(26.00, 2.0000, 0.0833) | 98(26.00, 2.0000, 0.2500) | 99(26.00, 2.0000, 0.5000) |
| 100(26.00, 2.0000, 0.7500) | 101(26.00, 2.5000, 0.0) | 102(26.00, 2.5000, 0.0833) |
| 103(26.00, 2.5000, 0.2500) | 104(26.00, 2.5000, 0.5000) | 105(26.00, 2.5000, 0.7500) |
| 106(26.00, 5.0000, 0.0) | 107(26.00, 5.0000, 0.2500) | 108(26.00, 5.0000, 0.7500) |
| 109(26.00, 10.00, 0.0) | 110(26.00, 10.00, 0.2500) | 111(26.00, 10.00, 0.7500) |
| 112(26.00, 20,00, 0.0) | 113(26.00, 20,00, 0.2500) | 114(26.00, 20.00, 0.7500) |

TABLE V-A

In order to determine temperature distribution at weldment nodes for the first pass of the HY-130 cylinder girth weld, the following parameters were used as input to the heat flow program:

Velocity of welding arc (v) = 0.2000 in/sec

Heat intensity (q) = 6084 $Joules/_{sec\ in}$

Where: $q = \frac{I \times V \times \eta_{arc}}{h}$ (Eq. 5-2)

I = welding current

V = arc voltage

h = plate thickness

$\eta_{arc}$ = welding arc efficiency

Density ($\rho$) = 0.282 $lbm/_{in^3}$

Specific heat ($\kappa$) = 124.4664 $Joules/_{lbm\ ^oF}$

Thermal conductivity (c) = 0.5250 $Joule/_{sec\ in\ ^oF}$

It should be noted that this stage of the computer analysis does not provide for temperature dependence of material properties. Values used in this case to determine temperature distribution are those valid at 400 $^oF$. It is also significant to note that for this analysis, an arc efficiency ($\eta_{arc}$) of 0.65 was assumed.

No modifications were required to the analytical or mathematical techniques required for generating temperature distributions to be used by the Muraki strain, stress, and distortion calculating program. However, since large amounts of numerical data were generated by the heat flow program for input to the Muraki program, it was necessary to modify the heat program output. Since weldment geometry and finite element representation of the nodes and elements were the same (except for coordinates) for both programs, the heat flow program was modified so as to provide its output in the form of punched cards suitable for use as input to the Muraki program. This reduced the probability of introducing numerical error between the two programs as well as improving the ease of program interaction.

V.C DESCRIPTION OF THE PROGRAM TO CALCULATE STRAIN, STRESS, AND DISTORTION:

1. Theoretical Background: The program used in this study to analytically generate strain, stress, and distortion distributions within the HY-130 cylinder girth weld was developed at MIT by Toyohiki Muraki for thermo elasto-plastic analyses of axisymmetric structural components. The Muraki program is written in FORTRAN IV language and uses finite element techniques in an incremental fashion to calculate strains, stresses, and distortion.

The Muraki program has great flexibility in terms of allowing temperature dependency of material properties to be considered as well as considering the effect of melting and deposition of metal which occurs during welding. Weldment restraint and concentrated loads are also considered in the analytical solution. In the "Manual on Axisymmetric Finite Element Program for Analysis of Thermal Stress and Metal Movement During Welding", Muraki[28] presents a brief synopsis of the theoretical background upon which this analysis is based. This synopsis is reproduced here as follows:

Principle of Virtual Work

The principle of virtual work for the quasi-static problem is, in general,

$$\iiint_V \{\delta\dot{\varepsilon}\}^T\{\dot{\sigma}\}dV - \iiint_V \{\delta\dot{u}\}^T\{\dot{\bar{P}}\}dV - \iint_{S_1} \{\delta\dot{u}\}^T\{\dot{\bar{F}}\}dS = 0 \quad (1)$$

where superscript T stands for the transpose of a vector or a matrix. $\{\dot{\varepsilon}\}$, $\{\dot{\sigma}\}$, and $\{\dot{u}\}$ are vectors of the time rates of strain, stress and displacement, respectively.

$\dot{\bar{P}}$ and $\dot{\bar{F}}$ denote the time rates of body force over the volume, V, and surface force on the boundary surface, $S_1$, respectively.

The boundary condition on the specified displacement on the surface, $S_2$, is given as

$$\{u\} = \{\dot{\bar{u}}\} \quad \text{on } S_2 \tag{2}$$

It is noted that the problem here is formulated in the small displacement theory based on the rectangular cartesian coordinate system.

Constitutive Equations

One of the important features in the analysis of thermal stress and distortion during welding is the temperature dependency of material properties and the yield criterion. Therefore the constitutive equations are provided here in a general form.

The rate of strain for the elasto-plastic state is given by:

$$\{\dot{\varepsilon}\} = \{\dot{\varepsilon}^{(e)}\} + \{\dot{\varepsilon}^{(p)}\} \tag{3}$$

where superscripts e and p refer to elastic and plastic components of the strain, respectively.

The rate of plastic strain is assumed as

$$\{\dot{\varepsilon}^{(p)}\} = \Lambda\{g\} \tag{4}$$

where $\Lambda$ is a proportional constant and g is derivatives of the yield function, f, with respect to the stress, $\sigma_{ij}$ (i,j = 1,2,3);

$$g = \frac{\partial f}{\partial \sigma_{ij}} \tag{5}$$

Using Hooke's law and Equation (4), we have

$$\{\dot{\varepsilon}\} = \frac{1}{E}|De|^{-1}\{\dot{\sigma}\} + \Lambda\{g\} \tag{6}^{*}$$

where $E|De|$ is the matrix form of Hooke's law.

Thermal strain and the temperature dependency of material properties are added to Equation (6) as follows:

$$\{\dot{\varepsilon}\} = \frac{1}{E}|De|^{-1}\{\dot{\sigma}\} - \frac{\dot{E}}{E^2}|De|^{-1}\{\sigma\} \Lambda + \dot{\varepsilon}^{\theta}\{\delta_{ij}\} + \Lambda\{g\} \tag{7}$$

where $\dot{\varepsilon}^{\theta}$ is the thermal strain, and $\delta_{ij}$ is the Kronecker symbol.

Equation (7) is rewritten for the rate of stress as,

$$\{\dot{\sigma}\} = E|De|\{\dot{\varepsilon}\} + \frac{\dot{E}}{E}\{\sigma\} - \dot{\varepsilon}^{\theta} E|De|\{\delta_{ij}\} - \Lambda E|De|\{g\} \tag{8}$$

*Note: $|\ |^{-1}$ stands for the inverse of the matrix

If the von Mises' yield criterion is adopted, f in Equation (5) is given by

$$f = \bar{\sigma} - C\ (\varepsilon_{ij}^{(p)},\ T) \tag{9}$$

where C is related to the strain hardening and given as a function of plastic strain, $\varepsilon_{ij}^{(p)}$ and temperature, T.

$\bar{\sigma}$ is referred to as the equivalent stress and given by

$$\bar{\sigma}^2 = 3/2\{\sigma'\}^T\{\sigma'\} \tag{10}$$

It is noted that $\{\sigma'\}$ is the vector of deviator stresses which is different from $\{\sigma\}$.

When a state of stress in a portion of a body is plastic and then changes to a new state of stress which is still plastic, the following relation is obtained from Equation (9):

$$\frac{\partial f}{\partial \bar{\sigma}}\dot{\bar{\sigma}} + \{\frac{\partial f}{\partial \varepsilon^{(p)}}\}^T \{\dot{\varepsilon}^{(p)}\} + \frac{\partial f}{\partial T}\dot{T} = 0 \tag{11}$$

Equation (11) with Equations (4), (9), and (10) leads to

$$\{\sigma'\}^T\{\dot{\sigma}\} = -2/3\bar{\sigma}(-\Lambda H' + \frac{\partial f}{\partial T}\dot{T}) \tag{12}$$

where

$$H' = -\frac{\partial f}{\partial \bar{\varepsilon}^{(p)}}$$

and $$\partial\bar{\varepsilon}^{(p)} = \sqrt{2/3\{\partial\varepsilon^{(p)}\}^T\{\partial\varepsilon^{(p)}\}}$$

From Equations (8) and (12), $\Lambda$ is obtained as follows:

$$\Lambda = \frac{1}{2/3\ \bar{\sigma}\ H' + E\{\sigma'\}^T|De|\{g\}} \times (E\{\sigma'\}^T|De|\{\dot{\varepsilon}\}$$

$$+ \frac{\dot{E}}{E}\{\sigma'\}^T \{\sigma\} - \dot{\varepsilon}^{\theta} E\{\sigma'\}^T|De|\{\delta_{ij}\}$$

$$+ 2/3\ \bar{\sigma}\ \frac{\partial f}{\partial T}\ \dot{T}) \qquad (13)$$

Substituting $\Lambda$ of Equation into (8) we have a general form of the stress-strain relationship as

$$\begin{aligned}\{\dot{\sigma}\} = {} & (E|De| - 1/S_o E|De|\{g\}\ E\{\sigma'\}^T|De|) \times \\ & (\{\dot{\varepsilon}\} - \dot{\varepsilon}^{\theta}\{\delta_{ij}\}) \\ & + \dot{E}/E\ \{|I| - 1/S_o\ E|De|\{g\}\{\sigma'\}^T)\{\sigma\} \\ & - 1/S_o\ E|De|\{g\}\ 2/3\bar{\sigma}\ \frac{\partial f}{\partial T}\ \dot{T}\end{aligned} \qquad (14)$$

where

$$S_o = 2/3\ \bar{\sigma}\ H' + E\{\sigma'\}^T|De|\{g\}$$

and $|I|$ is called the unit matrix.

Equation (14) covers the stress-strain relationship in the elastic as well as plastic state. This can be easily confirmed by eliminating terms related to the yield function from Equation (14).

Yield Criterion

As described in Equation (9) the yield function used here is that proposed by von Mises.

The yield function is to separate the region of elastic deformation from that of plastic deformation. Since the

deformation is closely related to the loading process, the yield function is also called a loading surface which is defined in stress space.

If a part of a material in question is in the region of plastic deformation, which means that the state of stress of the part is located on the loading surface, one of the following states will be realized at the next instance:

$$f = 0,\ \dot{f}' < 0 \quad \text{(unloading)}$$
$$f = 0,\ \dot{f}' = 0 \quad \text{(neutral)}$$
$$f = 0,\ \dot{f}' > 0 \quad \text{(loading)}$$

where

$$\dot{f} = \frac{\partial f}{\partial \sigma_{ij}} \dot{\sigma}_{ij} + \frac{\partial f}{\partial T} \dot{T}$$

If a part of the material is in the region of elastic deformation, one of the following states will be realized at the next instance:

$$\begin{aligned} f &< 0 \quad \text{(elastic)} \\ f &= 0 \quad \text{(plastic)} \end{aligned} \tag{16}$$

It is worth looking into Equation (15) more closely. Using Equations (10) and (12) with Equation (15), the following relationship is obtained:

$$\dot{f}' = \Lambda H' \tag{17}$$

Equation (17) indicates that when non-strain hardening is assumed of a material, Equation (15) cannot be used to

judge whether or not a part of the material recovers from the plastic to the elastic state of stress. To avoid this difficulty, Equation (17) will be written in the form of:

$$\lim_{H' \to 0} \frac{\dot{f}'}{H'} = \Lambda \tag{18}$$

Therefore Equation (15) is written as,

$$\begin{aligned} &f = 0, \ \Lambda < 0 \ \text{(unloading)} \\ &f = 0, \ \Lambda = 0 \ \text{(neutral)} \\ &f = 0, \ \Lambda > 0 \ \text{(loading)} \end{aligned} \tag{19}$$

to cover non-strain hardening materials.

Finite Element Approach

Various types of axisymmetric finite elements can be derived based on Equation (1).

In the computer program described in the Muraki[28] Manual, a four node-isoparametric element is used. Following a standard procedure to derive an element stiffness matrix and element forces, the coordinates and the displacements for the elements are assumed by

$$\begin{aligned} x &= \sum_{i=1}^{4} h_i x_i \\ y &= \sum_{i=1}^{4} h_i y_i \end{aligned} \tag{20}$$

$$u = \sum_{i=1}^{4} h_i u_i \tag{21}$$

$$v = \sum_{i=1}^{4} h_i v_i \tag{21}$$

where $h_1$, $h_2$, $h_3$, and $h_4$ are interpolation functions, $x_i$ and $y_i$ are nodal coordinates, and $u_i$ and $v_i$ are nodal displacements.

A key of the above derivation is use of the same interpolation functions for both the element coordinates and the element displacements. Details of the interpolation functions are

$$\begin{aligned} h_1 &= \tfrac{1}{4}(1 - r)(1 - s) \\ h_2 &= \tfrac{1}{4}(1 + r)(1 - s) \\ h_3 &= \tfrac{1}{4}(1 + r)(1 + s) \\ h_4 &= \tfrac{1}{4}(1 - r)(1 + s) \end{aligned} \tag{22}$$

where r and s are referred to as natural coordinates and vary from -1 to +1.

The element strains in the axisymmetric condition are

$$\begin{Bmatrix} \varepsilon_x \\ \varepsilon_y \\ \varepsilon_z \\ \gamma_{xy} \end{Bmatrix} = \begin{Bmatrix} \dfrac{\partial u}{\partial x} \\ \dfrac{\partial u}{\partial y} \\ \dfrac{u}{y} \\ \dfrac{\partial u}{\partial y} + \dfrac{\partial u}{\partial x} \end{Bmatrix} \tag{23}$$

Because u and v in the strain are a function of x and y, the following relation is first required between the x-y and r-s systems

$$\begin{Bmatrix} \frac{\partial}{\partial r} \\ \\ \frac{\partial}{\partial s} \end{Bmatrix} = \begin{bmatrix} \frac{\partial x}{\partial r} & \frac{\partial y}{\partial r} \\ \\ \frac{\partial x}{\partial s} & \frac{\partial y}{\partial s} \end{bmatrix} \begin{Bmatrix} \frac{\partial}{\partial x} \\ \\ \frac{\partial}{\partial y} \end{Bmatrix} \tag{24}$$

Derivatives of the displacements with regards to r and s are

$$\begin{aligned} \frac{\partial u}{\partial r} &= \sum_{i=1}^{x} \frac{\partial h_i}{\partial r} u_i \\ \\ \frac{\partial u}{\partial s} &= \sum_{i=1}^{x} \frac{\partial h_i}{\partial r} u_i \qquad (25) \\ \\ \frac{\partial u}{\partial r} &= \sum_{i=1}^{x} \frac{\partial h_i}{\partial r} v_i \\ \\ \frac{u}{s} &= \sum_{i=1}^{x} \frac{h_i}{r} v_i \end{aligned}$$

Using Equations (24) and (25), the strains in Equation (23) are given in terms of nodal displacements, $u_1$, $u_2$, $u_3$, and $u_4$ as follows:

$$\{\dot{\varepsilon}\} = |B|\{\dot{q}\} \tag{26}$$

where

$$\{\dot{\varepsilon}\}^T = \{\dot{\varepsilon}_x,\ \dot{\varepsilon}_y,\ \dot{\varepsilon}_z,\ \dot{\gamma}_{xy}\}$$

$$\{\dot{q}\}^T = \{\dot{u}_1,\ \dot{u}_2,\ \dot{u}_3,\ \dot{u}_4,\ \dot{v}_1,\ \dot{v}_2,\ \dot{v}_3,\ \dot{v}_4\}$$

and $\{B\}$ is the matrix which gives a relationship between the strains and the nodal displacements. It is noted that $\{B\}$ is a function of r and s.

The stress-strain relationship of Equation (14) is rewritten in a simple form as:

$$\{\dot{\sigma}\} = |D|\{\dot{\varepsilon}\} + \{\dot{\sigma}^{\theta}\} \tag{27}$$

where

$$\{\dot{\sigma}\}^T = \{\dot{\sigma}_x,\ \dot{\sigma}_y,\ \dot{\sigma}_z,\ \tau_{xy}\}$$

$\{D\}$ is the stress-strain relationship matrix and $\{\dot{\sigma}^{\theta}\}$ is the stress vector due to temperature change, and the temperature dependency of material properties and the yield function.

The element stiffness matrix $\{k\}$ is obtained using the principle of virtual work of Equation (1) and Castigliano's theorem as,

$$\{k\} = \int\int\int \{B\}^T\{D\}\{B\}y\ d\theta dxdy \tag{28}$$
$$2\pi\int\int \{B\}^T\{D\}\{B\}y|J|drds$$

where

$$|J| = \begin{vmatrix} \frac{\partial x}{\partial r} & \frac{\partial y}{\partial r} \\ \frac{\partial x}{\partial s} & \frac{\partial y}{\partial s} \end{vmatrix}$$

Introducing a numerical integration, we have

$$\{k\} = 2\pi \sum_{i,j} \{B\}_{ij}^T \{D\}\{B\}_{ij} |J|_{ij} Y_{ij} \alpha_{ij} \tag{29}$$

where subscripts i and j indicate that $Y_{ij}$, $\{B\}$, and $|J|$ are evaluated at points i and j. $\alpha_{ij}$ is weight factor at points i and j in the numerical integration.

The program in the Muraki manual uses the Gauss-Legendre numerical integration and $\alpha_{ij}$ in that scheme can be found in text books on numerical integration.

The element force vector $\{\dot{f}^{\theta}\}$ corresponding to the second term in the right side of Equation (27) is obtained in a similar manner.

$$\begin{aligned} \{\dot{f}^{\theta}\} &= \int\int\int \{B\}^T \{\dot{\sigma}^{\theta}\} y d\theta dx dy \\ &= 2\pi \int\int \{B\}^T \{\dot{\sigma}^{\theta}\} y |J| dr ds \end{aligned} \tag{30}$$

Again introducing the numerical integration we have

$$\{\dot{f}^{\theta}\} = 2\pi \sum_{i,j} \{B\}_{ij}^T \{\dot{\sigma}^{\theta}\} Y_{ij} |J|_{ij} \alpha_{ij} \tag{31}$$

In the current version of the computer program described in the Muraki manual, only the static load considered is the

is the concentrated load at nodal points. Therefore there is no other element force.

The stiffness matrix and force vector for the whole body (i.e. the whole system) are obtained by assembling the element stiffness matrices and force vectors.

The equilibrium equations for the whole system are obtained as

$$\sum_i \{k\}_i \{\dot{Q}\} + \sum_i \{\dot{f}^{\theta}\}_i = \sum_j \{\dot{\bar{F}}\}_j \qquad (32)$$

where i and j stand for the i-th element and the j-th node respectively.

$\{\dot{Q}\}$ is the vector of the time rate of nodal displacement. $\{\dot{\bar{F}}\}$ is the vector of the time rate of concentrated load.

Equation (32) is further written in the incremental form as follows:

$$\sum_i \{k\}_i \{\Delta Q\} + \sum_i \{\Delta f^{\theta}\}_i = \sum_j \{\Delta \bar{F}\}_j \qquad (33)$$

where

$$\Delta Q = \dot{Q}\Delta t$$

$$\Delta f^{\theta} = \dot{f}^{\theta}\Delta t$$

$$\Delta \bar{F} = \dot{\bar{F}}\Delta t$$

$\Delta t$ is the time increment.

It is noted that the time increment is included in Equation (33) implicitly.

Once the nodal displacements for the system, $\{\Delta Q\}$, are obtained, the element strains are calculated by Equation (26) and then the corresponding stresses by Equation (27).

When there is no further increment of concentrated and/or thermal loads, the analysis is complete.

When there is another increment of the loads, new equilibrium equations are calculated using the nodal displacements and stresses obtained in the preceding calculation. This procedure of incremental analysis continues until the final increment is solved.

2. Geometry of Weld Specimen and Finite Element Representation of Weldment used by Muraki Program:

Finite element representation of the weldment is depicted in Figure V-2. A comparison of Figure V-2 with the finite element representation of the weldment, Figure V-1, used in the heat flow program will show that an axis transformation as well as a shift of the origin were required in order to use heat flow program output as input for the Muraki Program.

For the Muraki program, the y-axis corresponds to the radial direction and the x-axis is along the cylinder length. The z-axis corresponds to the direction of welding arc travel, normal to the x-y plane as shown in Figure V-2, positive direction out of the paper. The origin (x=y=0) for the Muraki program analysis corresponds to a point at the center of the cylinder end. z=0 corresponds to the time of arc initiation.

The Muraki program also required the specification of nodal coordinates (x,y values). Element connectivity was input to the Muraki program by identification of the nodes, in counterclockwise fashion beginning with the node closest to the heat source, associated with each element. Nodal coordinates input to the Muraki program are listed in Table V-B and element connectivity is shown in Table V-C.

Thermophysical material properties required by the Muraki program were taken from Figures II-1 through II-10

in Chapter II of this study. Welding parameters required as input data for the first pass of the girth weld were the same as those used by the heat flow program. These parameters were discussed and values presented earlier in this chapter.

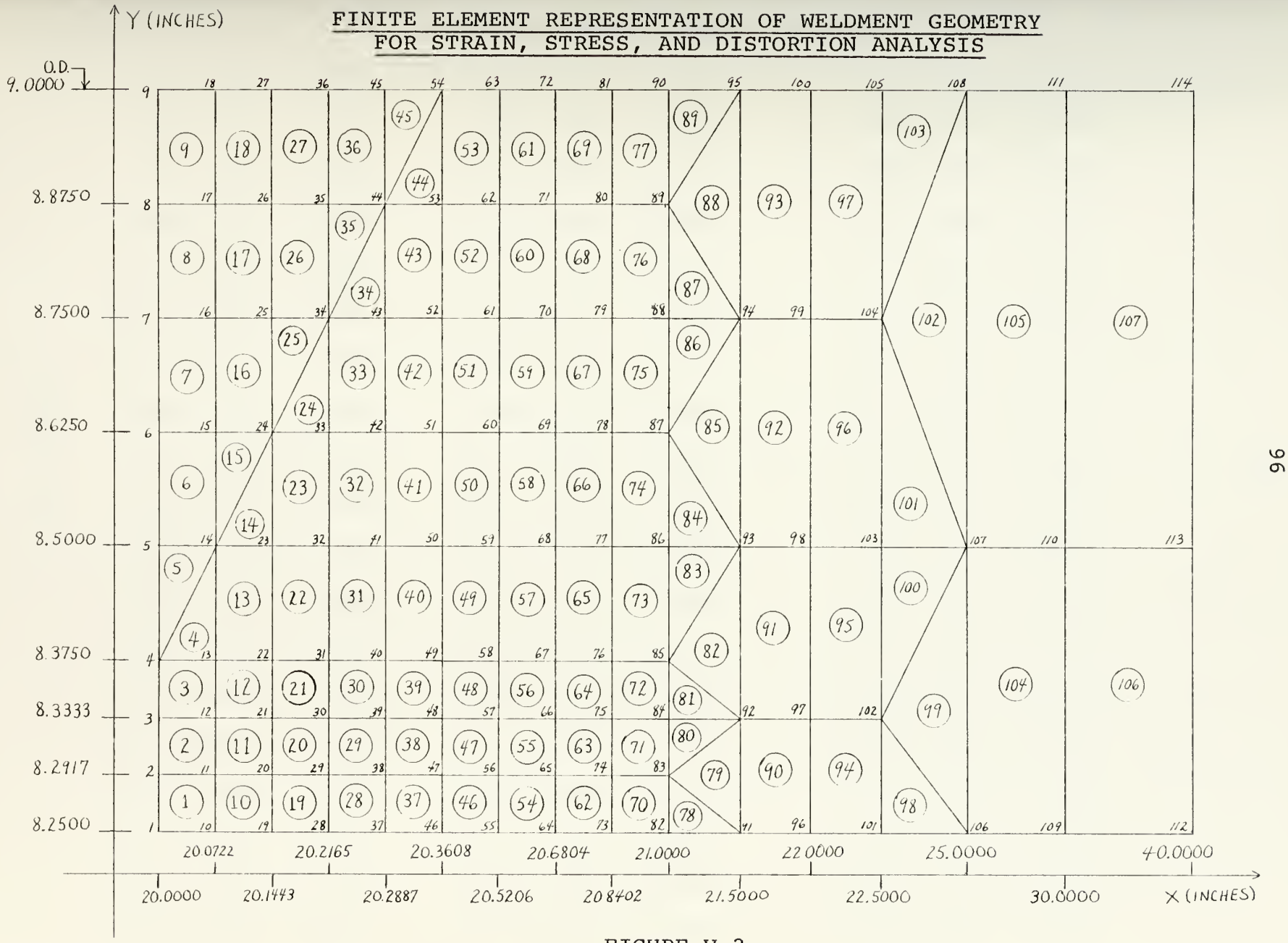
FINITE ELEMENT REPRESENTATION OF WELDMENT GEOMETRY
FOR STRAIN, STRESS, AND DISTORTION ANALYSIS
Y (INCHES)
O.D.
9.0000
8.8750
8.7500
8.6250
8.5000
8.3750
8.3333
8.2917
8.2500
20.0722
20.2165
20.3608
20.6804
21.0000
22.0000
25.0000
40.0000
20.0000
20.1443
20.2887
20.5206
20.8402
21.5000
22.5000
30.0000
X (INCHES)

FIGURE V-2

## NODE COORDINATES (MURAKI PROGRAM)

| | | |
|---|---|---|
| 1(20.0000, 8.2500) | 2(20.0000, 8.2917) | 3(20.0000, 8.3333) |
| 4(20.0000, 8.3750) | 5(20.0000, 8.5000) | 6(20.0000, 8.6250) |
| 7(20.0000, 8.7500) | 8(20.0000, 8.8750) | 9(20.0000, 9.0000) |
| 10(20.0722, 8.2500) | 11(20.0722, 8.2917) | 12(20.0722, 8.3333) |
| 13(20.0722, 8.3750) | 14(20.0722, 8.5000) | 15(20.0722, 8.6250) |
| 16(20.0722, 8.7500) | 17(20.0722, 8.8750) | 18(20.0722, 9.0000) |
| 19(20.1443, 8.2500) | 20(20.1443, 8.2917) | 21(20.1443, 8.3333) |
| 22(20.1443, 8.3750) | 23(20.1443, 8.5000) | 24(20.1443, 8.6250) |
| 25(20.1443, 8.7500) | 26(20.1443, 8.8750) | 27(20.1443, 9.0000) |
| 28(20.2165, 8.2500) | 29(20.2165, 8.2917) | 30(20.2165, 8.3333) |
| 31(20.2165, 8.3750) | 32(20.2165, 8.5000) | 33(20.2165, 8.6250) |
| 34(20.2165, 8.7500) | 35(20.2165, 8.8750) | 36(20.2165, 9.0000) |
| 37(20.2887, 8.2500) | 38(20.2887, 8.2917) | 39(20.2887, 8.3333) |
| 40(20.2887, 8.3750) | 41(20.2887, 8.5000) | 42(20.2887, 8.6250) |
| 43(20.2887, 8.7500) | 44(20.2887, 8.8750) | 45(20.2887, 9.0000) |
| 46(20.3608, 8.2500) | 47(20.3608, 8.2917) | 48(20.3608, 8.3333) |
| 49(20.3608, 8.3750) | 50(20.3608, 8.5000) | 51(20.3608, 8.6250) |
| 52(20.3608, 8.7500) | 53(20.3608, 8.8750) | 54(20.3608, 9.0000) |
| 55(20.5206, 8.2500) | 56(20.5206, 8.2917) | 57(20.5206, 8.3333) |

TABLE V-B

NODE COORDINATES (MURAKI PROGRAM - Cont'd)

| | | |
|---|---|---|
| 58(20.5206, 8.3750) | 59(20.5206, 8.5000) | 60(20.5206, 8.6250) |
| 61(20.5206, 8.7500) | 62(20.5206, 8.8750) | 63(20.5206, 9.0000) |
| 64(20.6804, 8.2500) | 65(20.6804, 8.2917) | 66(20.6804, 8.3333) |
| 67(20.6804, 8.3750) | 68(20.6804, 8.5000) | 69(20.6804, 8.6250) |
| 70(20.6804, 8.7500) | 71(20.6804, 8.8750) | 72(20.6804, 9.0000) |
| 73(20.8402, 8.2500) | 74(20.8402, 8.2917) | 75(20.8402, 8.3333) |
| 76(20.8402, 8.3750) | 77(20.8402, 8.5000) | 78(20.8402, 8.6250) |
| 79(20.8402, 8.7500) | 80(20.8402, 8.8750) | 81(20.8402, 9.0000) |
| 82(21.0000, 8.2500) | 83(21.0000, 8.2917) | 84(21.0000, 8.3333) |
| 85(21.0000, 8.3750) | 86(21.0000, 8.5000) | 87(21.0000, 8.6250) |
| 88(21.0000, 8.7500) | 89(21.0000, 8.8750) | 90(21.0000, 9.0000) |
| 91(21.5000, 8.2500) | 92(21.5000, 8.3333) | 93(21.5000, 8.5000) |
| 94(21.5000, 8.7500) | 95(21.5000, 9.0000) | 96(22.0000, 8.2500) |
| 97(22.0000, 8.3333) | 98(22.0000, 8.5000) | 99(22.0000, 8.7500) |
| 100(22.0000, 9.0000) | 101(22.5000, 8.2500) | 102(22.5000, 8.3333) |
| 103(22.5000, 8.5000) | 104(22.5000, 8.7500) | 105(22.5000, 9.0000) |
| 106(25.0000, 8.2500) | 107(25.0000, 8.5000) | 108(25.0000, 9.0000) |
| 109(30.0000, 8.2500) | 110(30.0000, 8.5000) | 111(30.0000, 9.0000) |
| 112(40.0000, 8.2500) | 113(40.0000, 8.5000) | 114(40.0000, 9.0000) |

TABLE V-B (Cont'd)

## FINITE ELEMENT CONNECTIVITY (MURAKI PROGRAM)
## NODE NUMBERS IN EACH ELEMENT

| | | |
|---|---|---|
| 1(1, 10, 11, 2) | 2(2, 11, 12, 3) | 3(3, 12, 13, 4) |
| 4(4, 13, 14, 0) | 5(4, 14, 5, 0) | 6(5, 14, 15, 6) |
| 7(6, 15, 16, 7) | 8(7, 16, 17, 8) | 9(8, 17, 18, 9) |
| 10(10, 19, 20, 11) | 11(11, 20, 21, 12) | 12(12, 21, 22, 13) |
| 13(13, 22, 23, 14) | 14(14, 23, 24, 0) | 15(14, 24, 15, 0) |
| 16(15, 24, 25, 16) | 17(16, 25, 26, 17) | 18(17, 26, 27, 18) |
| 19(19, 28, 29, 20) | 20(20, 29, 30, 21) | 21(21, 30, 31, 22) |
| 22(22, 31, 32, 23) | 23(23, 32, 33, 24) | 24(24, 33, 34, 0) |
| 25(24, 34, 25, 0) | 26(25, 34, 35, 26) | 27(26, 35, 36, 27) |
| 28(28, 37, 38, 29) | 29(29, 38, 39, 30) | 30(30, 39, 40, 31) |
| 31(31, 40, 41, 32) | 32(32, 41, 42, 33) | 33(33, 42, 43, 34) |
| 34(34, 43, 44, 0) | 35(34, 44, 35, 0) | 36(35, 44, 45, 36) |
| 37(37, 46, 47, 38) | 38(38, 47, 48, 39) | 39(39, 48, 49, 40) |
| 40(40, 49, 50, 41) | 41(41, 50, 51, 42) | 42(42, 51, 52, 43) |
| 43(43, 52, 53, 44) | 44(44, 53, 54, 0) | 45(44, 54, 45, 0) |
| 46(46, 55, 56, 47) | 47(47, 56, 57, 48) | 48(48, 57, 58, 49) |
| 49(49, 58, 59, 50) | 50(50, 59, 60, 51) | 51(51, 60, 61, 52) |
| 52(52, 61, 62, 53) | 53(53, 62, 63, 54) | 54(55, 64, 65, 56) |

TABLE V-C

NODAL CONNECTIVITY (Cont'd)

| | | |
|---|---|---|
| 55(56, 65, 66, 57) | 56(57, 66, 67, 58) | 57(58, 67, 68, 59) |
| 58(59, 68, 69, 60) | 59(60, 69, 70, 61) | 60(61, 70, 71, 62) |
| 61(62, 71, 72, 63) | 62(64, 73, 74, 65) | 63(65, 74, 75, 66) |
| 64(66, 75, 76, 67) | 65(67, 76, 77, 68) | 66(68, 77, 78, 69) |
| 67(69, 78, 79, 70) | 68(70, 79, 80, 71) | 69(71, 80, 81, 72) |
| 70(73, 82, 83, 74) | 71(74, 83, 84, 75) | 72(75, 84, 85, 76) |
| 73(76, 85, 86, 77) | 74(77, 86, 87, 78) | 75(78, 87, 88, 79) |
| 76(79, 88, 89, 80) | 77(80, 89, 90, 81) | 78(82, 91, 83, 0) |
| 79(83, 91, 92, 0) | 80(83, 92, 84, 0) | 81(84, 92, 85, 0) |
| 82(85, 92, 93, 0) | 83(85, 93, 86, 0) | 84(86, 93, 87, 0) |
| 85(87, 93, 94, 0) | 86(87, 94, 88, 0) | 87(88, 94, 89, 0) |
| 88(89, 94, 95, 0) | 89(89, 95, 90, 0) | 90(91, 96, 97, 92) |
| 91(92, 97, 98, 93) | 92(93, 98, 99, 94) | 93(94, 99, 100, 95) |
| 94(96, 101, 102, 97) | 95(97, 102, 103, 98) | 96(98, 103, 104, 99) |
| 97(99, 104, 105, 100) | 98(101, 106, 102, 0) | 99(102, 106, 107, 0) |
| 100(102, 107, 103, 0) | 101(103, 107, 104, 0) | 102(104, 107, 108, 0) |
| 103(104, 108, 105, 0) | 104(106, 109, 110, 107) | 105(107, 110, 111, 108) |
| 106(109, 112, 113, 110) | 107(110, 113, 114, 111) | |

TABLE V-C (Cont'd)

# CHAPTER VI

Comparison of temperatures and values of strain, stress, and distortion during production of the HY-130 cylinder girth weld with those predicted by use of the heat flow and Muraki programs follows in the form of tabulated data and in graphical presentations. During production of the girth weld, arc travel began at the seam weld opposite the cylinder seam about which thermocouples and strain gages were placed. Times at which data comparisons are presented were selected as representing a thermal cycle during which temperature, strains, stress, and distortion underwent greatest changes.

Temperatures determined experimentally at the eight thermocouple locations for the times of interest are shown in Table VI-A. Distances from weld centerline are indicated beside the column headings designated T1, T2, T3, T4, T4', T3', T2', and T1'. These temperatures are presented graphically in Figure VI-1. Temperature distribution predicted by use of the heat flow program is presented by a computer generated graph, Figure VI-2.

Qualitative comparison of the analytical and measured temperature distributions shows remarkable coincidence. The slightly higher overall values of the analytically generated values may be explained by the assumed welding arc efficiency ($\eta_{arc}$) of 0.65.

| TIME(SEC) | TEMPERATURE($^{o}$F) | | | | | | | |
|---|---|---|---|---|---|---|---|---|
| | T1(1.0) | T2(1.5) | T3(2.0) | T4(2.5) | T4'(2.5) | T3'(2.0) | T2'(1.5) | T1'(1.0) |
| 125.0 | 200 | 200 | 200 | 200 | 200 | 200 | 200 | 200 |
| 127.0 | 200 | 200 | 200 | 200 | 200 | 200 | 200 | 200 |
| 128.0 | 202 | 200 | 200 | 200 | 200 | 200 | 200 | 200 |
| 129.0 | 203 | 200 | 200 | 200 | 200 | 200 | 200 | 200 |
| 129.5 | 205 | 200 | 200 | 200 | 200 | 200 | 200 | 200 |
| 130.0 | 205 | 200 | 200 | 200 | 200 | 200 | 200 | 200 |
| 130.5 | 205 | 200 | 200 | 200 | 200 | 200 | 200 | 200 |
| 131.0 | 205 | 200 | 200 | 200 | 200 | 200 | 200 | 200 |
| 132.0 | 205 | 200 | 200 | 200 | 200 | 200 | 200 | 200 |
| 133.0 | 207 | 200 | 200 | 200 | 200 | 200 | 200 | 200 |
| 134.0 | 210 | 201 | 200 | 200 | 200 | 200 | 200 | 200 |
| 135.0 | 218 | 202 | 200 | 200 | 200 | 200 | 200 | 200 |
| 136.0 | 230 | 202 | 200 | 200 | 200 | 203 | 202 | 203 |
| 137.5 | 257 | 205 | 202 | 200 | 200 | 205 | 205 | 215 |
| 140.0 | 320 | 209 | 205 | 200 | 203 | 208 | 210 | 250 |
| 145.0 | 415 | 233 | 210 | 200 | 205 | 210 | 225 | 350 |
| 150.0 | 462 | 266 | 217 | 202 | 208 | 215 | 252 | 415 |
| 155.0 | 485 | 300 | 229 | 207 | 208 | 226 | 285 | 455 |
| 160.0 | 496 | 329 | 240 | 210 | 210 | 240 | 310 | 474 |
| 170.0 | 502 | 352 | 265 | 220 | 225 | 272 | 352 | 490 |
| 200.0 | 480 | 405 | 318 | 265 | 274 | 338 | 396 | 482 |

TABLE VI-A EXPERIMENTALLY DETERMINED TEMPERATURE DISTRIBUTION

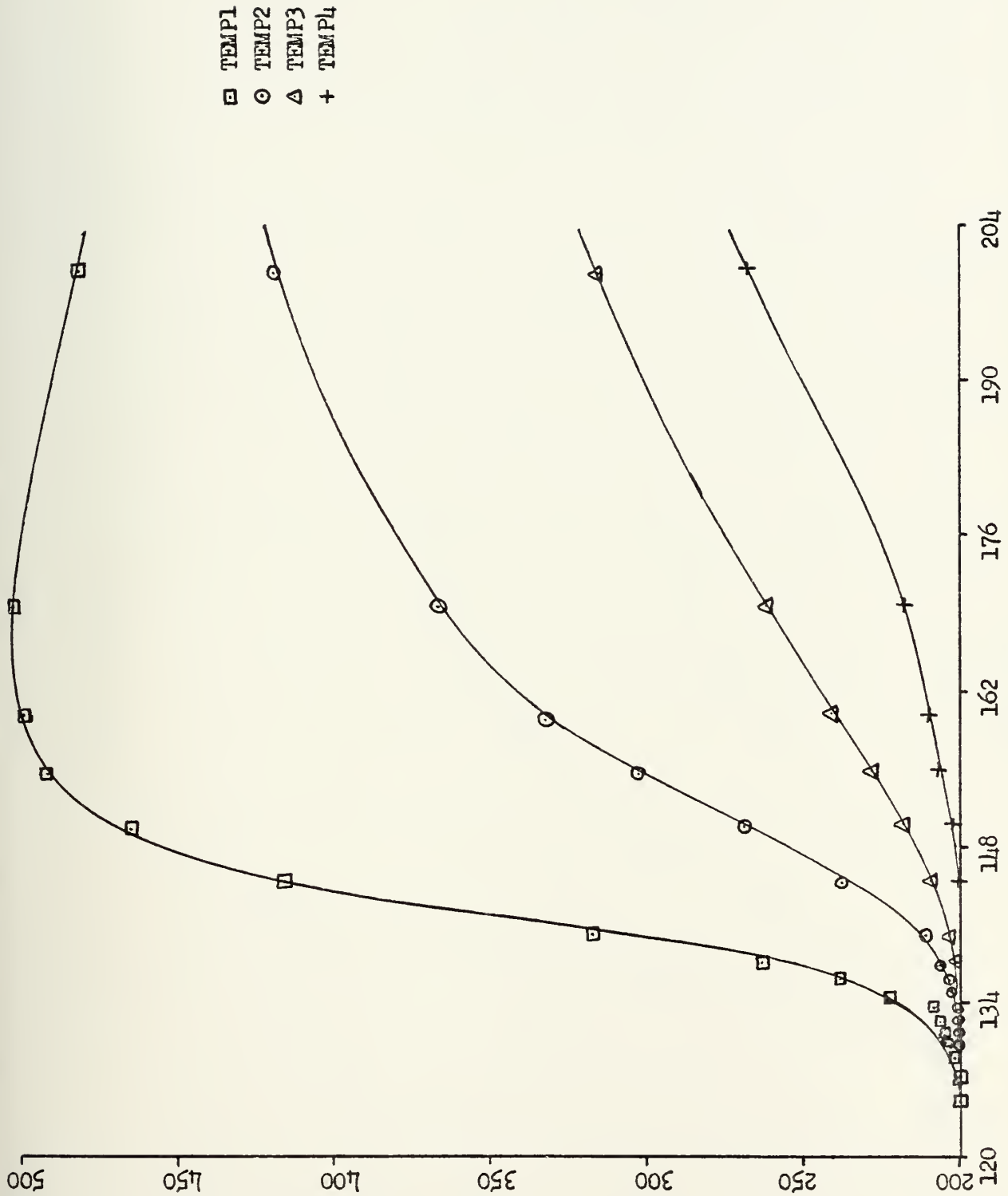


FIGURE VI-1 GRAPH OF EXPERIMENTALLY DETERMINED TEMPERATURES

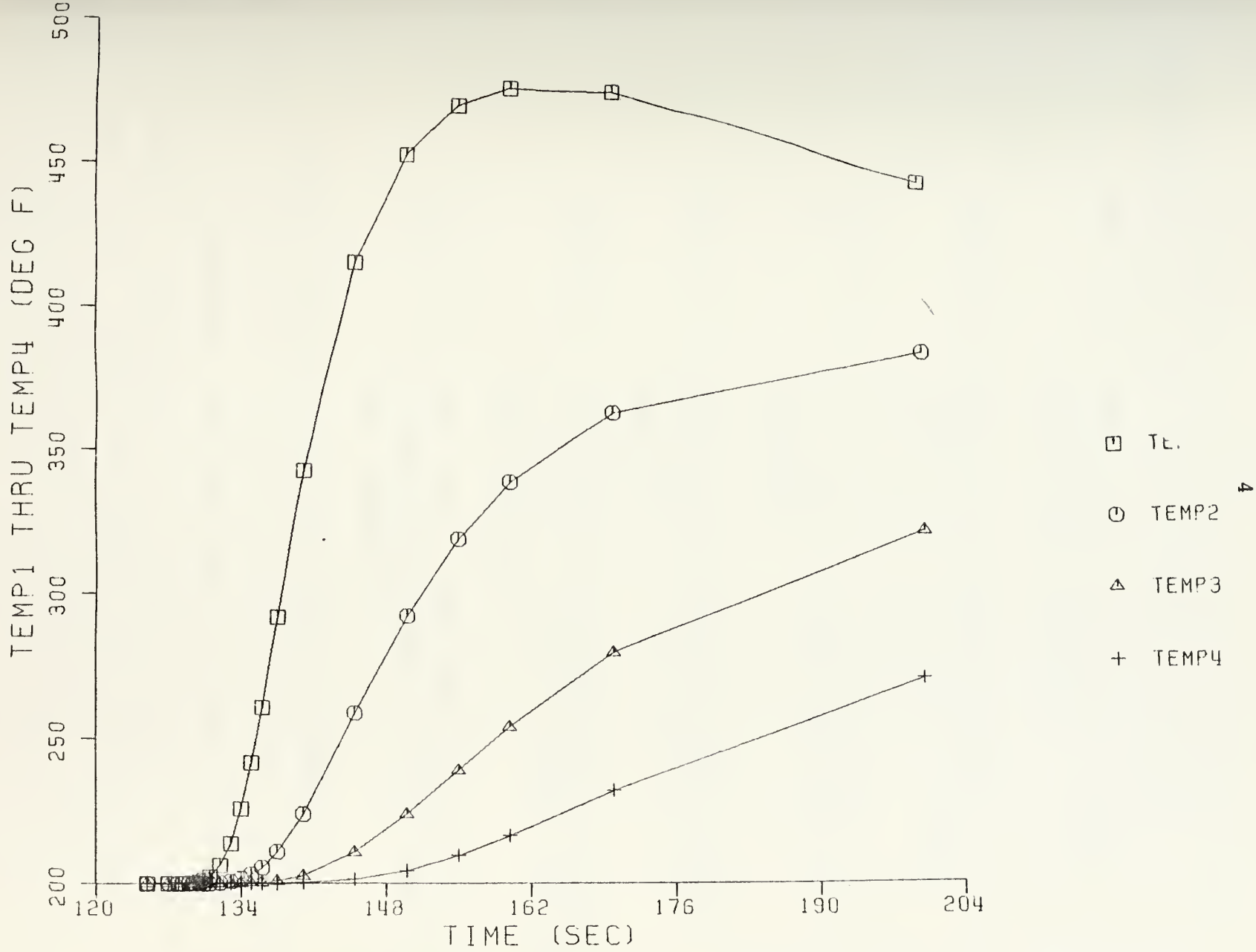


FIGURE VI-2 COMPUTER GENERATED GRAPH OF ANALYTICALLY PREDICTED TEMPERATURES

For the purpose of presenting comparative strain, stress, and distortion data, the following terms are defined:

STR(*.*)X = EXPERIMENTALLY DETERMINED STRAIN (MICROSTRAIN) AT A POINT *.* INCHES FROM THE WELD CENTERLINE.

STR(*.*)A = ANALYTICALLY PREDICTED STRAIN (MICROSTRAIN) AT A POINT *.* INCHES FROM THE WELD CENTERLINE.

STS(*.*)X = EXPERIMENTALLY DETERMINED STRESS ($lbf/_{in}^2$) AT A POINT *.* INCHES FROM THE WELD CENTERLINE.

STS(*.*)A = ANALYTICALLY PREDICTED STRESS ($lbf/_{in}^2$) AT A POINT *.* INCHES FROM THE WELD CENTERLINE.

DST(*.*)X = EXPERIMENTALLY MEASURED RADIAL DISTORTION IN INCHES AT A POINT *.* INCHES FROM THE WELD CENTERLINE.

DST(*.*)A = ANALYTICALLY PREDICTED RADIAL DISTORTION IN INCHES AT A POINT *.* INCHES FROM THE WELD CENTERLINE.

Positive values of strain and stress correspond to the tensile condition and negative values correspond to compressive strains and stresses. Positive values of radial distortion correspond to displacement in an outward direction from the cylinder center. Tables and graphs on the following pages use the terms as defined above to compare data. Strain and Stress directions correspond to directions shown in Figure V-2.

Tables VI-B through VI-E present in tabular form comparisons between strains measured during production of the HY-130 cylinder girth weld and those predicted by use of the Muraki program. Tables VI-F through VI-I present the analytically predicted stresses. Experimentally determined stresses were not tabulated since experimentally determined strains could not be transformed into stresses. There are three (ignoring creep) components of strain; elastic, plastic, and thermal. Elastic and thermal constitutive relations are simple and the stresses resulting therefrom could be calculated if these strains could be separated into their components. However, the constitutive relationships among elastic, plastic, and thermal strains are complex, made further so by the presence of a strain hardening material and by the dependence of all material properties on temperature. For this reason, experimentally determined strains could not be transformed into stresses. Values of radial distortion measured during production of the girth weld and predicted by the Muraki program are shown in Table VI-J. Comparative graphs of measured and predicted data are shown in Figures VI-3 through VI-9.

| | LONGITUDINAL STRAIN (X-DIRECTION) | | TRANSVERSE STRAIN (Z-DIRECTION) | |
|---|---|---|---|---|
| TIME(sec) | STR(1.0)X | STR(1.0)A | STR(1.0)X | STR(1.0)A |
| 125.0 | -44 | 0 | 200 | 0 |
| 127.0 | -130 | 0 | 235 | 0 |
| 128.0 | -153 | 0 | 277 | 0 |
| 129.0 | -177 | 10 | 318 | 18 |
| 129.5 | -190 | -2 | 365 | 32 |
| 130.0 | -198 | -23 | 370 | 51 |
| 130.5 | -198 | -127 | 405 | 132 |
| 131.0 | -185 | -305 | 420 | 279 |
| 132.0 | -185 | -420 | 475 | 391 |
| 133.0 | -228 | -350 | 607 | 387 |
| 134.0 | -390 | -271 | 780 | 401 |
| 135.0 | -608 | -177 | 922 | 420 |
| 136.0 | -823 | -68 | 967 | 446 |
| 137.5 | -933 | 127 | 902 | 481 |
| 140.0 | -818 | 474 | 527 | 531 |
| 145.0 | -464 | 1090 | -194 | 600 |
| 150.0 | -370 | 1530 | -319 | 641 |
| 155.0 | -4 | 1820 | -184 | 668 |
| 160.0 | 0 | 1930 | -129 | 680 |
| 170.0 | 49 | 2200 | -94 | 714 |
| 200.0 | 176 | 2250 | -49 | 726 |

TABLE VI-B EXPERIMENTAL AND ANALYTICAL STRAIN 1.0 IN FROM WELD CENTERLINE

| | LONGITUDINAL STRAIN (X-DIRECTION) | | TRANSVERSE STRAIN (Z-DIRECTION | |
|---|---|---|---|---|
| TIME(sec) | STR(1.5)X | STR(1.5)A | STR(1.5)X | STR(1.5)A |
| 125.0 | -245 | 0 | 320 | 0 |
| 127.0 | -310 | 0 | 365 | 0 |
| 128.0 | -325 | 0 | 395 | 1 |
| 129.0 | -345 | 2 | 410 | 16 |
| 129.5 | -345 | -70 | 425 | 27 |
| 130.0 | -345 | -21 | 450 | 41 |
| 130.5 | -340 | -105 | 470 | 92 |
| 131.0 | -340 | -259 | 485 | 185 |
| 132.0 | -330 | -358 | 505 | 260 |
| 133.0 | -330 | -318 | 570 | 263 |
| 134.0 | -320 | -297 | 626 | 277 |
| 135.0 | -325 | -288 | 681 | 293 |
| 136.0 | -330 | -283 | 706 | 311 |
| 137.5 | -335 | -265 | 750 | 336 |
| 140.0 | -340 | -205 | 749 | 373 |
| 145.0 | -330 | 11 | 664 | 433 |
| 150.0 | -350 | 276 | 560 | 477 |
| 155.0 | -400 | 527 | 496 | 513 |
| 160.0 | -390 | 651 | 427 | 530 |
| 170.0 | -330 | 1060 | 257 | 590 |
| 200.0 | -291 | 1490 | -246 | 666 |

TABLE VI-C EXPERIMENTAL AND ANALYTICAL STRAIN 1.5 IN FROM WELD CENTERLINE

| | LONGITUDINAL STRAIN (X-DIRECTION) | | TRANSVERSE STRAIN (Z-DIRECTION) | |
|---|---|---|---|---|
| TIME(sec) | STR(2.0)X | STR(2.0)A | STR(2.0)X | STR(2.0)A |
| 125.0 | -310 | 0 | 315 | 0 |
| 127.0 | -355 | 0 | 385 | 0 |
| 128.0 | -360 | 0 | 395 | 1 |
| 129.0 | -370 | -5 | 410 | 14 |
| 129.5 | -385 | -16 | 435 | 22 |
| 130.0 | -400 | -32 | 440 | 33 |
| 130.5 | -395 | -115 | 445 | 68 |
| 131.0 | -390 | -264 | 455 | 132 |
| 132.0 | -380 | -365 | 460 | 186 |
| 133.0 | -365 | -334 | 475 | 193 |
| 134.0 | -355 | -321 | 490 | 207 |
| 135.0 | -320 | -320 | 498 | 221 |
| 136.0 | -310 | -325 | 500 | 236 |
| 137.5 | -283 | -331 | 502 | 257 |
| 140.0 | -225 | -337 | 520 | 288 |
| 145.0 | -220 | -304 | 555 | 338 |
| 150.0 | -384 | -216 | 606 | 378 |
| 155.0 | -509 | -94 | 666 | 413 |
| 160.0 | -636 | -16 | 689 | 431 |
| 170.0 | -625 | 304 | 600 | 496 |
| 200.0 | -326 | 836 | 164 | 587 |

TABLE VI-D EXPERIMENTAL AND ANALYTICAL STRAIN 2.0 IN FROM WELD CENTERLINE

| | LONGITUDINAL STRAIN (X-DIRECTION) | | TRANSVERSE STRAIN (Z-DIRECTION) | |
|---|---|---|---|---|
| TIME(sec) | STR(2.5)X | STR(2.5)A | STR(2.5)X | STR(2.5)A |
| 125.0 | -175 | 0 | 295 | 0 |
| 127.0 | -220 | 0 | 310 | 0 |
| 128.0 | -250 | 0 | 320 | 1 |
| 129.0 | -265 | -5 | 325 | 11 |
| 129.5 | -265 | -8 | 335 | 16 |
| 130.0 | -265 | -13 | 355 | 24 |
| 130.5 | -265 | -30 | 355 | 47 |
| 131.0 | -265 | -61 | 365 | 88 |
| 132.0 | -265 | -86 | 365 | 124 |
| 133.0 | -260 | -85 | 365 | 132 |
| 134.0 | -260 | -89 | 355 | 143 |
| 135.0 | -255 | -93 | 355 | 154 |
| 136.0 | -245 | -98 | 350 | 166 |
| 137.5 | -223 | -104 | 340 | 182 |
| 140.0 | -125 | -114 | 340 | 205 |
| 145.0 | -115 | -123 | 355 | 244 |
| 150.0 | -249 | -118 | 457 | 276 |
| 155.0 | -379 | -99 | 552 | 305 |
| 160.0 | -501 | -83 | 625 | 320 |
| 170.0 | -560 | 1 | 624 | 377 |
| 200.0 | -376 | 203 | 365 | 463 |

TABLE VI-E EXPERIMENTAL AND ANALYTICAL STRAIN 2.5 IN FROM WELD CENTERLINE

| | LONGITUDINAL STRESS (X-DIRECTION) | | TRANSVERSE STRESS (Z-DIRECTION) | |
|---|---|---|---|---|
| TIME(sec) | STS(1.0)X | STS(1.0)A | STS(1.0)X | STS(1.0)A |
| 125.0 | | 0 | | 0 |
| 127.0 | | 3 | | 22 |
| 128.0 | | 143 | | 374 |
| 129.0 | | 436 | | 593 |
| 129.5 | | 207 | | 888 |
| 130.0 | | -295 | | 1236 |
| 130.5 | | -2658 | | 2669 |
| 131.0 | | -6614 | | 5369 |
| 132.0 | | -9464 | | 11431 |
| 133.0 | | -8670 | | 6405 |
| 134.0 | | -8263 | | 5400 |
| 135.0 | | -8235 | | 3860 |
| 136.0 | | -8420 | | 1908 |
| 137.5 | | -8619 | | -1588 |
| 140.0 | | -8727 | | -7665 |
| 145.0 | | -7337 | | -16930 |
| 150.0 | | -4913 | | -21859 |
| 155.0 | | -2501 | | -24190 |
| 160.0 | | -1321 | | -24732 |
| 170.0 | | 2508 | | -25156 |
| 200.0 | | 6329 | | -21790 |

TABLE VI-F PREDICTED X AND Z DIRECTION STRESSES 1.0 IN FROM WELD CENTERLINE

| | LONGITUDINAL STRESS (X-DIRECTION) | | TRANSVERSE STRESS (Z-DIRECTION) | |
|---|---|---|---|---|
| TIME(sec) | STS(1.5)X | STS(1.5)A | STS(1.5)X | STS(1.5)A |
| 125.0 | | 0 | | 0 |
| 127.0 | | 0 | | 2 |
| 128.0 | | 7 | | 29 |
| 129.0 | | 222 | | 518 |
| 129.5 | | 54 | | 741 |
| 130.0 | | -226 | | 1031 |
| 130.5 | | -2336 | | 1709 |
| 131.0 | | -6161 | | 2950 |
| 132.0 | | -8488 | | 4195 |
| 133.0 | | -7210 | | 4717 |
| 134.0 | | -6482 | | 5298 |
| 135.0 | | -6155 | | 5751 |
| 136.0 | | -6047 | | 6131 |
| 137.5 | | -5846 | | 6464 |
| 140.0 | | -5495 | | 6320 |
| 145.0 | | -4303 | | 4198 |
| 150.0 | | -2819 | | 1155 |
| 155.0 | | -1363 | | -1724 |
| 160.0 | | -612 | | -3085 |
| 170.0 | | 2010 | | -7334 |
| 200.0 | | 5202 | | -10709 |

TABLE VI-G PREDICTED X AND Z DIRECTION STRESSES 1.5 IN FROM WELD CENTERLINE

| | LONGITUDINAL STRESS (X-DIRECTION) | | TRANSVERSE STRESS (Z-DIRECTION) | |
|---|---|---|---|---|
| TIME(sec) | STS(2.0)X | STS(2.0)A | STS(2.0)X | STS(2.0)A |
| 125.0 | | 0 | | 0 |
| 127.0 | | 0 | | 1 |
| 128.0 | | -6 | | 20 |
| 129.0 | | -13 | | 382 |
| 129.5 | | -293 | | 487 |
| 130.0 | | -716 | | 608 |
| 130.5 | | -3141 | | 612 |
| 131.0 | | -7513 | | 621 |
| 132.0 | | -10343 | | 974 |
| 133.0 | | -9197 | | 1626 |
| 134.0 | | -8632 | | 2215 |
| 135.0 | | -8436 | | 2661 |
| 136.0 | | -8476 | | 3045 |
| 137.5 | | -8508 | | 3563 |
| 140.0 | | -8571 | | 4237 |
| 145.0 | | -8168 | | 4976 |
| 150.0 | | -7258 | | 4859 |
| 155.0 | | -6154 | | 4135 |
| 160.0 | | -5498 | | 3548 |
| 170.0 | | -2939 | | 887 |
| 200.0 | | 1115 | | -3872 |

TABLE VI-H PREDICTED X AND Z DIRECTION STRESSES 2.0 IN FROM WELD CENTERLINE

| | LONGITUDINAL STRESS (X-DIRECTION) | | TRANSVERSE STRESS (Z-DIRECTION) | |
|---|---|---|---|---|
| TIME(sec) | STS(2.5)X | STS(2.5)A | STS(2.5)X | STS(2.5)A |
| 125.0 | | 0 | | 0 |
| 127.0 | | 0 | | 1 |
| 128.0 | | -2 | | 17 |
| 129.0 | | -23 | | 295 |
| 129.5 | | -50 | | 450 |
| 130.0 | | -89 | | 656 |
| 130.5 | | -269 | | 1301 |
| 131.0 | | -595 | | 2465 |
| 132.0 | | -827 | | 3487 |
| 133.0 | | -780 | | 3687 |
| 134.0 | | -772 | | 4001 |
| 135.0 | | -782 | | 4299 |
| 136.0 | | -807 | | 4618 |
| 137.5 | | -842 | | 5036 |
| 140.0 | | -889 | | 5658 |
| 145.0 | | -958 | | 6567 |
| 150.0 | | -1025 | | 7051 |
| 155.0 | | -1140 | | 7139 |
| 160.0 | | -1231 | | 7013 |
| 170.0 | | -1689 | | 5963 |
| 200.0 | | -2710 | | 2510 |

TABLE VI-I PREDICTED X AND Z DIRECTION STRESSES 2.5 IN FROM WELD CENTERLINE

| | RADIAL DISTORTION (Y-DIRECTION) | | RADIAL DISTORTION (Y-DIRECTION) | |
|---|---|---|---|---|
| TIME(sec) | DST(0.5)X | DST(0.5)A | DST(1.0)X | DST(1.0)A |
| 125.0 | 0.0000 | 0.0000 | 0.0000 | 0.0000 |
| 127.0 | 0.0000 | 0.0000 | 0.0000 | 0.0000 |
| 128.0 | 0.0000 | 0.0000 | 0.0000 | 0.0000 |
| 129.0 | 0.0000 | 0.0000 | 0.0000 | 0.0000 |
| 129.5 | 0.0000 | 0.0002 | 0.0000 | 0.0000 |
| 130.0 | * | 0.0002 | * | 0.0005 |
| 130.5 | * | 0.0009 | * | 0.0013 |
| 131.0 | * | 0.0026 | * | 0.0028 |
| 132.0 | 0.001 | 0.0035 | 0.001 | 0.0038 |
| 133.0 | 0.001 | 0.0029 | 0.001 | 0.0037 |
| 134.0 | 0.001 | 0.0028 | 0.001 | 0.0037 |
| 135.0 | 0.001 | 0.0028 | 0.001 | 0.0037 |
| 136.0 | 0.002 | 0.0029 | 0.002 | 0.0038 |
| 137.5 | 0.002 | 0.0032 | 0.002 | 0.0039 |
| 140.0 | 0.003 | 0.0035 | 0.003 | 0.0041 |
| 145.0 | 0.003 | 0.0039 | 0.004 | 0.0044 |
| 150.0 | 0.003 | 0.0041 | 0.004 | 0.0045 |
| 155.0 | 0.003 | 0.0043 | 0.004 | 0.0046 |
| 160.0 | 0.003 | 0.0044 | 0.004 | 0.0047 |
| 170.0 | 0.002 | 0.0046 | 0.004 | 0.0049 |
| 200.0 | 0.002 | 0.0049 | 0.003 | 0.0052 |

*DEFLECTION TOO SMALL TO QUANTIFY

TABLE VI-J EXPERIMENTAL AND ANALYTICAL DISTORTION 0.5 IN AND 1.0 IN FROM WELD CENTERLINE

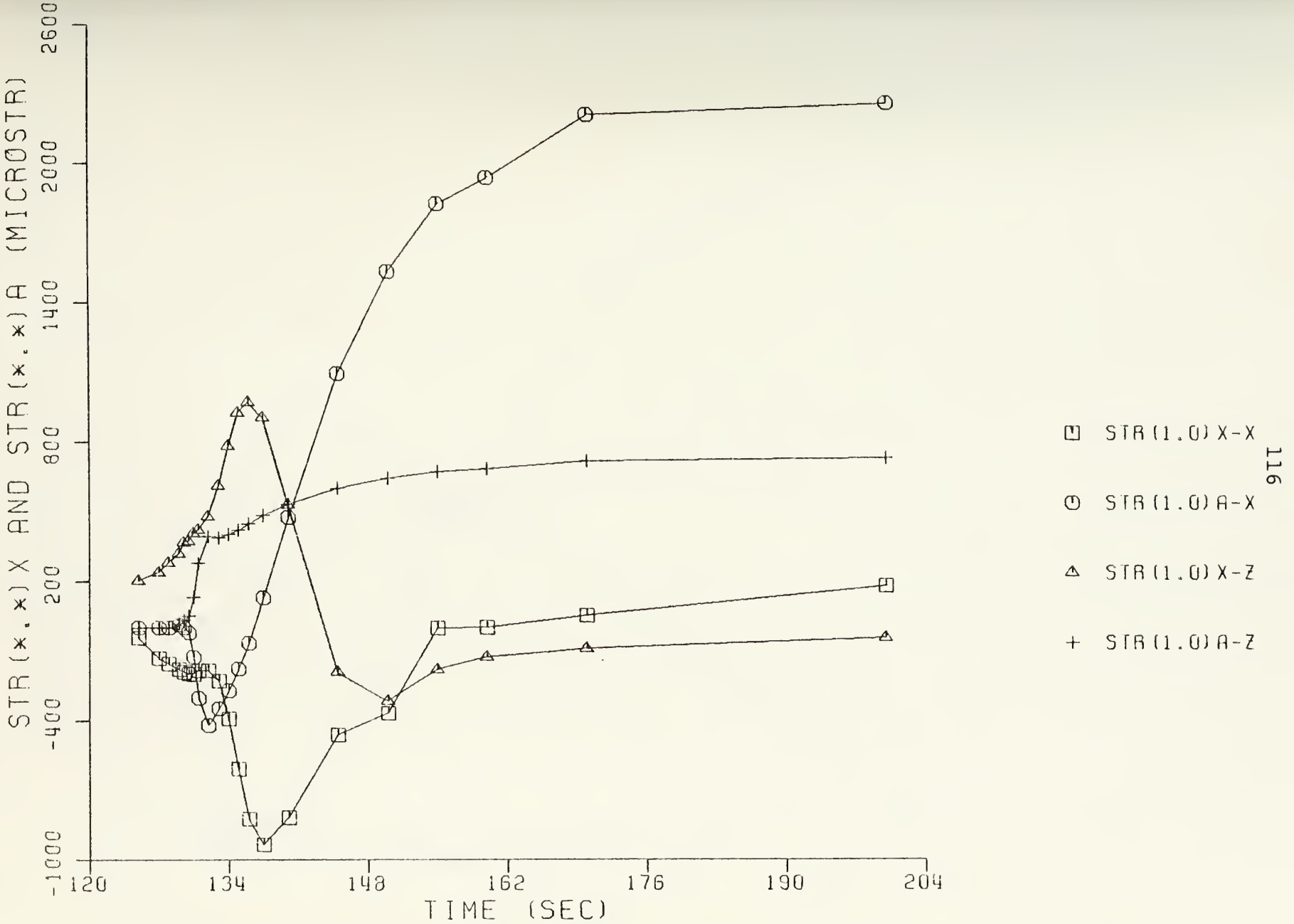




FIGURE VI-3 COMPARATIVE PLOT OF EXPERIMENTAL AND ANALYTICAL STRAIN 1.0 IN FROM WELD CENTERLINE

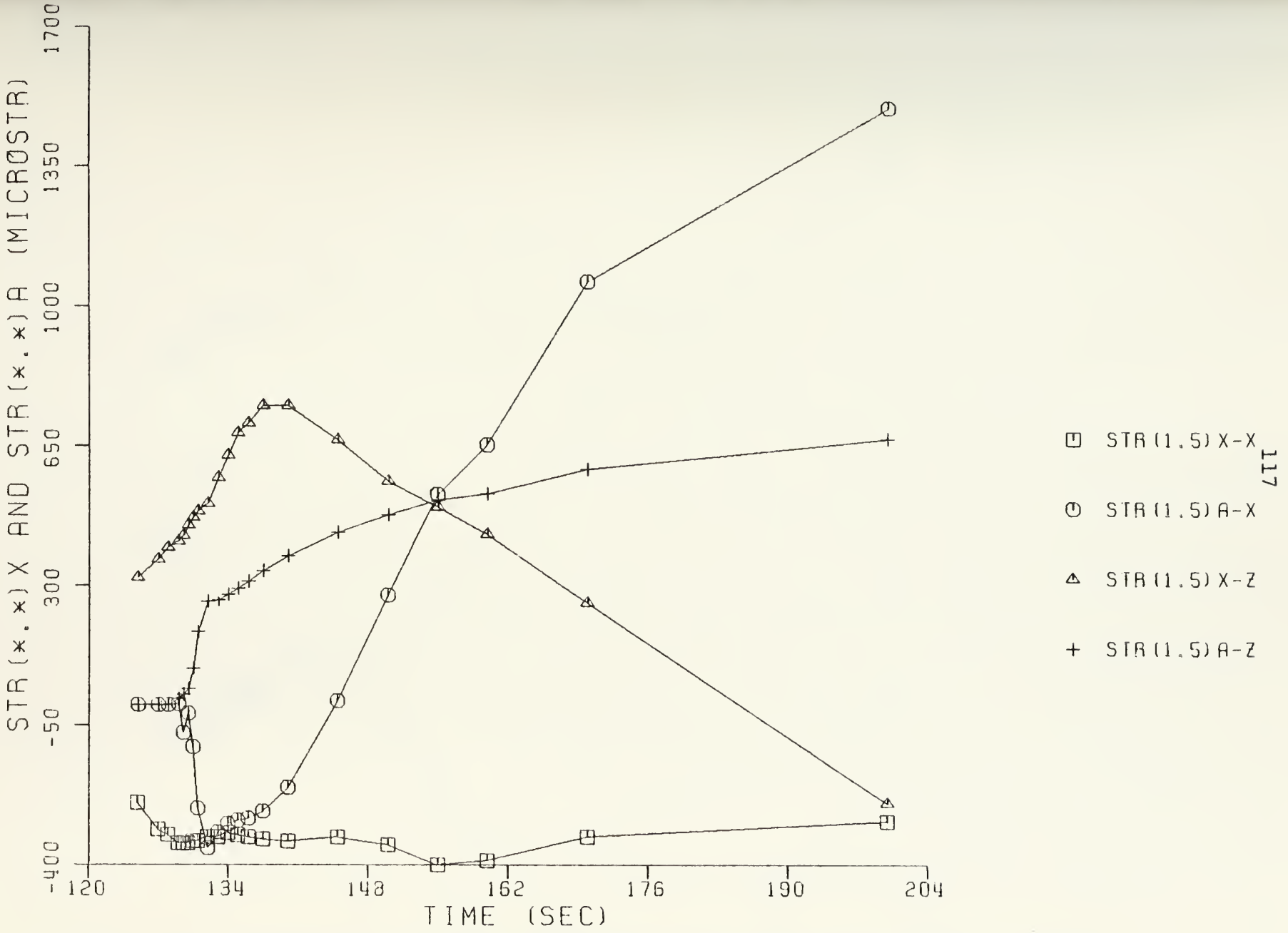


FIGURE VI-4 COMPARATIVE PLOT OF EXPERIMENTAL AND ANALYTICAL STRAIN 1.5 IN FROM WELD CENTERLINE

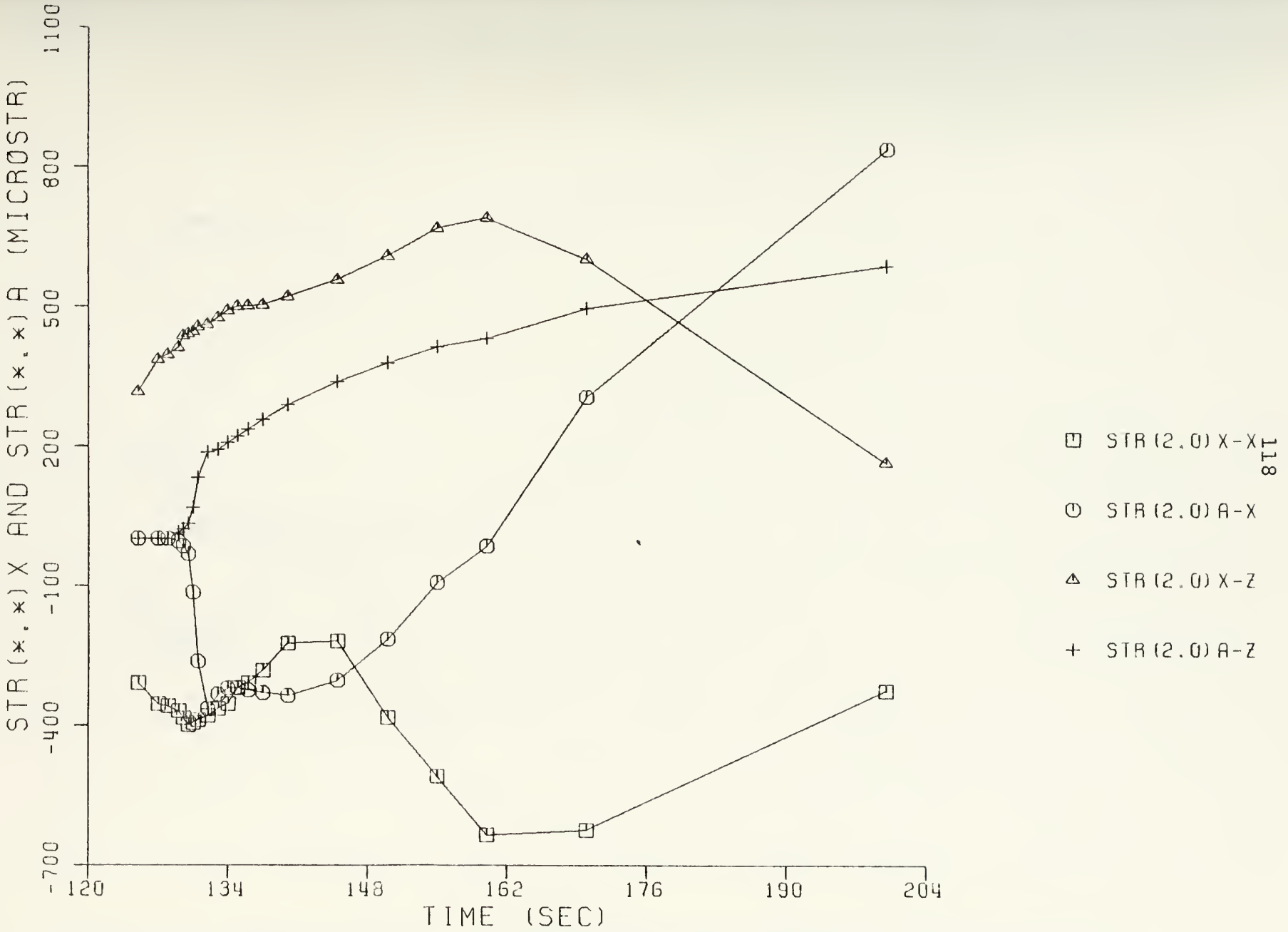




FIGURE VI-5 COMPARATIVE PLOT OF EXPERIMENTAL AND ANALYTICAL STRAIN 2.0 IN FROM WELD CENTERLINE

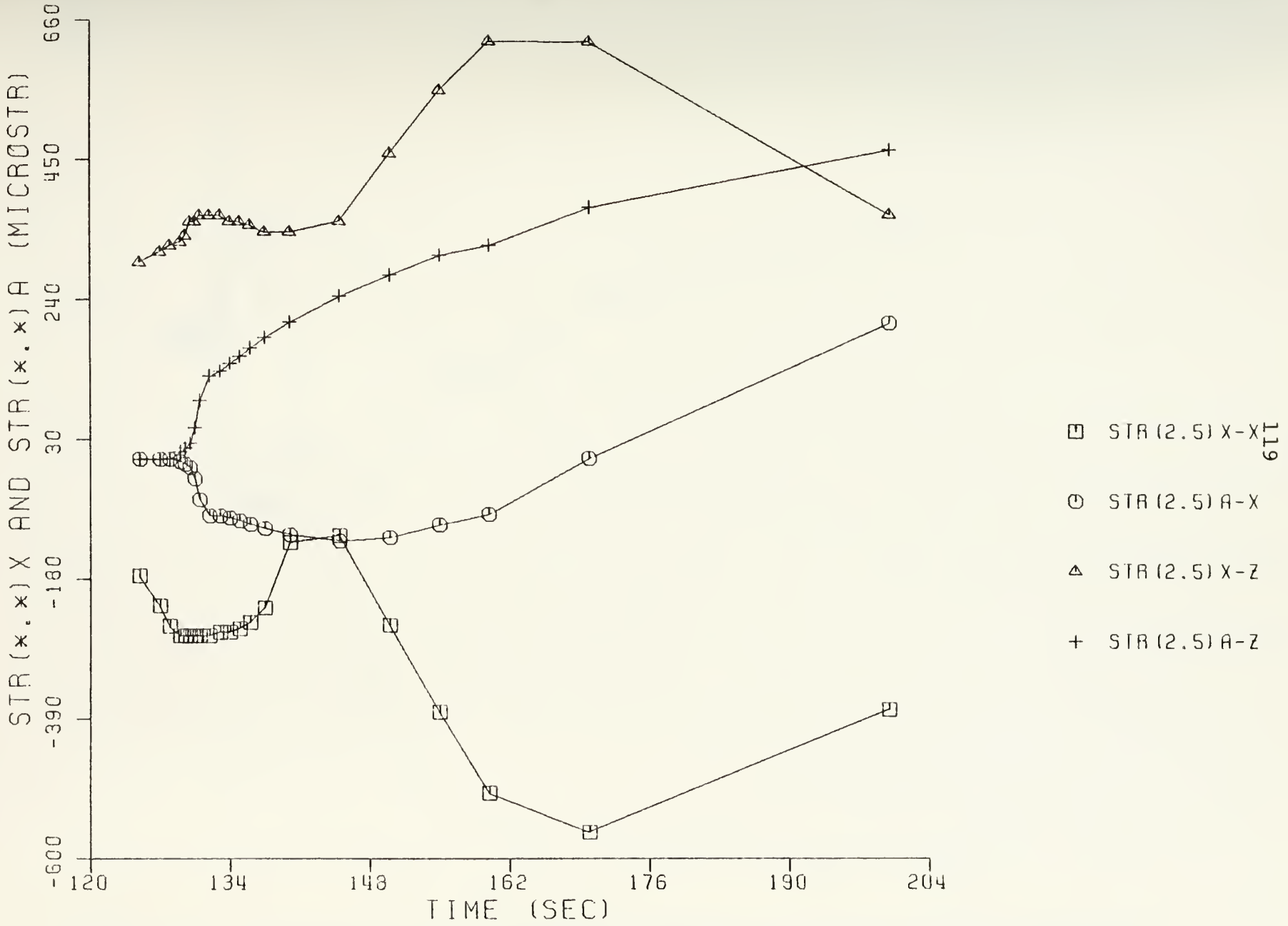


FIGURE VI-6 COMPARATIVE PLOT OF EXPERIMENTAL AND ANALYTICAL STRAIN 2.5 IN FROM WELD CENTERLINE

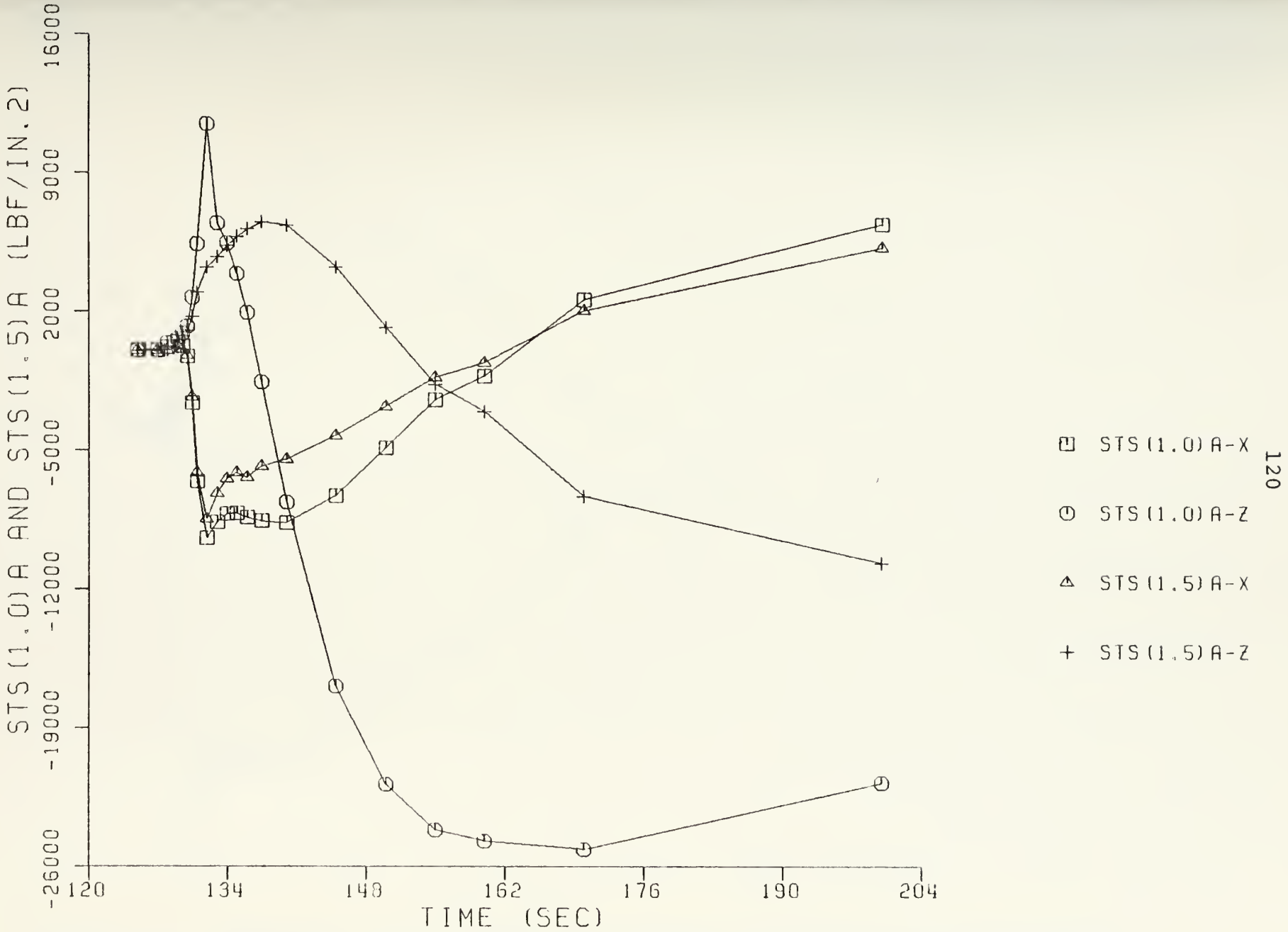


FIGURE VI-7 PREDICTED X AND Z DIRECTION STRESSES 1.0 IN AND 1.5 IN FROM WELD CENTERLINE

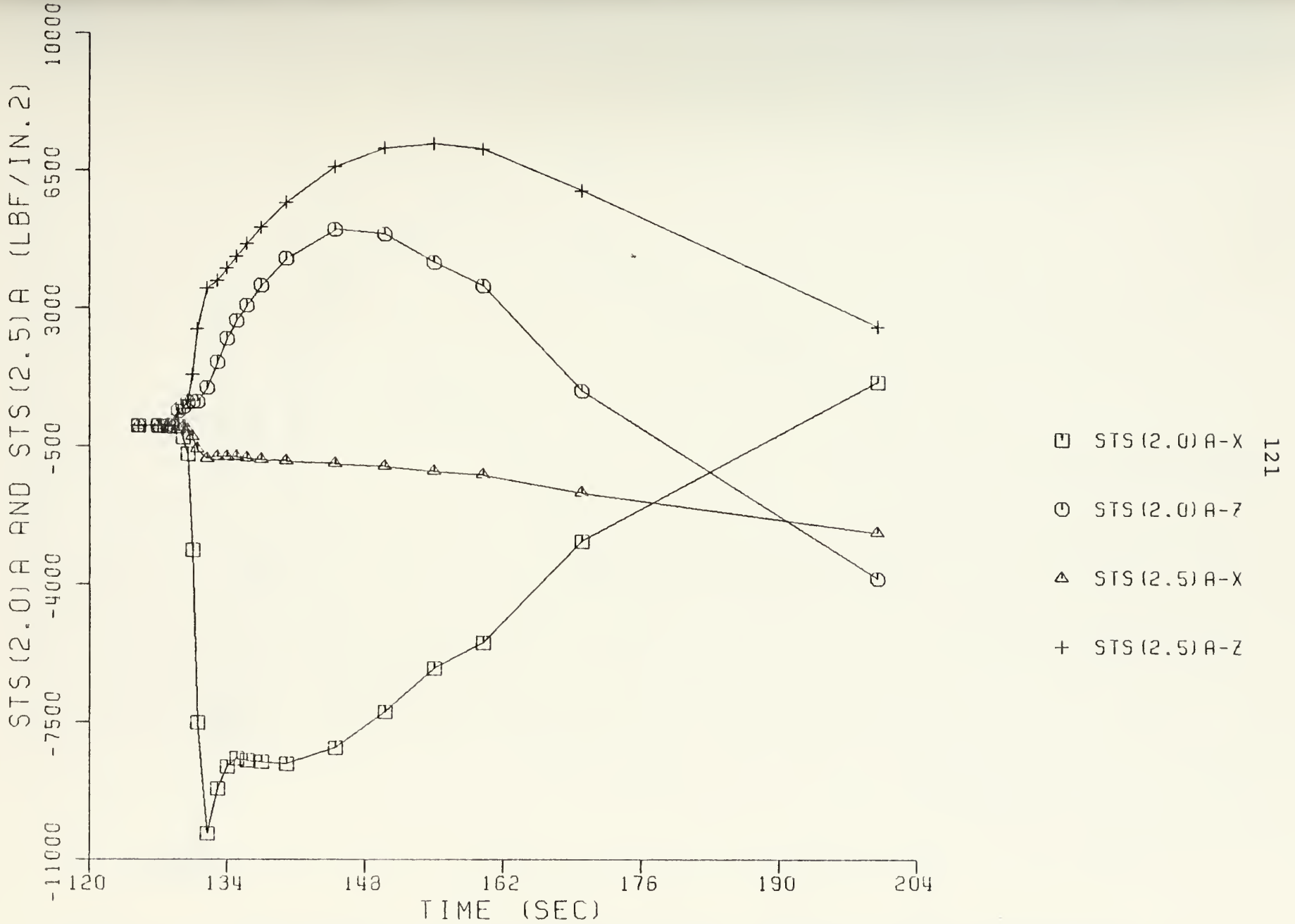


FIGURE VI-8 PREDICTED X AND Z DIRECTION STRESSES 2.0 IN AND 2.5 IN FROM WELD CENTERLINE

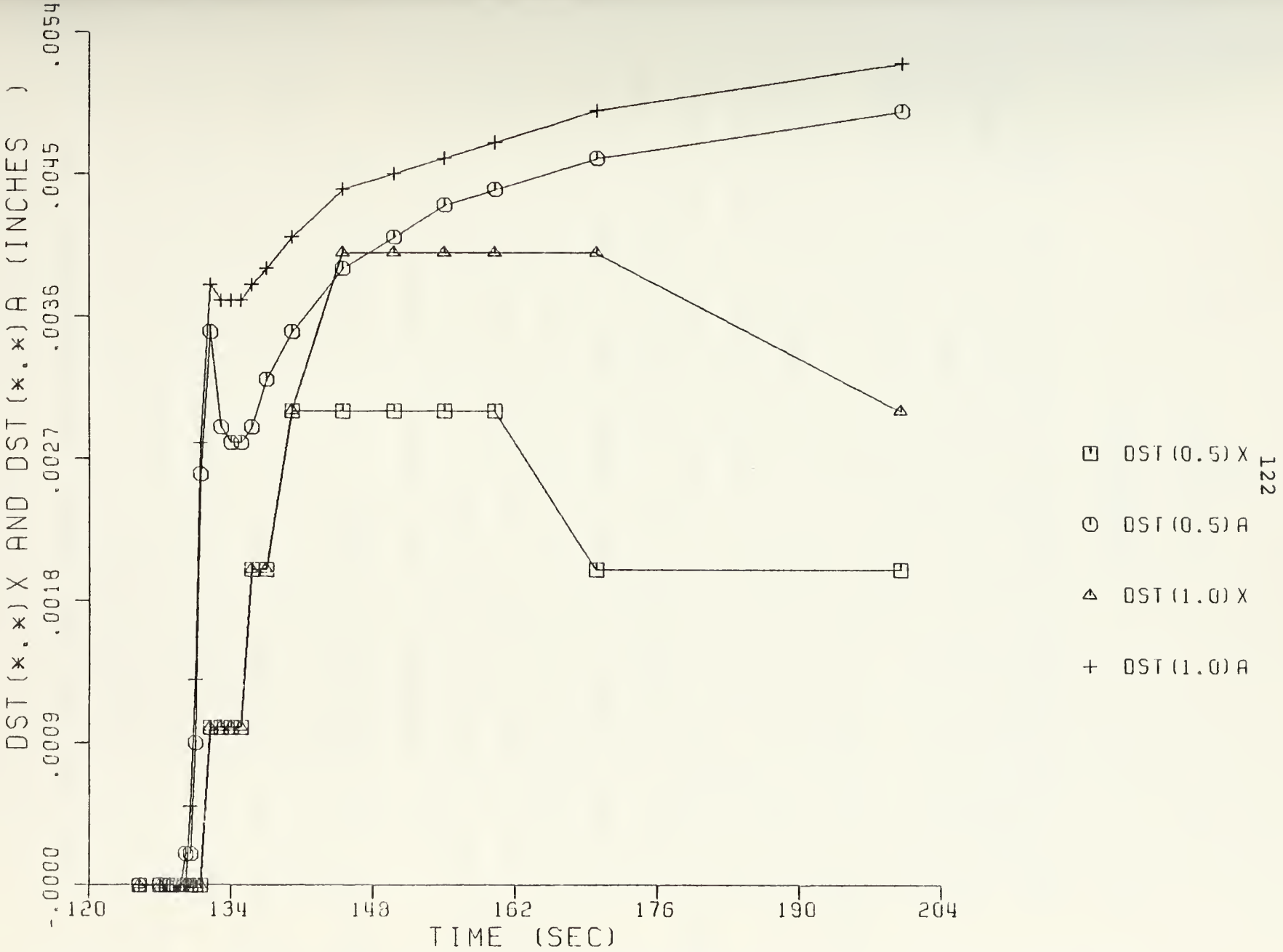


FIGURE VI-9 COMPARATIVE PLOT OF EXPERIMENTAL AND ANALYTICAL RADIAL DISTORTION 0.5 IN AND 1.0 IN FROM WELD CENTERLINE

# CHAPTER VII

## CONCLUSIONS

This study of residual stresses and distortion in high strength steel weldments has shown that existing computer programs require further refinement in order to be used as a day-to-day tool of the welding engineer.

The occurrence of residual stresses and distortion during production of a weldment is a complex phenomena. Past efforts to simulate the welding process involved clever simplifying assumptions followed by attempts to carry out experiments which supported these assumptions. The new approach to welding simulation employs the enormous power of computer techniques to analyze what actually takes place during the welding process. However, if a large computational process is used to model the complex welding process, the thermophysical material properties on which the analysis is based must be accurately known.

The axisymmetric finite element program which was developed by Muraki for analysis of thermal stress and metal movement during welding is promising in that it showed good qualitative agreement with carefully generated experimental data. Heat flow and resulting temperature distributions within weldments can be accurately predicted by existing methods. Qualitative and quantitative comparison between analytical and measured temperature distributions showed remarkable coincidence.

# CHAPTER VIII

## RECOMMENDATIONS

Inasmuch as analytical methods to predict stresses and distortion resulting from thermal cycles can only be as good as the thermophysical material properties on which they are based, it is recommended that studies be undertaken to accurately determine the temperature dependence of high strength steel properties at alevated temperatures. This would enhance further efforts to simulate the welding process.

For further study of computer simulation of multi-pass welding, it is recommended that a micro-processor be used to process welding parameter data. Reduction of strains requiring temperature compensation is a tedious task, especially if measurements are made at several locations and recorded on one photo tape. This additional source of error could be reduced or eliminated if parameters of interest could be calculated internally and displayed directly.

High temperature strain gages could significantly contribute toward a more meaningful study. The 400 $^{o}$F limitation of gages used in this study severely restricted their location.

# REFERENCES


1 Masubuchi, K. "Thermal Stresses and Metal Movement During Welding, especially High Strength Steels", London, 15-17 Nov 77, The Welding Institute, Cambridge.

2 Tall, L. "Residual Stresses In Welded Plates - a theoretical study". Weld. J., 43(1), 1964, 10s-23s.

3 Masubuchi, K., Simmons, F.B., and Monroe, R.E., "Analysis of Thermal Stresses and Metal Movement During Welding". RSIC-820, Redstone Scientific Information Center, Redstone Arsenal, Ala, Jul 1968.

4 Masubuchi, K. and Iwaki, T. "Thermo-elastic analysis of orthotropic plastic by the finite element method". J. Soc Naval Architects of Japan, 130, 1971, 195-204.

5 Muraki, T. and Masubuchi, K. "Finite Element Analysis based upon the generalized variational principle of Plastic and Elastic Distortion of Plates and Shells". Paper V-2 presented at the Int's Conference 'Computer Applications in the Automation of Shipyard Operation and Ship Design', Tokyo, 28-30 Aug 1973.

6 Andrews, J.B., Arita, M., and Masubuchi, K. "Analysis of Thermal Stresses and Metal Movement during Welding", NASA Contract Report NASA CR-61351, prepared for the G.C. Marshall Space Flight Center, Dec 1970.

7 Klein, K.M., "Investigation of Welding Thermal Strains in Marine Steels", MS Thesis, MIT, May 1971.

8 Klein, K.M., and Masubuchi, K. "Investigation of Welding Strains in High Strength Steels for Marine Application", Paper presented at 2nd Int'l Ocean Development Conference, Tokyo, 5-7 Oct 1972.

9 Johnson, E.K. "Study of Flame Heating of Steel Plate", MS Thesis, MIT, May 1971.

10 Hirsch, A.K. "Investigation of Thermal Stress and Buckling during Welding of Tantalum and Columbium Sheet", MS Thesis, MIT, May 1973.

[11] Muraki, T., Bryan, J.J., and Masubuchi, K. "Analysis of Thermal Stresses and Metal Movement during Welding, Pt. 1: Analytical Study, Pt 2: Comparison of Experimental Data and Analytical Results", Trans ASME, Series H, J., Eng'g Materials and Technology, 97 (1), 1975, 81-4, 85-91.

[12] Bryan, J.J. "Analysis of two-dimensional Thermal Stresses and Metal Movement during Welding", Thesis for Ocean Engineer's Degree, MIT, May 1973.

[13] Yamamoto, G. "Study of Longitudinal Distortion of Welded Beams", MS Thesis, MIT, May 1975.

[14] Masubuchi, K. et al. "Analysis of Thermal Stresses and Metal Movement of Weldments: a basic study toward computer-aided analysis and control of welded structures", Paper presented at Annual Meeting of Soc. of Naval Architects and Marine Engineers, New York, NY, 13-15 Nov 1975.

[15] Serotta, M.D. "Reduction of Distortion in Weldments", Thesis for Ocean Engineer's Degree, MIT, Aug 1975.

[16] Hwang, J.S. "Residual Stresses in Weldments in High Strength Steels", MS Thesis, MIT, Jan 1976.

[17] Nishida, M. "Analytical Prediction of Distortion in Welded Structures", MS Thesis, MIT, Mar 1976.

[18] Schrodt, C.J. "Fracture of High Restraint Welds in High Strength Quenched and Tempered Steel", MIT O.E. Thesis, May 1974.

[19] Lipsey, M.D., "Investigation of Welding Thermal Strains in High Strength Quenched and Tempered Steel", MIT O.E. Thesis, June 1978.

[20] Shackleton, D.N. "Welding HY-100 and HY-130 Steels", A Literature Review, The Welding Institute, Abington Hall, Abington, Cambridge CB16AL England.

[21] Schrodt, C.J. "Fracture of High Restraint Welds in High Strength Quenched and Tempered Steel", MIT O.E. Thesis, May 1974.

[22] Tsai, C.L., MIT Research Associate, Personal Conferences, October-November 1978.

[23] Radziminski, J.B. and Lawrence, F.V. Jr. "Fatigue of High Strength Weldments", Welding Research Supplement, Aug 1970, p. 365S.

[24] Doty, W.D. "Welding of Quenched and Tempered Alloy Steels", Metals Engineering Quarterly, ASM Feb 1969.

[25] Nunez, J.M. "Development Welding of HY-140 Steel", Welding Journal, Nov 1969, p. 882.

[26] Connor, L.P., Rathbone, A.M. and Gross, J.H. "Development of Procedures for Welding HY-130(T) Steel. Welding Research Supplement, Jul 1967, p. 309S.

[27] Muraki, T. and Masubuchi, K. "Computer Programs Useful for the Analysis of Heat Flow in Weldments", MIT OSP # 81499 and # 22016, June 30, 1974.

[28] Muraki, T. "Manual on Axisymmetric Finite Element Program for Analysis of Thermal Stress and Metal Movement During Welding", MIT, Cambridge, Mass., Jan 1978.

Thesis
M106
c.1

190661

Mabry
Prediction and control of residual stresses and distortion in HY-130 thick pipe weldments.